ENG470-Engineering Honours Thesis

MURDOCH
UNIVERSITY
PERTH, WESTERN AUSTRALIA

Thesis submitted to the School of Engineering and Information Technology, Murdoch University, to fulfil the requirements for the degree of Chemical and Metallurgical Engineering Honours.

The leaching of α-spodumene

Written by: Bryce Martin Albertani

Unit Coordinator(s): Dr Gareth Lee, Professor Parisa Arabzadeh Bahri

Thesis Supervisor: Assoc. Prof. Aleksandar Nikoloski

Co-Supervisor: Dr. Rorie Gilligan

This page was intentionally left blank

Author's Declaration

I declare that this thesis is my own account of my research and contains as its main content work which has not previously been submitted for a degree at any tertiary education institution.

_____

Bryce Martin Albertani

Acknowledgements

I would like to express my deepest gratitude to my supervisors in Associate Professor Alexander Nikoloski and Dr Rorie Gilligan for their continuous support and guidance throughout this project. Their encouragement and willingness to help has enabled me to learn and develop throughout the entirety of my undergraduate studies. Thank you so much.

I would like to take this opportunity to thanks ALS Metallurgy for providing me the assays results and knowledge to formulate a thesis of which I am proud of. I would particularly like to thank Mr Matthew Ameron and Mr Simon Bagas as it was they who enabled this to happen.

I would also like to thanks Mrs Nasim Khoshdel for her amazing support thought out this project. Without your knowledge and support I would not have had this wonderful opportunity, nor had the amazing year I had. Thankyou.

To my friends all I can do is say thank you. Your support, kindness and caring mean the world to me. I would like to shout out to Mitch, Lia, Chris, Sadie, Brett and Nic for the constant support throughout my studies, you guys are the best. I would like to give special thanks to Chris Buhlmann for the constant supply of coffee and support. You are the best!

Lastly to my family, for their love and support throughout my whole life, thank you.

Abstract

An investigation into the direct leaching of α-spodumene has being warranted due to increasing societal interest in lithium-ion battery technology. The direct leaching of α-spodumene utilising a caustic autoclave process was investigated, in aspirations of leaching significant quantities of lithium from the silicate matrix of α-spodumene. The influence of reagent dosage, temperature, reaction time and particle size on the extraction efficiency of lithium were investigated. From the investigations conducted it became evident that the leaching efficiency of α-spodumene was consistently greater than 40.00% under the optimal conditions. The optimal conditions evaluated throughout the investigation were found to occur at 573.15 kelvin, 14 molar NaOH, a 6 hour residence time and a P_{80} of 325 μm.

The lithium recovered to solution is present as a hydroxide species, of which is in significant demand within the lithium-ion battery production industry. Sodium silicate or 'water glass' was also found to be present within the leach products adding a potential valuable by-product to the process investigated.

Table of Contents

List of Figures

List of Tables

1. Introduction

The societal push towards renewable technologies has resulted in a rapid expansion of the lithium-ion battery (LIB) industry (Vikström et al. 2013). As the name suggests lithium is a fundamental component of LIB's and hence the processing and refining of lithium compounds has attracted lots of attention in recent years.

Spodumene ($LiAlSi_2O_6$) naturally exists as an insoluble alumino-silicate with a significant theoretical lithium contents of 8.03% (Brown 2016). The relatively high abundance of spodumene compared to other hard rock sources has seen it become the dominant mineralogical source of lithium worldwide. Current extraction techniques utilised in the processing of spodumene utilise a series of calcination, roasting and consequential water leach systems to efficiently recovery economical quantities of lithium (Meshram et al. 2014). Due to the intrinsic drawbacks associated with these processing methods, investigations into simplifying and reducing the constraints associated with the processing of spodumene is a subject worthy of detailed investigation.

Lithium hydroxide (LiOH) has been identified as a key material in the production of LIB's cathodic and electrolytic components (Gains et al. 2011). The current world market for refined lithium compounds is dominated by the production of lithium carbonate (Li_2CO_3). Current technologies enable lithium carbonate to be readily converted to lithium hydroxide, however investigations into the direct production of lithium hydroxide are warranted in aspirations of creating a simplified and environmentally friendly process.

1.1 Research aim and objectives

The aim of this research project was to study the direct leaching of α-spodumene in different alkaline media by addressing the following research objectives:

1. Investigate and quantify the influence of key process parameters on the leaching system including the following:
    i. The effect of reagent dosage
    ii. The effect of residence time
    iii. The effect of particle size
    iv. The effect of temperature.
2. Analyse and interpret the collected results and propose directions for further research.

2. Literature review

2.1 Introduction

The increasing demand for the production of lithium has been on the rise since the introduction of the lithium-ion battery. The global desire to reduce carbon emissions by embracing renewable technologies is driving society towards the development of electronic vehicles and enhanced energy storage devices. Lithium has been identified as a source of interest due to its significant energy density and high electrochemical potential (3.045 V) (Meshram et al. 2014). The Deutsche Bank estimated the global consumption of Lithium Carbonate Equivalent will increase from 181 kilo tonnes in 2015 to 535 kilo tonnes by 2025, due to the expected expansion of the LIB industry (Hocking et al. 2016). Lithium is the critical element within the chemistry of lithium ion batteries, hence the demand appears certain. Major applications of lithium are present in the aeronautical and ceramic industries, of which further encouraging lithium's growing demand (Wanhill 2014) (Figure 1). By 2025 the *Association of Mining and Exploration Companies* (AMEC) estimate the net worth of the lithium resource sector to be in excess of $ 2 trillion dollars (USD), with the LIB industry holding a primary stake over the market (AMEC 2018).

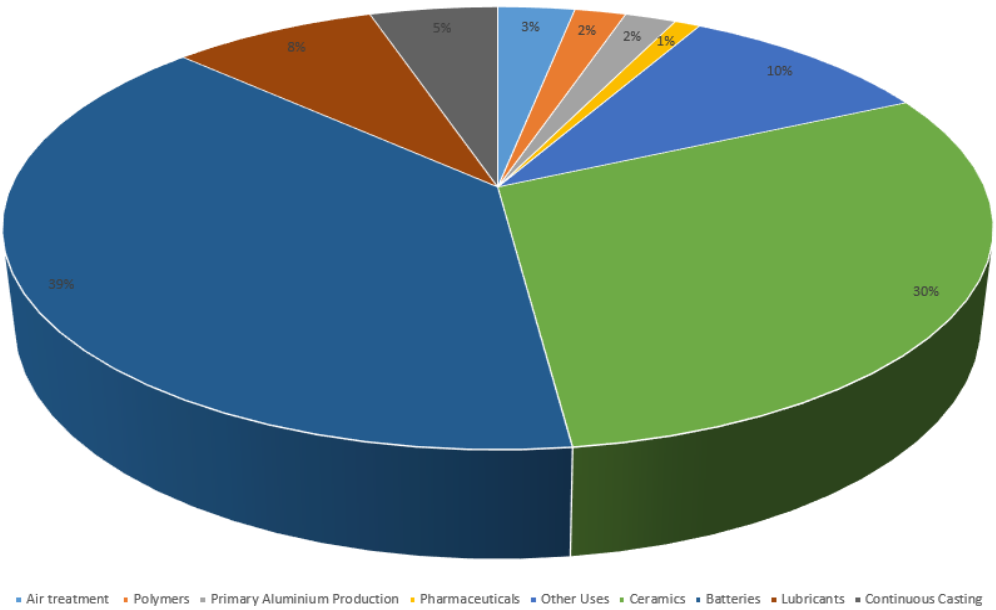

Figure 1: Global lithium demand for end uses in 2011, adopted from Jaskula (2017)

In order to satisfy the growing demand for lithium, investigations into alternative sources and refined processing techniques are warranted. Spodumene is a hard rock mineralogical source of lithium that has attracted significant amounts of attention in recent years, due to its relatively high grade (Meshram et al. 2014). Current commercial extraction techniques often require sophisticated and energy intense processes in order to produce marketable

quantities of lithium from spodumene ore (Meshram et al. 2014, Choubey et al. 2016). In order to understand the benefits and constraints of the current spodumene market, a literature review has been conducted. The literature review developed a baseline of knowledge, directed towards understanding the global supply of spodumene as well as understanding the various extraction techniques currently utilised in the production of saleable lithium products. The downstream processing that is utilised in the production of metallic lithium and lithium ion batteries was also assessed. This was conducted in an attempt to understand key attributes of lithium products, and is used to identify points of potential improvement in the earlier extraction phases. From the analysis conducted relevant technological advances are discussed and areas of potential improvement were identified in a concluding summary.

2.2 Mineralogical aspects of lithium

Lithium exists in various natural resources such as clays, salt lakes, brine reserves and hard rock minerals. The worlds current primary source of lithium exist as salt brines, of which are geographically concentrated in South America (Grosjean et al. 2012) (Figure 2). When assessing the geographical distribution of lithium deposits, *Grosjean et al* highlighted how existing brine deposits are "*geo-strategically and geo-economically"* restricted. The constraints associated with the brine deposits limit the amount of lithium that these sources can produce, encouraging investigation into alternative sources such as spodumene.

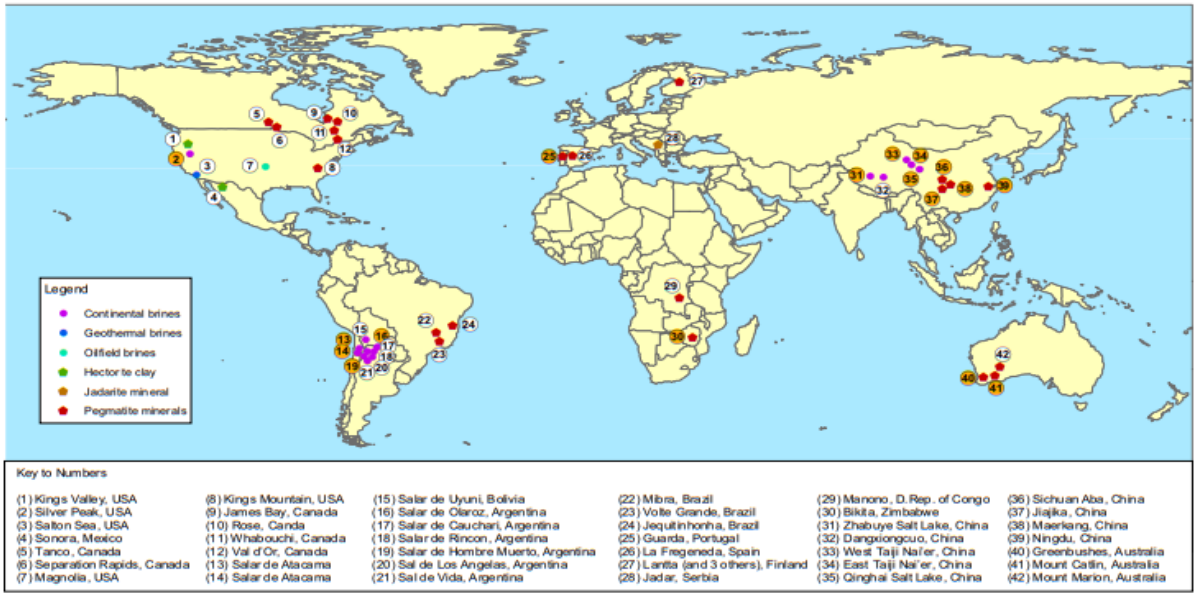

Figure 2: Locations of lithium deposits worldwide, adopted from (Brown 2016)

2.2.1 Geological overview of spodumene

Spodumene ($LiAlSi_2O_6$ or $Li_2O.Al_2O_3.(SiO_2)_4$) is the primary hard rock mineralogical source of lithium worldwide (Brown 2016). This is due to spodumene having a high theoretical lithium content (8.03% Li_2O) in comparison to other lithium bearing minerals such as lepidolite (3.58%), zinnwaldite (1.59%) and amblygonite (3.44%) (Table 5). The mineralogical characteristics of spodumene has been associated with the pegmatite mineralogical family. *London (2014)* identified these mineralogical characteristics and categorised spodumene as being an igneous rock formation of granitic composition. *London* concluded that the extremely coarse and variable grain-size with the abundance of crystal growth allowed for spodumene to be distinguished from other igneous ores. Spodumene is often associated with gangue minerals such as quartz and feldspar (Zelikman et al. 1996). As often associated with such deposits, the highly siliceous composition of spodumene indicates that it derives from a felsic igneous origin (Brown 2016, University of Minnesota 2010).

The formation of pegmatitic deposits occur under high temperature and pressure, where the slow cooling of magmatic fluids provides optimal conditions for silicate formation (University of Minnesota). Spodumene is understood to form as intrusive veins under 250-300 MPa and 438-538 K in pegmatitic deposits, coring itself towards the interior of the silicate vein, where the thermal diffusivity of the magmatic material is slowest (London 2014). Ferrous (Fe^{2+}) and manganese (Mn) material can be substituted into the formation of spodumene, resulting in impurities in the crystal lattice structure (Souza et al. 2004). The presence of these impurities are one of the reasons why various existing lithium deposits are not economically viable to recover, with few containing a significant lithium content able to produce economical amounts of lithium product. One of the few economically viable pegmatite's discovered is the Greenbushes deposit owned by Talison Lithium Pty Ltd (Talison Pty Ltd 2018).

Studies into the formation of the Greenbushes deposit have being investigated since the discovery of alluvial tin in 1886 (Bridgetown 2016). The investigation conducted by *Partington and McNaughton (1995)* accessed the formation geology of the Greenbushes pegmatite's (Figure 3). The journal article published states: "*The Greenbushes pegmatite is a giant pegmatite dike of Archean age with substantial Li-Sn-Ta mineralization, including half the world's Ta resource." Partington* theorised that the high tantalum (Ta) and tin (Sn) contents associated with the greenbushes deposit, occurred as paragenetic inclusions into

the pegmatite ore during early formation. Research conducted by *Thomas and Davidson* (2016) further suggests that pegmatite mineralisation occurs at 1023 K and 500 MPa. *Thomas and Davidson* also identified that when pegmatite is cooled to 893 K Ta/Sn mineralisation occurs simultaneously within the pegmatitic material, allowing for the intrusion of magmatic material to occur prior to spodumene crystallisation. Zircon ($ZrSiO_4$) growth has been associated with Ta/Sn mineralisation, allowing for isotropic age dating to be conducted for greater formation assessments (Wang et al. 2007, Partington and McNaughton 1995).

A recent report conducted by *Ingham et al. (2011)* was released to the Toronto Stock Exchange (TSX) in June of 2011, regarding the current regional geology of the Greenbushes deposit. The report surmised by the *British Geological Survey* (Brown 2016) states that the "*pegmatite orebody is approximately five kilometres in length and three hundred meters in width. It lies within the Donnybrook-Bridgetown Shear Zone and intrudes rocks of the Balingup Metamorphic Belt in the south of the Yilgarn Craton."* It is understood that deposits located within this region are often obscured by tertiary sediments and laterites at depths up to forty meters (Partington and McNaughton 1995). This provides unique challenges when mining such deposits, often having to be classified into distinct groups to undergo economically viable processing (Ingham et al. 2011). The distinct groups of pegmatite identified by *Ingham et al* are separated into five distinct mineralogical zones. This includes the contact; potassium feldspar; albite; mixed and a spodumene zones of which it is estimated that spodumene represents 26% of the total pegmatitic ore (Figure 3). Studies conducted in September of 2012 estimated approximately 0.6 million tonnes of lithium ore readily available at an average grade of 3.2% Li_2O (Ingham et al. 2011). Recently *Talison Pty Ltd (2018)* released a press statement in February of 2017 announcing a $320-million-dollar expansion to the Greenbushes ore deposit towards the south- west (Williams 2017). The expansion is estimated to double production outputs to 165 000 tonnes per annum by 2021, with more information to be released by the estimated end of commissioning date in 2019 (Tianqi Lithium 2018).

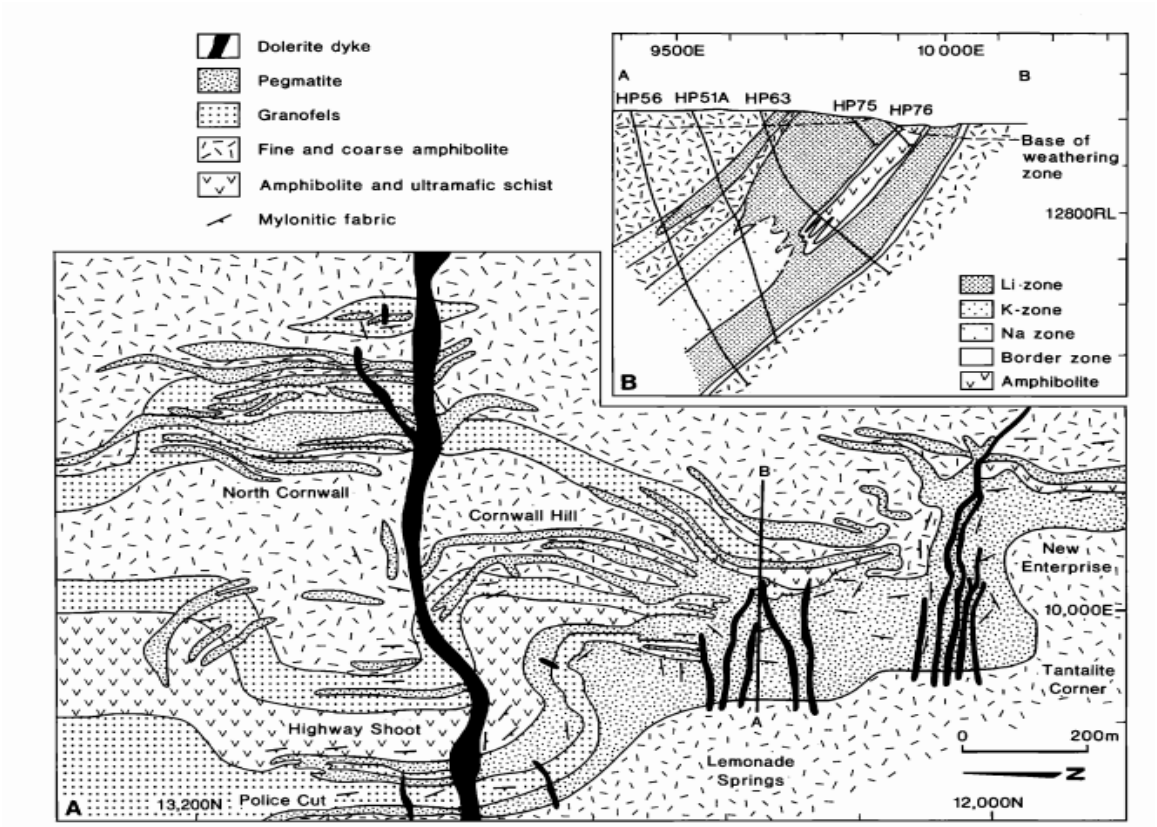

Figure 3: Greenbushes pegmatite (A) with (B) displaying the mineralogical zonation of the region, adopted from Partington and McNaughton (1995)

2.2.1 Crystal chemistry of spodumene

The crystal structure of spodumene is transparent and composes of 8.03% Li_2O, 27.4% Al_2O_3 and 64.6 % SiO_2 (Hurlbut 1971). Naturally α-spodumene exists as a silicate ($[SiO_3]^2$) in a tetrahedral coordination (Figure 4a). An investigation conducted by *Moon and Douglas (2003)* surmised the crystallography of spodumene. In the article spodumene is understood to contain two distinctive regions of interstitial cations, of which the smaller aluminium ion (Al^{3+}) and larger lithium ion (Li^+) exist within the silicate structure. The aluminium ions exist within the silicate structure in an octahedral coordination with six oxygen atoms *(two non-bridging basal oxygen atoms plus four apical oxygen atoms)*. The lithium contained within spodumene is arranged in an irregular octahedral coordination with six oxygen atoms *(two non-bridging basal oxygen's, two bridging basal oxygen's and two apical oxygen's)*, due to its small size. This explanation satisfies *Pauling's (1932)* principle on electroneutrality, as the strength of electrostatic bonds become 1/6 for the lithium ion in octahedral coordination with the oxygen atoms, 1/2 for the aluminium ion in octahedral coordination with the oxygen atoms and one for the silicon atom at the centre of silicate tetrahedra (Moon and Douglas 2003, Pauling's 1932, Hazen and Finger 1984). The lateral

bonding of the silicate chains occurs due to the ionic bonds that exist between the lithium and aluminium ions, leading to the cell formula of $LiAlSi_2O_6$.

Spodumene with its monoclinic crystal structure indicates that it belongs to the clinopyroxene subgroup of the pyroxene family (University of Minnesota 2010) (Figure 4A). The formation conditions of pyroxene (pegmatitic conditions) allows for the substitution of aluminium and lithium ions with transitional elements such as manganese (Mn), iron (Fe) and chromium (Cr). The potential substitutions that can occur, can lead to polymorphs of spodumene forming. This includes kunzite ($LiAlSi_2O_6$) of which due to its high manganese content contains pink hues and hiddenite ($LiAlSi_2O_6$) of which contains a significant chrome content giving the silicate crystal a green tinge. Larger mineralogical substitutions such as the formation of ferromagnesian minerals are likely to occur in the place of spodumene formation (Souza et al. 2004). Such minerals include clinoferrosilite ($Fe^{2+}SiO_3$), jadeite ($Na\ (Al, Fe^{3+})\ Si_2O_6$) and johannsenite ($CaMn^{2+}Si_2O_6$) (Hurlbut 1971). The most common impurities associated with spodumene are feldspars ($KAlSi_3O_8 – NaAlSi_3O_8 – CaAl_2Si_2O_8$), quartz ($SiO_2$) and micas ($(AB_{2-3})\ (X, Si)_4O_{10}\ (O, F, OH)_2$) of which are gangue minerals and are not included in elemental substitution reactions that occur with spodumene.

Table 1: Mineralogical characteristics of spodumene, adopted and modified from Mindat (1993-2018)

Chemical Formula	$LiAlSi_2O_6$
Colour	Colourless, yellow, light green, emerald-green, pink to violet, purple, white, grey.
Hardness	6.5-7
Specific Gravity	3.1-3.2
Crystal Structure	Monoclinic

(A)

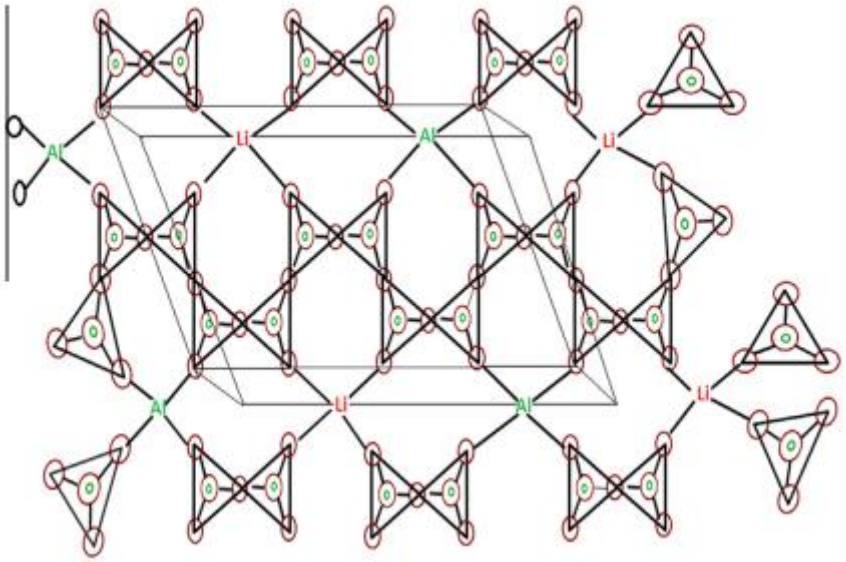

(B)

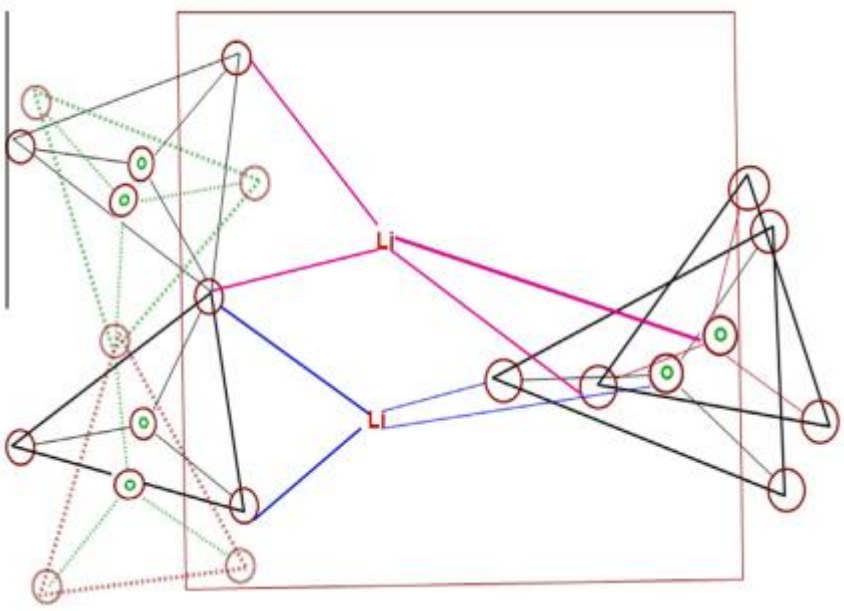

Figure 4: Crystal structure of α-spodumene (A) and β-spodumene (B), adopted from Choubey et al. (2016)

2.3 Processing of spodumene

Spodumene naturally exists as an insoluble monoclinic aluminium silicate, referred to as α-spodumene (Brown 2016). The molecular arrangement of α-spodumene consists of a sixfold tetrahedra of silicon atoms, centralised around aluminium and lithium ions (Botto 1985, Salakjani et al. 2016) (Figure 4A). It has been found that due to the highly siliceous nature of the mineral, numerous difficulties arise when trying to extract valuable constituents (Meshram et al. 2014, Kuang et al. 2018). Currently the most efficient extraction techniques utilise an energy intensive calcination step prior to leaching. The calcination of α-spodumene promotes a physical transformation to occur resulting in a reactive polymorph forming known as β-spodumene. When calcination occurs the sixfold coordination of the silicon atoms become five membered rings of (Si, Al) O_4 (Botto 1985, Salakjani et al. 2016) (Figure 4B). The transformation provides a passage for the liberation of lithium to occur, by thermally weakening the intermolecular bonds that exist between Li - (Si, Al) O_4 atoms (Salakjani et al. 2016). The consequential volumetric expansion (by 30%) and decrease in specific gravity (from 3.15 g/cm^3 to 2.40 g/cm^3) assists in allowing external reagents to penetrate the β-spodumene and liberate the lithium present (Salakjani et al. 2016, Rosales et al. 2014).

Thermodynamic studies based around the conversion of spodumene has been extensively researched and Gibbs energy diagrams established (Choubey et al. 2016, Munoz 1969, Konar et al. 2018). *Choubey et al.* (2016) identified that the conversion of α to β-spodumene at standard ambient conditions was not feasible. However, the thermodynamic data collected suggested that conversion could be achieved at elevated temperatures as displayed in equations (1) and (2) below:

$$\alpha\text{-spodumene} \xrightarrow{\Delta G_{1073\ K} = -0.45\ kcal} \beta\text{-spodumene} \quad (1)$$

$$\alpha\text{-spodumene} \xleftarrow{\Delta G_{298\ K} = 4.63\ kcal} \beta\text{-spodumene} \quad (2)$$

The Ellingham diagram (Figure 5) reveals the possibility of a phase conversion at ≥ 1073.15 K, however investigations conducted suggests that higher temperatures are required (Meshram et al. 2014, Salakjani et al. 2016, Konar et al. 2018, Barbosa et al. 2014). Spodumene is currently the most commercially active mineralogical source of lithium product worldwide, of which four prominent processing techniques have been established.

The four techniques include sulfation, chlorination, fluorination and alkaline processing (Meshram et al. 2014) of which are surmised in Table 6 and discussed in detail below.

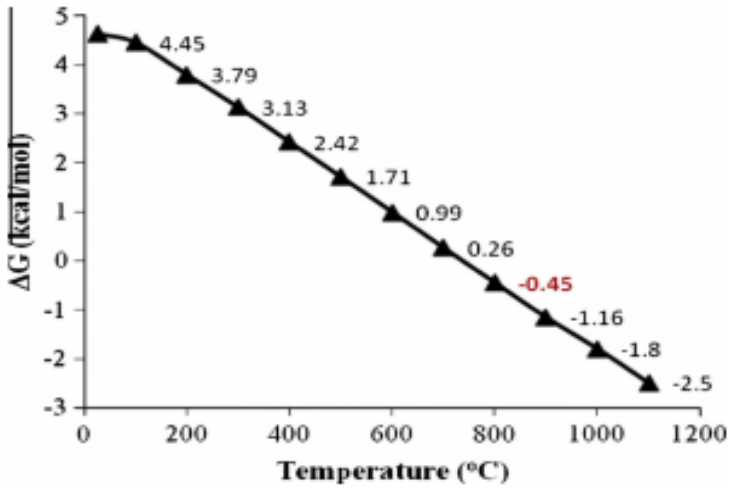

Figure 5: Ellingham diagram for the phase transformation of α to β-spodumene, adopted from Choubey et al. (2016)

2.3.1 Sulfation process

The sulfation process is the most common technique utilised in the extraction of lithium from spodumene, and is currently in commercial application with Galaxy Resources Ltd (Galaxy Resources Limited 2011). This is due to the relatively high stability of lithium sulfate (Li_2SO_4) in aqueous solutions (Figure 6) and its corresponding high solubility factor (Table 8). *Meshram et al.* (2014) analysed studies conducted around the sulfation process and found that the trend for treating spodumene concentrates consisted of four fundamental stages. Stage one consisted of a thermal pre-treatment phase of which was followed by a sulfuric acid roast, water leach and consequential precipitation stage with the desire to produce a lithium carbonate (Li_2CO_3) product.

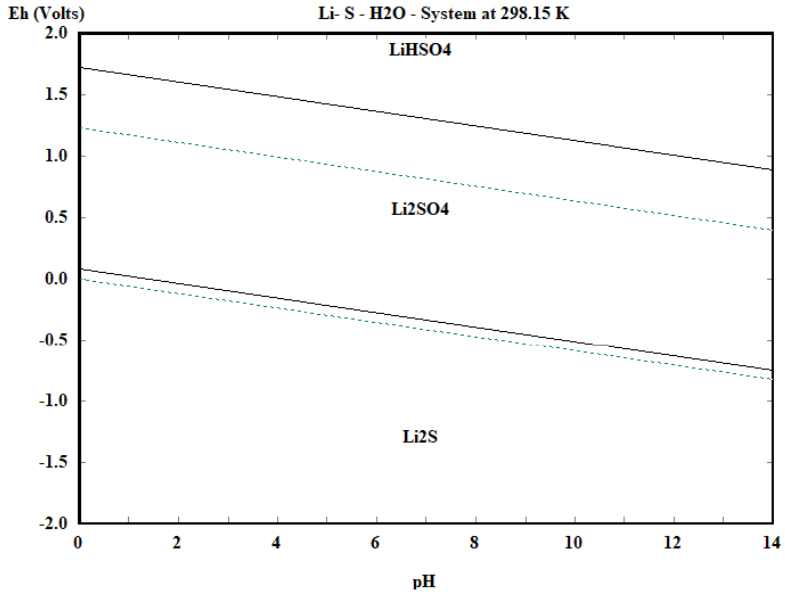

Figure 6: Eh-p.H diagram for the Li-S-H_2O system at 298.15 K, adopted form OutoTec (2017)

The calcination of α-spodumene at 1273.15-1373.15 K for approximately 1 hour, converts the α-spodumene to its more reactive β phase (Salakjani et al. 2016, Kuang et al. 2018). Post calcination, the material is cooled and then mixed with concentrated sulfuric acid (H_2SO_4). The mixture is then roasted at 483.15 K where a cation exchange occurs between the spodumene and the sulfuric acid (Choubey et al. 2016). From this reaction a roast product containing lithium sulfate (Li_2SO_4) is produced, represented by equation (3) below:

$$\beta\text{-}LiAlSi_2O_{6\,(s)} + H_2SO_{4\,(conc)} \xrightarrow{\Delta G^{o}_{483\,K} = -375.28\ kcal} Li_2SO_{4\,(s)} + Al_2O_3.4SiO_{2\,(s)} + H_2O_{(g)} \quad (3)$$

The roast product is then screened at ± 150 µm with the oversize reporting to a regrind stage (Ellestad and Leute 1950). The undersize is subjected to a water leach in order to produce an aqueous lithium sulfate product (Meshram et al. 2014, Kuang et al. 2018, Ellestad and Leute 1950). The extent of leaching is controlled by the addition of limestone ($CaCO_3$), of which is utilised to neutralise the excess sulfuric acid (Kuang et al. 2018). The operating temperature of the leaching vessel is approximated around 448.15-498.15 K allowing for the complete dissolution of lithium sulfate to occur as represented in equation (4) below (Ellestad and Leute 1950).

$$Li_2SO_{4\,(s)} + Al_2O_3.4SiO_{2\,(s)} + H_2O_{(aq)} \xrightarrow{\Delta G^{o}_{498\,K} = -0.71\ kcal} Li_2SO_{4\,(aq)} + Al_2O_3.4SiO_{2\,(s)} + H_2O_{(aq)} \quad (4)$$

Lithium carbonate (Li_2CO_3) can be recovered by the addition of sodium carbonate (Na_2CO_3) to the leach solution (Nicholson 1946). This is completed by the precipitation reaction below:

$$Li_2SO_{4\,(aq)} + Na_2CO_{3\,(aq)} \xrightarrow{\Delta G^o_{298\,K} = -48.88\ \text{kcal}} Li_2CO_{3\,(s)} + Na_2SO_{4\,(aq)} \quad (5)$$

Further downstream processing can be implemented to maximise the recovery of lithium. This is achieved by implementing a closed loop re-leach circuit post the lithium carbonate precipitation stage (Kuang et al. 2018). Doing so does have respective drawbacks such as increased capital costs, intense energy requirements and complicated running conditions (Kuang et al. 2018).

2.3.2 Alkaline process

The process of producing lithium chloride (LiCl) in alkaline conditions is conducted in a two-step process: 1) calcination of the α-spodumene, and 2) a water leach for lithium chloride production (Meshram et al. 2014). *Averill and Olson (1978)* reported that the recovery of this method is approximately 85-90% efficient. The drawbacks on the process involve a complex reagent scheme and a high reagent expenditure. Furthermore the costs associated with constructing corrosion resistant equipment are much greater than that of alternative processes (Kuang et al. 2018).

The calcination of α-spodumene into its reactive β phase is conducted at 1098.15-1323.15 K in the presence of limestone ($CaCO_3$). A product containing lithium oxide (β-Li_2O) is formed under alkaline conditions outlined by equation (6) below:

$$(\alpha)\text{-}LiAlSi_2O_{6\,(s)} + CaCO_{3\,(aq)} \xrightarrow{\Delta G^o_{1323\,K} = -63.52\ kcal} (\beta)\text{-}Li_2O_{\,(s)} + CaAlSi_2O_{6\,(s)} + CO_{2\,(g)} \quad (6)$$

The resulting calcine (β-Li_2O) is crushed, milled and leached in water to yield aqueous lithium hydroxide, as displayed by equation (7), below. The lithium hydroxide is then converted to lithium chloride (LiCl) by reacting with hydrochloric acid (HCl) (8).

$$\beta\text{-}Li_2O_{\,(s)} + H_2O_{\,(aq)} \xrightarrow{\Delta G^o_{298\,K} = -19.01\ kcal} 2LiOH_{\,(aq)} \quad (7)$$

$$LiOH_{\,(aq)} + HCl_{\,(aq)} \xrightarrow{\Delta G^o_{298\,K} = -12.60\ kcal} LiCl_{\,(aq)} + H_2O_{\,(aq)} \quad (8)$$

Post lithium chloride production the lithium bearing eluate is sent for further downstream processing, to be utilised in the production of lithium metal (Brown 2016) (refer to section 2.4.1 for more information).

Archambault and Olivier (1968) proposed an alternative alkaline process by utilising sodium carbonate (Na_2CO_3) as a cationic exchange lixiviant. The recovery of the process is reported

to be 75% efficient at producing a lithium carbonate product. The drawbacks associated with the process involve a complex reagent scheme and high capital/operating expenditures due to the requirement of corrosion resistant materials of construction.

Archambault and Olivier (1968) reported that the calcination of α-Spodumene to its reactive β phase was conducted at 1272.15 K. The β-spodumene was then mixed with sodium carbonate and roasted at 848.15-948.15 K represented in equation (9) below:

$$2\beta\text{-}LiAlSi_2O_{6\,(s)} + Na_2CO_{3\,(s)} \xrightarrow{\Delta G^o_{948\,K} = -450.32\ kcal} Li_2CO_{3\,(s)} + 2NaAlSi_2O_{6\,(s)} \quad (9)$$

The roast product was then subjected to a warm water leach, where the injection of carbon dioxide (CO_2) promotes the formation of lithium bicarbonate ($LiHCO_3$).

$$Li_2CO_{3\,(s)} + CO_{2\,(g)} + H_2O_{\,(aq)} \xrightarrow{\Delta G^o_{298\,K} = -8.48\ kcal} 2LiHCO_{3\,(s)} \quad (10)$$

Lithium bicarbonate has a relatively high solubility in comparison to lithium carbonate (Figure 7), making it an ideal feed for highly soluble lithium applications such as pharmaceutical production (Vikström et al. 2013). Lithium bicarbonate is predominantly present at pH ranges 6-8, at which the process must be maintained for sufficient conversion to be achieved. Once the dissolution of the lithium carbonate is complete the solution is cooled and filtered, where the residue is collected as an upgraded product (≥85%).

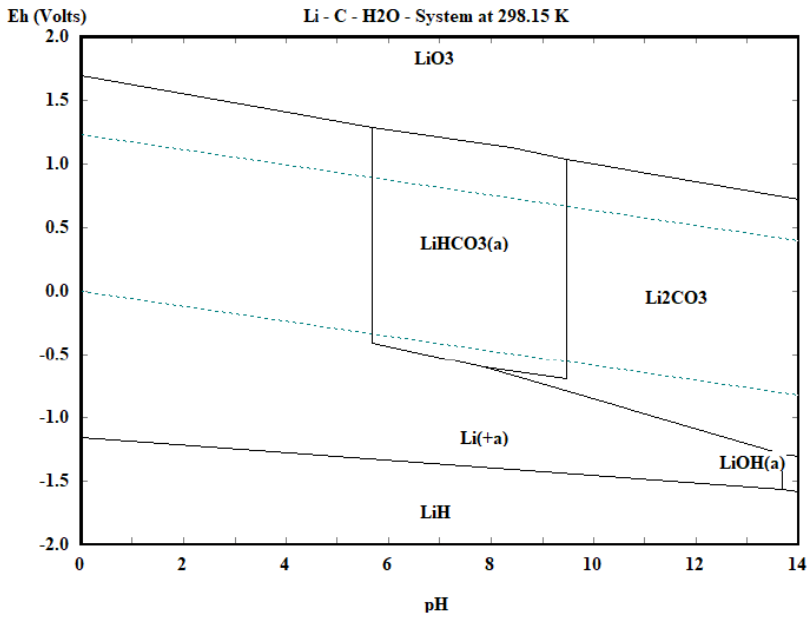

Figure 7: Eh- pH diagram for a Li-C-H_2O system at 298.15 K, adopted from OutoTec (2017)

2.3.3 Chlorination process

The chlorination of β-spodumene utilising chlorine based additives was investigated in detail by *Zelikman et al. (1996)*. The research conducted indicated that the chlorination process was 98% efficient at producing lithium chloride crystals via a chloride roast and subsequent water leach. It was suggested that the efficiency of the process was due to the high reactivity of chloride gas with the metal oxides and silicates resulting in the formation of water soluble chloride complexes (Choubey et al. 2016). The current drawbacks identified with this treatment include the requirement for corrosion resistant materials of construction, high reagent expenditures and the intrinsic dangers associated with utilising chlorine gas (Barbosa et al. 2014).

The sintering of spodumene with a combination of ammonium chloride (NH_4Cl) and calcium chloride ($CaCl_2$) was conducted at 1023.15 K. It was found that 98% of the lithium contained within the spodumene was converted to lithium chloride (LiCl) within the sinter product, as displayed by equation (11) below:

$$\beta\text{-}LiAlSi_2O_{6\,(s)} + 4CaCO_{3\,(s)} + 2NH_4Cl_{\,(s)} \xrightarrow{\Delta G^o_{1023\,K} = -179.15\ kcal} 2LiCl_{\,(s)} + 4CaSiO_{3\,(s)} + Al_2O_{3\,(s)} + 4CO_{2\,(g)} + 2NH_{3\,(g)} + H_2O_{\,(aq)} \quad (11)$$

Zelikman et al. (1996) later investigated the leaching of the sinter product and found that it was water soluble. The leach liquor obtained from the water leach upgraded the purity of the lithium chloride eluate, justifying a re-leach.

$$LiCl_{\,(s)} + CaAlSi_2O_{8\,(s)} + Al_2O_{3\,(s)} + H_2O_{\,(aq)} \xrightarrow{\Delta G^o_{298\,K} = -2.74\ kcal} LiCl_{\,(aq)} + CaAlSi_2O_{8\,(s)} + Al_2O_{3\,(s)} + H_2O_{\,(aq)} \quad (12)$$

The liquor from the water leach is filtered and separated from the solid residue. The solution is then evaporated allowing for the crystallisation of lithium chloride to occur, resulting in a 98% pure lithium chloride product (Meshram et al. 2014, Zelikman et al. 1996). The crystallised product is sent for further downstream processing, to be utilised in the production of lithium metal (Brown 2016) (refer to section 2.4.1 for more information).

Barbosa et al. (2014) investigated the roasting of β-spodumene with chlorine gas and reported a recovery of 90%. From the research conducted an equilibrium composition system consisting of Si-Al-Li-O-Cl (Figure 8) was derived, of which accounted for the complexes formed during the chlorination of spodumene. The test work conducted by

Barbosa et al established that the optimal conditions for chlorinating spodumene occurred a 1323.15-1373.15 K for approximately 2.5 hours, of which is represented by equation (13) below:

$$\beta\text{-}LiAlSi_2O_{6\,(s)} + \frac{1}{2}\,Cl_{\,(g)} \xrightarrow{\Delta G^{o}_{1373\,K} = -202.00\ kcal} LiCl_{\,(aq)} + \frac{1}{6}\,Al_6Si_2O_{13\,(s)} + \frac{1}{4}\,O_{2\,(g)} \qquad (13)$$

The chlorination process resulted in an overall mass reduction of the feed material, indicating the formation of lithium chloride complexes. The rate of formation for the lithium chloride was evaluated to increase with increasing temperatures, as displayed by in Figure 8 (Barbosa et al. 2014, OutoTec 2017). The formation of solid by-products such as mullite ($Al_6Si_2O_{13}$) and cristobalite (SiO_2) assisted in distinguishing the efficiency of the process. This is more evident at temperature in excess of 1273.15 K, as lithium chloride becomes preferentially concentrated in an aqueous phase above 453.15 K (Figure 8). The elimination of iron-based impurities was found to occur below 1273.15 K, with other impurities requiring removal via distillation (Habashi 1986). From the results gathered the activation energy for the chlorination process was determined to be 85.80 kcal/mol (please refer to Figure 42) (Barbosa et al. 2014).

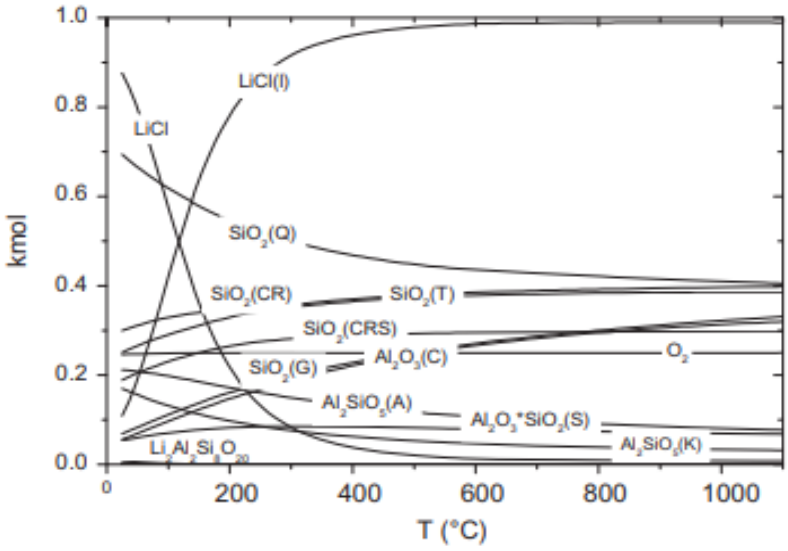

Figure 8: Equilibrium composition of the system Si-Al-Li-O-Cl, as a function of temperature, adopted from Barbosa et al. (2014)

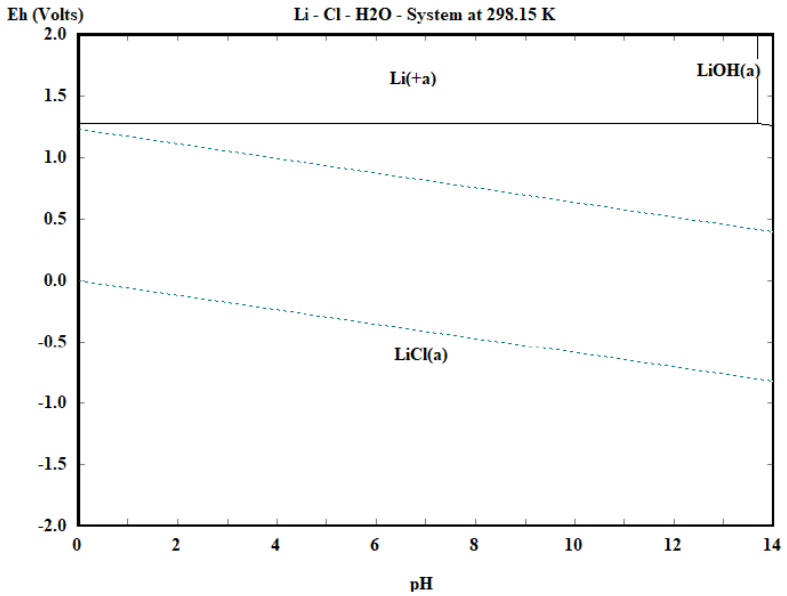

Figure 9: Eh-pH diagram for a Li-Cl-H_2O system at 298.15 K, adopted from OutoTec (2017)

2.3.4 Fluorination process

Rosales et al. (2014) conducted an investigation into the leaching of β-spodumene, utilising hydrofluoric acid (HF) as leachate. A recovery of 90% was reported under the optimised conditions, however due to the intrinsic drawbacks associated with HF acid, the process has not been commercialised (Kuang et al. 2018).

The optimised hydrofluoric leach conducted by *Rosales et al. (2014)* operated under the following conditions: A solid–liquid ratio of 1.82% (w/v); Temperature of 348.15 K; HF concentration, 7% (v/v); stirring speed, 330 rpm and a residence time of 10 minutes. The lithium present in the β-spodumene readily dissolves and complexes into lithium fluoride (LiF) (Figure 10). Meanwhile the silicon and aluminium atoms present were also dissolved into solution. This is all represented by equation (14) below:

$$LiAlSi_2O_{6\,(s)} + 19HF_{\,(aq)} \xrightarrow{\Delta G^o_{348\,K} = -91.974\ kcal} LiF_{\,(aq)} + H_3AlF_{6\,(aq)} + 2H_2SiF_{6\,(aq)} + 6H_2O_{\,(aq)} \quad (14)$$

The silicon and aluminium present are later recovered by precipitating as sodium hexafluorosilicate (Na_2SiF_6) and cryolite (Na_3AlF_6) via the addition of sodium hydroxide. Simultaneously, the fluoride species containing lithium are converted into soluble lithium hydroxide, represented by equation (15) below:

$$LiF_{(aq)} + NaOH_{\,(aq)} \xrightarrow{\Delta G^o_{298\,K} = -7.25\ kcal} LiOH_{\,(aq)} + NaF_{\,(aq)} \quad (15)$$

The lithium hydroxide concentrate is then subject to evaporation and purification. The purification process involves the heating of the lithium hydroxide concentrate to 368.15 K for approximately 20 minutes, under the presence of a carbon dioxide atmosphere (16). This promotes the formation of lithium carbonate, of which is sparged with carbon dioxide to convert the lithium carbonate to soluble lithium bi-carbonate. The formation of lithium bi-carbonate allows for further purification to occur, where the lithium carbonate produced is upgraded to a more concentrated product (Rosales et al. 2014).

$$2LiOH_{(aq)} + CO_{2\,(g)} \xrightarrow{\Delta G^{o}_{368\,K} = -25.10\ kcal} Li_2CO_{3\,(s)} + H_2O_{(aq)} \qquad (16)$$

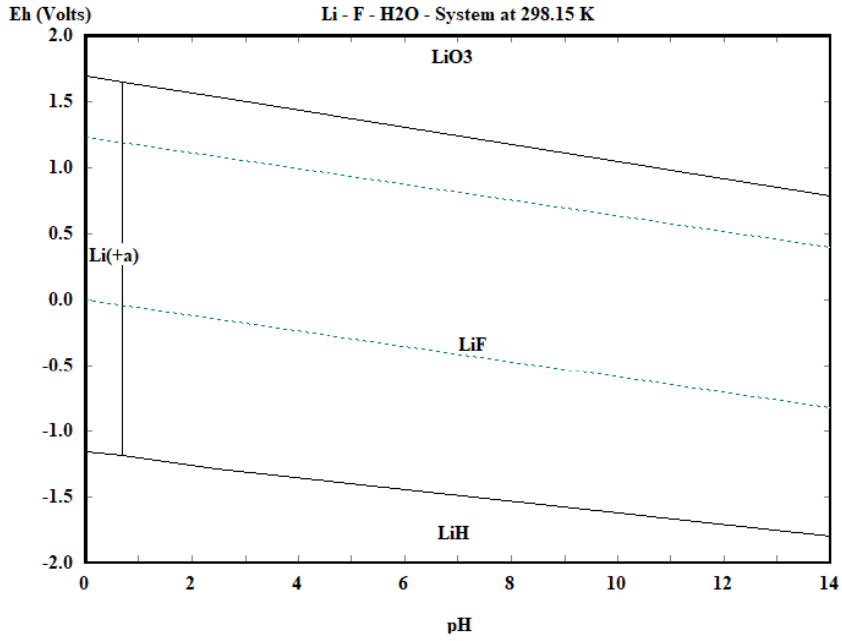

Figure 10: Eh-pH diagram for a Li-F-H_2O system at 298.15 K, adopted from OutoTec (2017)

Guo et al. (2017) conducted research utilising hydrofluoric acid as an additive to the sulfuric acid roasting process. The results showed that the addition of hydrofluoric acid to the sulfuric acid process was successful in increasing the overall extraction efficiency to 96%. It was further found that the process could be replicated with α-spodumene, and similar recoveries achieved. However, a major drawback of this process is to the highly toxic nature of the hydrofluoric acid, which has restricted the processes commercial application.

The hydrofluoric leach conducted by *Guo et al* utilised a α-spodumene feed of which was mixed in a 1:3:2 ore/HF/H_2SO_4 ratio (Guo et al. 2017). This mixture was placed into an agitated tank at 150 rpm and 373.15 K for the optimal time of 3 hours. The dissolution

reaction of the α-spodumene and formation of lithium sulfate are represented by equation (17) below:

$$2\alpha\text{-}LiAlSi_2O_{6\,(s)} + 24HF_{\,(aq)} + 4H_2SO_{4\,(aq)} \xrightarrow{\Delta G^o_{373\,K} = -206.61\ kcal} LiSO_{4\,(aq)} + Al_2(SO_4)_{3\,(aq)} + 4H_2SiF_{6\,(aq)} + 12H_2O_{\,(aq)} \quad (17)$$

The aqueous product from the leach contains lithium sulfate, aluminium sulfate ($Al_2(SO_4)_3$) and hexafluorosilicic acid (H_2SiF_6). The aqueous species produced then undergo a purification process which consists of a water leach where the addition of sodium carbonate promotes the precipitation of lithium carbonate (18). The product from the water leach is then filtered, to recover the solid residue which contains ≥96% lithium carbonate (Guo et al. 2017).

$$Li_2SO_{4\,(aq)} + Na_2CO_{3\,(aq)} \xrightarrow{\Delta G^o_{323\,K} = -48.88\ kcal} Li_2CO_{3\,(s)} + Na_2SO_{4\,(aq\}} \quad (18)$$

2.4 Downstream processing of lithium

The downstream processing of lithium products has a significant influence on the extraction process selected. This can be due to the relative costs and complexity associated with refining particular lithium products for commercial applications, such as LIB's (Averill and Olson 1978, Vikström et al. 2013). As displayed in Figure 11 below lithium hydroxide, chloride and carbonate are the main lithium products utilised in current commercial applications (Yaksic and Tilton 2009). Lithium consumption is estimated to rise by 20% per annum past the year 2020 (Kuang et al. 2018). Lithium carbonate has been identified as the most robust and important lithium product on the market, due to its wide spread applications (Yaksic and Tilton 2009). Lithium chloride is predominantly utilised in the electrolytic production of lithium metal, due to its relatively high solubility and reactive interface (Nicholson 1946). Lithium hydroxide is rapidly becoming the dominant lithium product utilised in the production of lithium ion batteries (Mao 1996). Lithium hydroxide is often utilised in converting any lithium carbonate to lithium chloride, due to its high reactivity and simple chemistry (Mao 1996). The downstream processing of lithium carbonate, chloride and hydroxide are discussed in detail below.

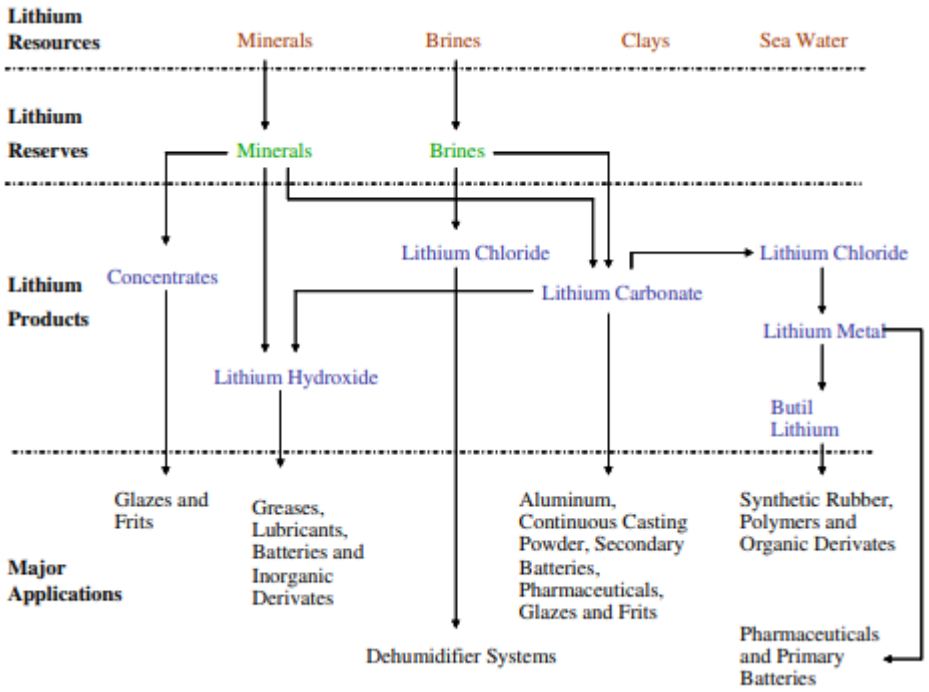

Figure 11: Types of lithium resources, reserves, products and applications, adopted from Yaksic and Tilton (2009)

2.4.1 Electrorefining for the production of lithium metal

The electrowinning of lithium chloride is the dominant refining method utilised in the production of lithium metal (Kipouros and Sadoway 1998). The process has been utilised in the lithium refining industry for many years with the first commercial production of lithium metal occurring in 1923 by Metallgesellschaft AG, formerly one of Germany's largest industrial conglomerates (Rio Tinto 2014). The process operates with an efficiency ≥ 98%, however significant drawbacks and hazards are present in the process, especially the dangers associated around the evolution of chlorine gas at the anode. Chlorine gas is a corrosive substance, of which can lead to respiratory problems in people (U.S. Department of Health and Human Services 2004). Mitigating the potential risks associated with the corrosive nature of the process is the most significant cost to the refining process. Research into alternative refining methods have been investigated, however the lithium chloride electrorefining method remains the most economically viable process to date.

The most dominant lithium species utilised in the production of metallic lithium is lithium chloride (Hampel 1972). This is due to lithium chloride having the largest deposition potential of all lithium products, suggesting that it has the greatest potential for being reduced (Takeda et al. 2014). A method for converting lithium carbonate to lithium chloride has been found to be economically viable within the constraints of the electrorefining process (Kipouros and Sadoway 1998, DeYoung 1991). Lithium carbonate is initially converted to lithium hydroxide by the addition of calcium hydroxide ($Ca(OH)_2$). The lithium hydroxide produced is then converted to lithium chloride by the addition of a chlorination agent such as hydrochloric acid (DeYoung 1991). The respective lithium hydroxide and lithium chloride conversions are represented by equations (19) and (20) below.

$$Li_2CO_{3\,(s)} + Ca(OH)_{2\,(aq)} \xrightarrow{\Delta G^o_{298\,K} = -0.41\ kcal} 2LiOH_{(aq)} + CaCO_{3\,(s)} \quad (19)$$

$$LiOH_{(aq)} + HCl_{(aq)} \xrightarrow{\Delta G^o_{298\,K} = -12.60\ kcal} LiCl_{(aq)} + H_2O_{(aq)} \quad (20)$$

The electrorefining of lithium chloride is conducted between a central cathode composed of stainless steel and two anodes consisting of pure graphite (DeYoung 1991). The electrorefining process produces liquid lithium which agglomerates above the stainless steel cathode. A bell-shaped structure positioned above the cathode collects the rising liquid product and prevents it from reacting with the chlorine off gas (Figure 12). The evolution of chlorine gas at the anode provides an oxidative reaction, allowing for the reduction to lithium metal at the cathode.

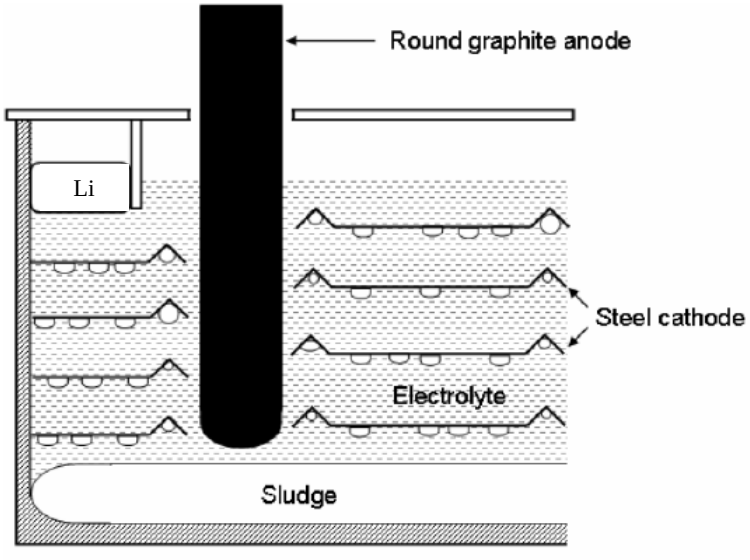

Figure 12: Electrowinning cell utilised for the production of metallic lithium, adopted from Yan and Fray (2010)

Overall Cell Reaction

$$LiCl_{(aq)} \rightarrow Li_{(l)} + \tfrac{1}{2} Cl_{2\,(g)} \text{ of which } E^{o}_{700\,K} = 3.63\ V \quad (21)$$

Cathodic Reaction

$$Li^{+}_{(aq)} + e^{-} \rightarrow Li_{(l)} \quad (22)$$

Anodic Reaction

$$Cl^{-}_{(aq)} \rightarrow \tfrac{1}{2} Cl_{2\,(g)} + e^{-} \quad (23)$$

Potassium chloride (KCl) is utilised in conjunction with lithium chloride to create a feed stock solution. Potassium chloride is utilised as a solvent and supporting electrolyte in the electrorefining process as it has a higher decomposition potential than lithium chloride (Figure 13) (Kipouros and Sadoway 1998). The eutectic point of LiCl-KCl is 623.15 K and 42 mole percent KCl (Hampel 1972). At 673.15 K, the liquid range extends to 35–45 mole percent (mol%) KCl. At this temperature lithium metal is molten and its vapour pressure is acceptably low, preventing the oxidation of the molten lithium (Figure 14). Other important information regarding the operational conditions of the process include the current density at 2 A/m^2 and the predicted energy consumption which is estimated at 35 kWh/kg of lithium refined (Tran and Luong 2015).

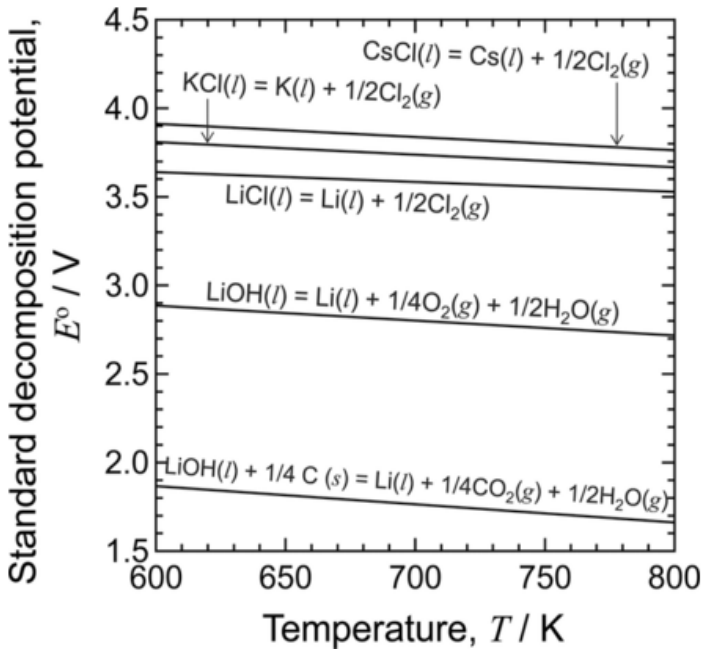

Figure 13: Standard decomposition potential vs temperature of lithium electro refining system, adopted from Takeda et al. (2014)

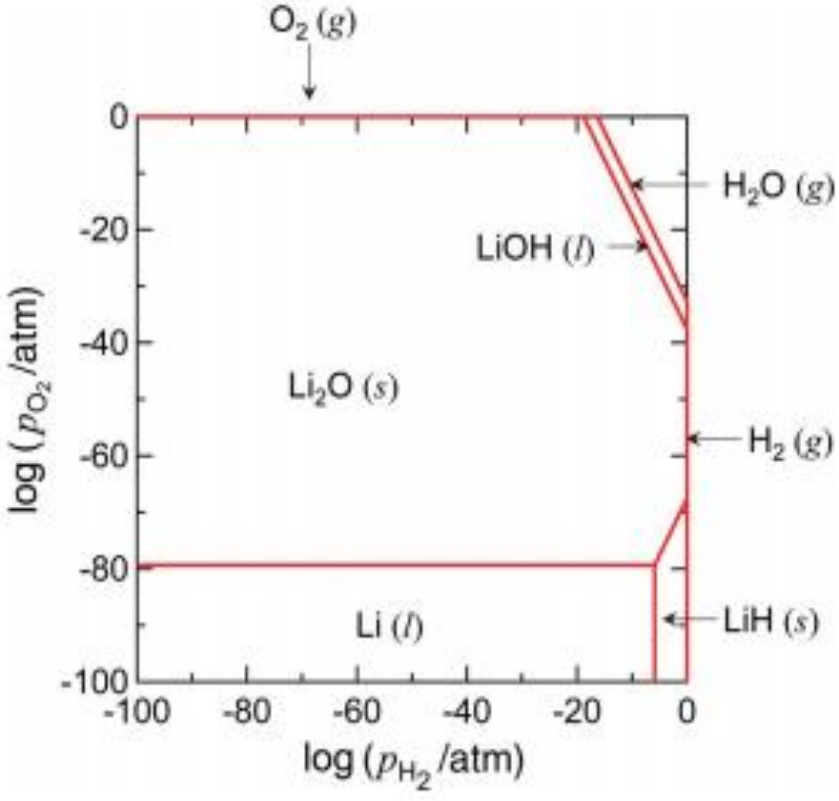

Figure 14: Partial pressures of O_2 vs H_2 and the corresponding lithium stability diagram, adopted from Takeda et al. (2014)

Takeda et al. (2014) conducted an investigation into the electrowinning of metallic lithium from lithium hydroxide in a molten chloride solution. From the thermodynamic studies

conducted, it was predicted that lithium metal cannot be electrowon from lithium hydroxide solution, due to the metallic lithium generated readily reacting with lithium hydroxide to form lithium oxide (24). In order to overcome the unfavourable formation of lithium oxide an electrorefining method utilising lithium chloride, potassium chloride (KCl) and caesium chloride (CsCl) has been proposed (Takeda et al. 2014).

$$Li^{+}_{(aq)} + LiOH_{(aq)} \xrightarrow{\Delta G^{o}_{623.15\,K} = -23.14\ kcal} Li_2O_{(s)} + \tfrac{1}{2} H_{2\,(g)} \qquad (24)$$

Electrolysis of LiOH in molten LiCl (43 mol%)–KCl and LiCl (17 mol%)–KCl–CsCl (26 mol%) solutions were investigated. Lithium hydroxide was fed into the anodic compartment and separated from the lithium metal deposited at the cathode by a porous magnesia diaphragm (Takeda et al. 2014). The addition of the diaphragm prevented the transportation of lithium hydroxide into a cathode compartment. Utilising this arrangement, lithium metal was successfully obtained with a current efficiency of 84–86%. The electrode potentials of the hydroxide evolution reaction (25) are lower than that of the chloride gas (26), therefore suggesting that the evolution of hydroxide species will be preferential to the evolution of chloride species (Averill and Olson 1978). This was evident in *Takeda et al. (2014)* investigations as they witness no chlorine gas emission when they conducted either of their hydroxide tests. This suggests that the evolution of hydroxide at the anode occurred and that the lithium collected at the cathode, was from the electrorefining of the lithium hydroxide.

$$OH^{-} \rightarrow \tfrac{1}{2} H_2O_{(g)} + \tfrac{1}{4} O_{2\,(g)} + e^{-} \text{ of which } E^{o}=2.78 \text{ V vs } Li^{+}/\text{ Li at } 623.15 \text{ K} \qquad (25)$$

$$Cl^{-} \rightarrow \tfrac{1}{2} Cl_{2\,(g)} + e^{-} \text{ of which } E^{o}=3.63 \text{ V vs } Li^{+}/\text{ Li at } 623.15 \text{ K} \qquad (26)$$

2.4.2 Thermochemical reduction of lithium compounds

The pyrometallurgical reduction of lithium hydroxide by the addition of magnesia, aluminium and calcium additives are represented by equations (27)-(33), below (Kipouros and Sadoway 1998). The pyrometallurgical processes operates under the principles of redox of which favourable conditions are created in order to promote the formation of metallic lithium. The pyrometallurgical recovery of lithium is a process that has become less commercially popular with recent technological developments (Meshram et al. 2014, Averill and Olson 1978). Its declining popularity is due to the conversion of lithium to gaseous state, which results in a lower recovery compared to alternative processes (Kipouros and Sadoway 1998). The conversion of lithium to gaseous state is an energy intensive process which

requires the utilisation of a condenser in order to capture the lithium gas (Kipouros and Sadoway 1998). With present technological capabilities, the recovery of lithium by pyrometallurgical processes is estimated to be between 80%-95% efficient (Tran and Luong 2015). Recent studies have identified three methods of thermochemical reduction that have displayed the most promise for the extraction of lithium. The carbothermic, oxide and hydroxide reduction processes have been discussed and surmised below (Kipouros and Sadoway 1998).

Carbothermic reduction utilises carbon as a reducing agent in order to produce gaseous lithium (Halmann et al. 2012). The process is conducted in a furnace at a temperature range between 1000-2100 K. The lithium gas produced is captured by a condensing system that is operated in conjunction with the furnace. The carbothermic process has been identified to work on both lithium oxide and lithium hydroxide feeds, represented by equations 27-29 below.

$$Li_2O_{(s)} + C_{(s)} \xrightarrow{\Delta G^o_{2000\,K} = -2.57\ kcal} 2Li_{(g)} + CO_{(g)} \quad (27)$$

$$6LiOH_{(aq)} + 2C_{(s)} \xrightarrow{\Delta G^o_{1600\,K} = -0.65\ kcal} 2Li_{(g)} + 2Li_2CO_{3\,(s)} + 3H_{2\,(g)} \quad (28)$$

$$3LiOH_{(aq)} + FeC_{2\,(s)} \xrightarrow{\Delta G^o_{2173\,K} = -19.55\ kcal} 3Li_{(g)} + Fe_{(s)} + 3/2H_{2\,(g)} + CO_{(g)} + CO_{2\,(g)} \quad (29)$$

Oxide reduction also known as the pigeon process, reduces lithium to the gaseous phase by introducing calcium, silicon and aluminium additives as reducing agents (Pidgeon and Touguri 1962). The formation of calcium silicate under reducing conditions (1500 K-1773 K) is preferential over the formation of solid lithium products, as displayed in equations 30 and 31 below. Therefore, lithium tends to be converted to gaseous state which reports to the downstream condensing system.

$$2Li_2O_{(s)} + 2CaO_{(s)} + Si_{(s)} \xrightarrow{\Delta G^o_{1773K} = -2.81\ kcal} 4Li_{(g)} + Ca_2SiO_{4\,(s)} \quad (30)$$

$$3Li_2O_{(s)} + 2Al_{(s)} \xrightarrow{\Delta G^o_{1673\,K} = -9.19\ kcal} 6Li_{(g)} + Al_2O_{3\,(s)} \quad (31)$$

Hydroxide reduction utilises manganese and aluminium additives to reduce lithium to its gaseous state (Kulifeev et al. 2007). This is conducted at temperatures ranging 353K – 1103

K. The process is conducted in a furnace of which the off gas is collected in a condenser and metallic lithium recovered, as displayed by equations (32) and (33) below.

$$3LiOH_{(aq)} + 2Mg_{(s)} \xrightarrow{\Delta G^{o}_{353\ K} = -0.633\ kcal} 2Li_{(g)} + 2MgO_{(s)} + H_{2(g)} \quad (32)$$

$$2LiOH_{(aq)} + Al_{(s)} \xrightarrow{\Delta G^{o}_{1103\ K} = -0.455\ kcal} Li_{(g)} + LiAlO_{2(s)} \quad (33)$$

Di et al. (2013) investigated the roasting of lithium carbonate under the influence of a vacuumed atmosphere. Calcium oxide and aluminium oxide were added to the roasting process as reducing agents. The feed mixture was initially roasted at 1073.15 K for 2 hours. The roasted product consisted of a lithium aluminate calcine which was then pressure briquetted and mixed with aluminate powder (34). This product was further roasted at 1423.15 K for approximately 3 hours, promoting the liberation of gaseous lithium (35). The vacuum alumina-thermic reduction process liberated 95% of the lithium present which is collected by a downstream condenser (Di et al. 2013).

$$Li_2CO_{3(s)} + Al_2O_{3(s)} \xrightarrow{\Delta G^{o}_{1073\ K} = -13.73\ kcal} 2LiAlO_{2(s)} + CO_{2(g)} \quad (34)$$

$$3LiAlO_{2(s)} + 2CaO_{(s)} + Al_{(s)} \rightarrow 2[CaO.Al_2O_3]_{(s)} + 3Li_{(g)} \quad (35)$$

Furthermore, *Di et al. (2013)* proposed a scheme utilising a coarse ferrosilicon-aluminium alloy containing 28.83% aluminium and 41.10% silicon as a reductant to extract lithium from lithium oxide (Tran and Luong 2015). It was reported that 95.26% of the total lithium present was extracted, under the optimised conditions of 1273.15 K over the course of 3 hours (Di et al. 2013).

2.4.3 The direct electrolysis of lithium carbonate to produce lithium metal

DeYoung (1991) developed a method for the direct electrolytic production of metallic lithium from lithium carbonate. The method utilises two electrolytic cells which are separated by a porous non-conductive membrane. One cell contains the anode with the other cell containing the corresponding cathode (Figure 15) with lithium carbonate is introduced as an anolyte to the anode compartment. When a charge is introduced to the system the lithium ions begin migrating from the anodic compartment to the cathodic compartment. The cathodic compartment is separated from the anode by a magnesia diaphragm. The diaphragm assists in preventing backflow of lithium ions, promoting the reduction of metallic lithium to occur at the cathode. The functionality and convenience associated with

this refining method are the main constraints of the process, as only small quantities of lithium can be efficiently refined.

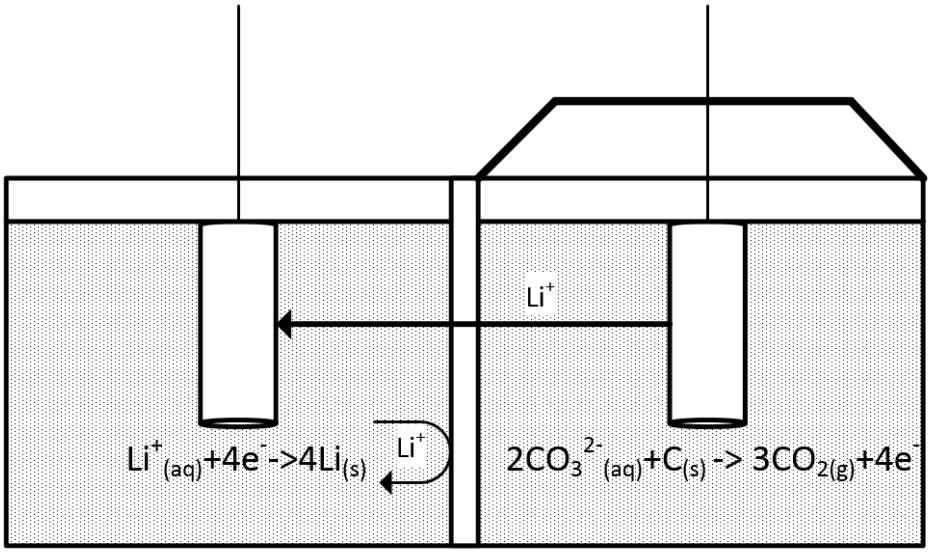

$$Li_2CO_{3(aq)} + C_{(s)} \rightarrow 3CO_{2(g)} + 4Li_{(s)}$$

Figure 15: Electrolytic cell setup for the direct production of lithium metal from lithium carbonate, adopted and altered from DeYoung (1991)

DeYoung achieved a current efficiency of 89.09%, with the respective yield near 99.3% for the test work conducted. Mitigating the formation of lithium oxide and carbon are essential if the process is to be run efficiently. Both lithium oxide and carbon are present as by-products in the electrolytic production of lithium metal (36). They exist as insoluble sludge that forms in the cathodic cell, causing the efficiency of the process to decrease. *DeYoung*'s utilisation of the magnesium diaphragm assisted in preventing the formation of sludge by restricting the undesirable backflow of the lithium ions from the cathodic compartment.

$$Li^+_{(aq)} + Li_2CO_{3\,(s)} \rightarrow 3Li_2O_{\,(s)} + C_{(s)} \qquad (36)$$

The lithium carbonate present within the anolyte composed of 0.5 - 10 weight % of the anolyte solution. Upon receiving a charge, the ions in solution begin migrating from the anode towards the cathode. The anode consists of pure graphite which assists in promoting the evolution of carbon dioxide at the anodic interface (38). The cathode utilised was made from stainless steel, allowing for the deposition of metallic lithium to occur. This is represented by equation (39) below.

Overall Cell reaction

$$2Li_2CO_{3\,(s)} + C \rightarrow 4Li^+_{\,(s)} + 3CO_{2\,(g)} \text{ of which } E^o = 1.85\ V \qquad (37)$$

Anodic reaction

$$2CO_3^{2-}{}_{(aq)} + C_{(s)} \rightarrow 3CO_{2\,(g)} + 4e^- \quad (38)$$

Cathodic Reaction

$$4Li^+{}_{(aq)} + 4e^- \rightarrow 4Li_{(s)} \quad (39)$$

The decomposition voltage for pure lithium carbonate is estimated to be 1.85 volts which when diluted to a 1% standard solution becomes 2.2 volts. Lithium chloride deposition comparatively is 3.46 volts at 923.15 K which is significantly higher than that of the carbonate production method. As lithium carbonate is depleted in the cell, the cell voltage will tend to rise. As a result, by monitoring the cell voltage one may obtain an indication of whether the lithium carbonate concentration in the anolyte is within the desired range. *DeYoung (1991)* electrolysis tests were optimised at 923 K and 140.26 Ampere's for approximately 6.05 hours. 32.36 grams of pure (>99.95%) lithium metal was recovered from solution of which contained minor traces of impurities.

2.4.4 Lithium ion batteries

The cathode and electrolyte utilised in lithium ion batteries are considered fundamental components. These components utilise three different lithium products, as a means to allow redox flow within the battery to occur. The most common lithium products utilised in the manufacturing of cathodic material are lithium cobalt oxide ($LiCoO_2$) and lithium nickel manganese cobalt oxide ($Li_{0.33}Ni_{0.33}Mn_{0.33}CoO_2$ or NMC) (Gains et al. 2011). The refining process undertaken to produce these cathodic materials from lithium sources is discussed below.

Cho et al. (2000) surmised the synthesising process that is undertaken to produce cathodic battery grade material. The process identified by *Cho et al* outlined how lithium cobalt oxide contains an energy dense medium which is capable of high functioning energy storage. The synthesis of lithium cobalt oxide was originally developed by *Gummow et al. (1992)*, however as the market for LIB's has expanded in recent years so too has the research into refining lithium cobalt oxide. *Cho et al* outlines a refining method that is commercially utilised in the direct production of lithium cobalt oxide from lithium hydroxide. *Cho et al* explains that lithium cobalt oxide is produced by conducting a roast at 1173.15 K for 24 hours. The feed to the roast consists of a 1:1.05 ratio between lithium hydroxide and cobalt

oxide (Co_3O_4) (Cho et al. 2000). Lithium carbonate can be substituted into the roast in place of lithium hydroxide, however it has been found to produce a lower grade product (Gains et al. 2011). The roast product is then pulverised and screened to -63µm which is then compressed into pellets at 4500 lb/inch. The reacted pellets are then re crushed, ground and heated a second time under the presence of flowing oxygen at 1023.15 K for 16 hours. The product is then pulverised and screened over -32 µm, of which it is then combined with various binding agents to create the paste that covers the reactive face cathode (refer to Appendix A3 – Lithium Ion Batteries).

The primary process for producing NMC cathodic material was surmised by *Julien et al. (2000)*. The ideal NMC cathodic material identified by *Julien et al* was formed via a precipitation technique utilising metal acetates and lithium hydroxide as raw feed material. This precipitate is then neutralized to a pH range of 5-6 with sodium hydroxide (NaOH) and the solid/aqueous phases separated by filtration. The final refining step involves collecting the solid residue from the filtration process and roasting it at 1173.15 K for approximately 3 hours. The roast product is then collected and pulverised to -32µm, which it is then combined with various binding agents (refer to Appendix A3-Lithium Ion Batteries).

The other main component of lithium ion batteries that it utilises lithium products is the electrolyte of which consists of a super saturated lithium hexafluorophosphate ($LiPF_6$) solution (Mayer 1999). Mao (1996) developed a simplified method for the synthesis of $LiPF_6$. Mao's process utilises lithium hydride (LiH) and ammonium hexafluorophosphate (NH_4PF_6) as reactants, of which are combined with solvents that consists of chain esters and cyclic ester functional groups (refer to Appendix A3- Lithium Ion Batteries). In order to produce lithium hydride, aqueous lithium hydroxide must first be combined with magnesium power and heated to 823.15 K. This promotes the reaction represented by equation (40) to occur (Alexander 1947).

$$LiOH_{(aq)} + Mg_{(s)} \xrightarrow{\Delta G^{o}_{823\ K} = -43.04\ kcal} MgO_{(s)} + LiH_{(aq)} \qquad (40)$$

The lithium hydride produced is then filtered, where the aqueous solution is collected and combined with the ammonium hexafluorophosphate (Mao 1996). The mixture containing the reactants is then combined with diethyl carbonate (DEC) and ethylene carbonate (EC) solvents. The resulting solution is heated to 323.15 K which promotes the reaction represented by equation (41). The electrolyte produced can be sparged with inert gasses such as helium (He) as a means to drive off residual ammonia (Mao 1996). The resulting

electrolyte is suitable for use in lithium ion batteries without the need for additional processing.

$$NH_4PF_{6\,(aq)} + LiH_{\,(aq)} \xrightarrow{solvents} LiPF_{6\,(aq)} + NH_{3\,(g)} + H_{2\,(g)} \quad (41)$$

2.5 Technological advances in lithium extraction from spodumene

Research into the more efficient extraction processes from hard rock lithium minerals has been of much industrial interest since the commercial rise of LIB batteries (Kuang et al. 2018). A study conducted by *Vikström et al. (2013)* identified the rapid expansion of the lithium market, with *Jaskula (2017)* confirming a 40% to 60% rise in the spot prices of lithium carbonate worldwide, in 2015 alone . In order to capitalise on this growing industry, research has been conducted into improving the efficiency of extracting lithium from spodumene. The two most promising developments to date are the applications of high pressure leaching and *Lithium Australia's* SiLeach® (Lithium Australia 2016), which are discussed in detail below.

2.5.1 High pressure leaching

The application of high pressure leaching conditions has been found to promote the formation of valuable lithium products (Munoz 1969). This is achieved by the increased rate of reaction induced by the high pressure environment (Free 2013). The improved physio-chemical interactions and preferential thermodynamic conditions of the high pressure environment, allows for the selective formation of desirable products to be achieved. The mineralogical decomposition of the leach reactants occurs with respect to each minerals redox potential (Fuerstenau and Han 2003). Often the cathodic portion of redox reactions occur with respect to the oxygen present under the following conditions:

$$4H^+ + 4e^- + O_2 \leftrightarrow 2H_2O \text{ (Acidic pH)} \quad (42)$$

$$2H_2O + 4e^- + O_2 \leftrightarrow 4OH \text{ (Alkaline pH)} \quad (43)$$

Thus mineral decomposition is often increased with increasing oxygen pressure. This increased oxygen pressure further stimulates the reaction by increasing the rate of reaction, by raising the activation energy (Free 2013). Investigations conducted by *Nicholson (1946)*, *Chen et al. (2011)* and *Kuang et al. (2018)* were found to successfully produce a lithium product from a high pressure leach. These methods were derived around reducing the high energy expenditure of current processing techniques, mitigating the use of toxic reagents and simplifying sophisticated recovery schemes. An in-depth analysis of each process is discussed in detail below.

2.5.1.1 Lithium hydroxide production utilising an alkaline pressurised digestion process

Nicholson (1946) investigated the pressurised leaching of β-spodumene under alkaline conditions. An extraction of 84% lithia from β-spodumene was registered, with an overall recovery of 1-4% lithium hydroxide reported. The process *Nicholson* derived was patented in 1946, and is current utilised as a foundation for current lithium based research (Choubey et al. 2016, Meshram et al. 2014).

Nicholson's process highlights how a β-spodumene concentrate that is treated in a water leach, with the addition of lime at 478.15 K and 17.27 Barr is able to produce a lithium hydroxide product (44) (Nicholson 1946).

$$4\beta\text{-}LiAlSi_2O_{6\,(s)} + 2CaO_{\,(s)} + 9H_2O_{\,(aq)} \xrightarrow{\Delta G^o_{478\,K} = -47.50\ kcal} 4LiOH_{(aq)} + 2CaO.2Al_2O_3.8SiO_{2\,(s)} + 7H_2O_{\,(aq)} \quad (44)$$

The leach product is then subject to filtration where the filtrate is collected, containing 1-4% lithium hydroxide (Nicholson 1946). The filtrate is then evaporated to concentrate the solution which is then sparged with carbon dioxide to precipitate lithium carbonate. The product produced consists of 97.8 5 lithium carbonate (Choubey et al. 2016).

2.5.1.2 Lithium Carbonate Production Utilising Sodium Carbonate Autoclave Process

Chen et al. (2011) investigated the production of lithium carbonate utilising a sodium carbonate additive. The reported process resulted in a 94% lithium carbonate conversion efficiency, obtained under optimal operational conditions. The drawbacks of the process involve the complexity and strict operational parameters preventing the process becoming robust enough for commercial application (Kuang et al. 2018). This includes a complex and expensive reagent scheme which needs to be addressed or simplified before commercial application becomes viable (Guo et al. 2017).

α-spodumene in its natural inert state is converted to its reactive β phase in a muffle furnace at 1323.15 K for 30 minutes (Chen et al. 2011). This is represent by equation 45 below.

$$\alpha\text{-}Li_2AlSi_2O_{6\,(s)} \xrightarrow{\Delta G^o_{1323K} = -0.45\ kcal} \beta\text{-}LiAlSi_2O_{6\,(s)} \quad (45)$$

The calcined β-spodumene is placed into the autoclave at a liquid/solid (L/S) ratio of 4 and sodium/lithium ratio of 1.25 and heated at 278.15 K/min up to the operating temperature of 498.15 K. During the pressure leaching lithium carbonate (Li_2CO_3) and analcime ($NaAlSi_2O_6$) slurry is formed (46) (Meshram et al. 2014, Chen et al. 2011).

$$2\beta\text{-}LiAlSi_2O_{6\,(s)} + Na_2CO_{3\,(s)} + 2H_2O_{(aq)} \xrightarrow{\Delta G^o_{498\,K} = -6.17\ kcal} Li_2CO_{3\,(s)} + 2NaAlSi_2O_6.H_2O_{(aq)} \quad (46)$$

The slurry produced has its L/S ratio adjusted to 8 as it is leached in water and sparged with carbon dioxide (CO_2) at 0.5 L/min for 120 minutes. The resulting bicarbonate solution is filtered and washed with dilute sulfuric acid and deionized water (DI). The lithium bicarbonate filtrate is heated to 363.15 K for 120 minutes to drive off excess CO_2. The resulting slurry is re-filtered and lithium carbonate is recovered (Chen et al. 2011).

$$Li_2CO_{3\,(s)} + CO_{2\,(g)} + H_2O_{(aq)} \xrightarrow{\Delta G^o_{298\,K} = -8.48\ kcal} 2LiHCO_{3\,(aq)} \quad (47)$$

$$2LiHCO_{3\,(aq)} \xrightarrow{\Delta G^o_{363\,K} = -1.25\ kcal} Li_2CO_{3\,(s)} + CO_{2\,(g)} + H_2O_{(aq)} \quad (48)$$

2.5.1.3 Lithium Sulfate Production Utilising Sodium Sulfate Additive in Autoclave Process

Kuang et al. (2018) investigated the production of lithium carbonate (Li_2CO_3), utilising a sodium sulfate (Na_2SO_4) solution under high pressure leaching (HPL) conditions. The addition of calcium oxide (CaO) and sodium hydroxide (NaOH) as leaching additives, and their corresponding effect on the formation of lithium sulfate (Li_2SO_4) is also analysed. Under the optimal conditions tested, *Kuang et al* determined that the highest lithium extraction efficiency for CaO and NaOH was 93.30% and 90.70% respectively. The drawbacks on the process involve the complex operating conditions and the high capital expenditure required for the construction of downstream processing circuit, to produce a lithium carbonate product.

The initial conversion of α-spodumene to its reactive β phase is conducted via calcination at 1373.15 K for approximately 1 hour (Kuang et al. 2018).

$$\alpha\text{-}Li_2AlSi_2O_{6\,(s)} \xrightarrow{\Delta G^o_{1373\,K} = -0.45\ kcal} \beta\text{-}LiAlSi_2O_{6\,(s)} \quad (49)$$

Under the optimal conditions tested by *Kuang* the calcined β spodumene is leached in an autoclave at: Na_2SO_4: Additive: ore mass ratio of 9:0.4:20, leaching temperature of 503.15 K, leaching time of 3 hours, liquid/ solid ratio of 7.5 mL/g and a particle size of 39.23 µm. It was found that analcime residue ($NaAlSi_2O_6$) formed as a by product of the lithium sulfate (Li_2SO_4) production (50).

$$2\beta\text{-}LiAlSi_2O_{6\,(s)} + Na_2SO_{4\,(s)} + 2H_2O_{(aq)} \xrightarrow{\Delta G^o_{503\,K} = -1.61\ kcal} 2NaAlSi_2O_6.H_2O_{(s)} + Li_2SO_{4\,(aq)} \quad (50)$$

The autoclave leach product is filtered and purified by the addition of limestone ($CaCO_3$). The pH adjustment allows for the removal of impurities present in the solution. The addition of sodium carbonate (Na_2CO_3) to the lithium sulfate eluate allows for the precipitation of lithium carbonate (Li_2CO_3) to occur. The by product of this reaction is the formation of sodium sulfate which can be recycled back as mother liquor to be used in the autoclave leach, creating a closed loop system.

$$Li_2SO_{4\,(aq)} + Na_2CO_{3\,(aq)} \xrightarrow{\Delta G^o_{298\,K} = -8.11\ kcal} Li_2CO_{3\,(s)} + Na_2SO_{4\,(aq)} \quad (51)$$

2.5.2 Lithium Australia's SiLeach®

Lithium Australia (2016) has developed a process which it has claimed to recover all significant metals from a wide range of lithium sources. The process is claimed to operate with low energy consumption and has the ability to produce an extensive range of valuable by-products.

The process outlined by *Lithium Australia* ^{NL} highlights how unlike conventional processing, SiLeach® does not require a roasting phase. It utilises a combination of sulfuric acid and halides to dissociate the silicate lattice under atmospheric conditions. The reactions of SiLeach® occur rapidly at 90˚C, which is provided by utilising the waste heat generated during the production of sulfuric acid. The SiLeach® process produces very clean lithium solutions, in the form of lithium carbonate, lithium hydroxide and sulfate salts. Further information is not readily available to the public about SiLeach®, as *Lithium Australia*^{NL} is seeking to patent its process at the present time. *Birney (2017)* identified a key shift in the lithium market after the announcement of SiLeach® as a 50% rise in *Lithium Australia's* ^{NL} share price occurred shortly after the announcement was made. In the corporate position statement released in August of 2017, Adrian Griffin the managing director for Lithium Australia ^{NL} released a statement addressing that the current status of the SiLeach® process. In his statement Griffin estimated that the second piloting campaign for the SiLeach® process will run towards the closure of 2018, with more optimisation investigations to be conducted heading into early 2019 (Griffin 2017).

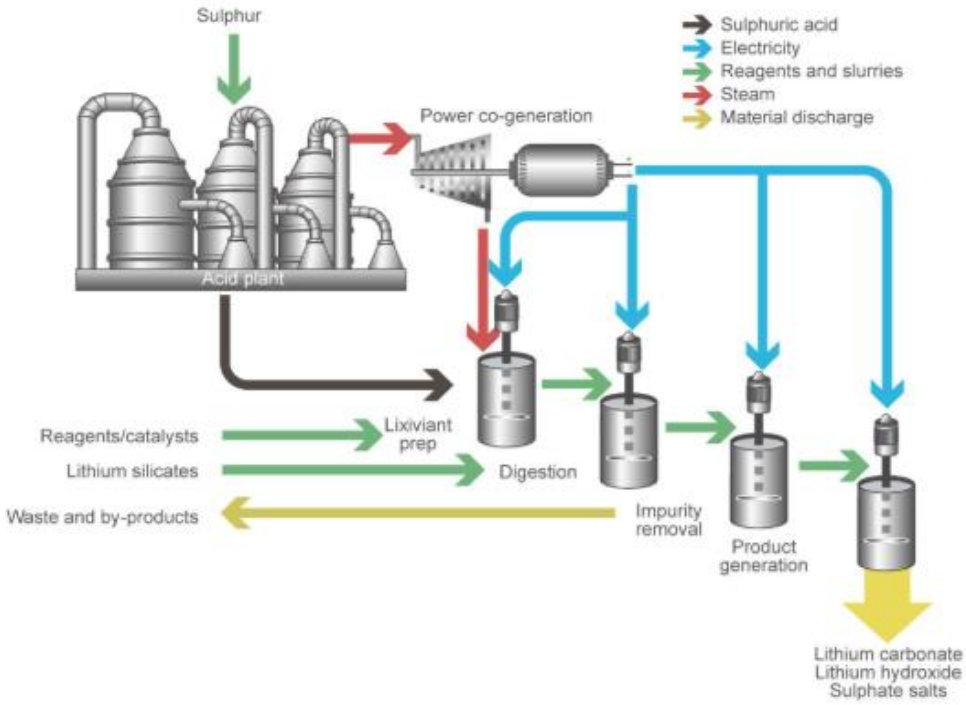

Figure 16: A summation schematic of Lithium Australia's SiLeach® which is adopted from Lithium Australia (2016)

2.6 Summary and concluding remarks

The literature review conducted assisted in identifying key areas of interest with regards to improving the efficiency of extracting lithium compounds from spodumene. The current commercial practises of sulfation, carbonation and chlorination all contain intrinsic drawbacks such as toxic operational environments, high reagent expenditures and complex processing steps (Kuang et al. 2018). All processes utilise the energy intensive calcination step of converting α-spodumene to its reactive β phase, of which if mitigated could provide a means to produce more economical quantities of lithium products (Meshram et al. 2014). Companies such as *Lithium Australia*^{NL} (Griffin 2017) have recognised this and have already began developing processing techniques that mitigate the utilisation of energy intense processes.

The investigation of increasing the leaching efficiency of spodumene with hydrofluoric acid provided promising results. The dissolution of α and β spodumene due to the influence of hydrofluoric acid proved to be an efficient way of extracting lithium from the interlocking silicate structures. However as often found when utilising hydrofluoric acid, the toxic nature of the process limits its ability to become commercially applicable.

Lithium hydroxide appears to be the domain lithium product utilised in the production of lithium ion batteries (Mao 1996, Walker 2015). Therefore, refinement and simplification of extraction processes towards developing lithium hydroxide appear to be most appealing to the lithium market moving forward. Lithium carbonate is still the most robust of the lithium compounds in current commercial production. However, in foresight the mitigation of carbon dioxide produced by processing lithium carbonate has to be addressed sufficiently, if it is to remain a sustainable option moving in the renewables future.

Recent technological advances regarding the *Lithium Australia*^{NL} SiLeach® display a lot of promise based off the marketing statements made (Griffin 2017). The actual efficiency of the process isn't fully accessible until the patent is approved and released to the public domain. The application of high pressure systems appears to be area worthy of further research, with the journal articles assessed in this literature review producing promising results. The application of a high pressure system promotes unique leaching kinetics, which has the potential to address the limitations of current processes for extracting all of the valuable metals that exist in spodumene ores.

3. Experimental summary

The experimental approach that was adopted throughout this project towards achieving the research objectives outlined in section 1.1, are summarised in this chapter. Due to the investigative nature of this project, the test work conducted was completed in designated phases. Four phases of test work were conducted over the course of this project, with each phase progressing towards maximising the dissolution of lithium from the spodumene concentrate. The project test work flowsheet is attached in Figure 17 below.

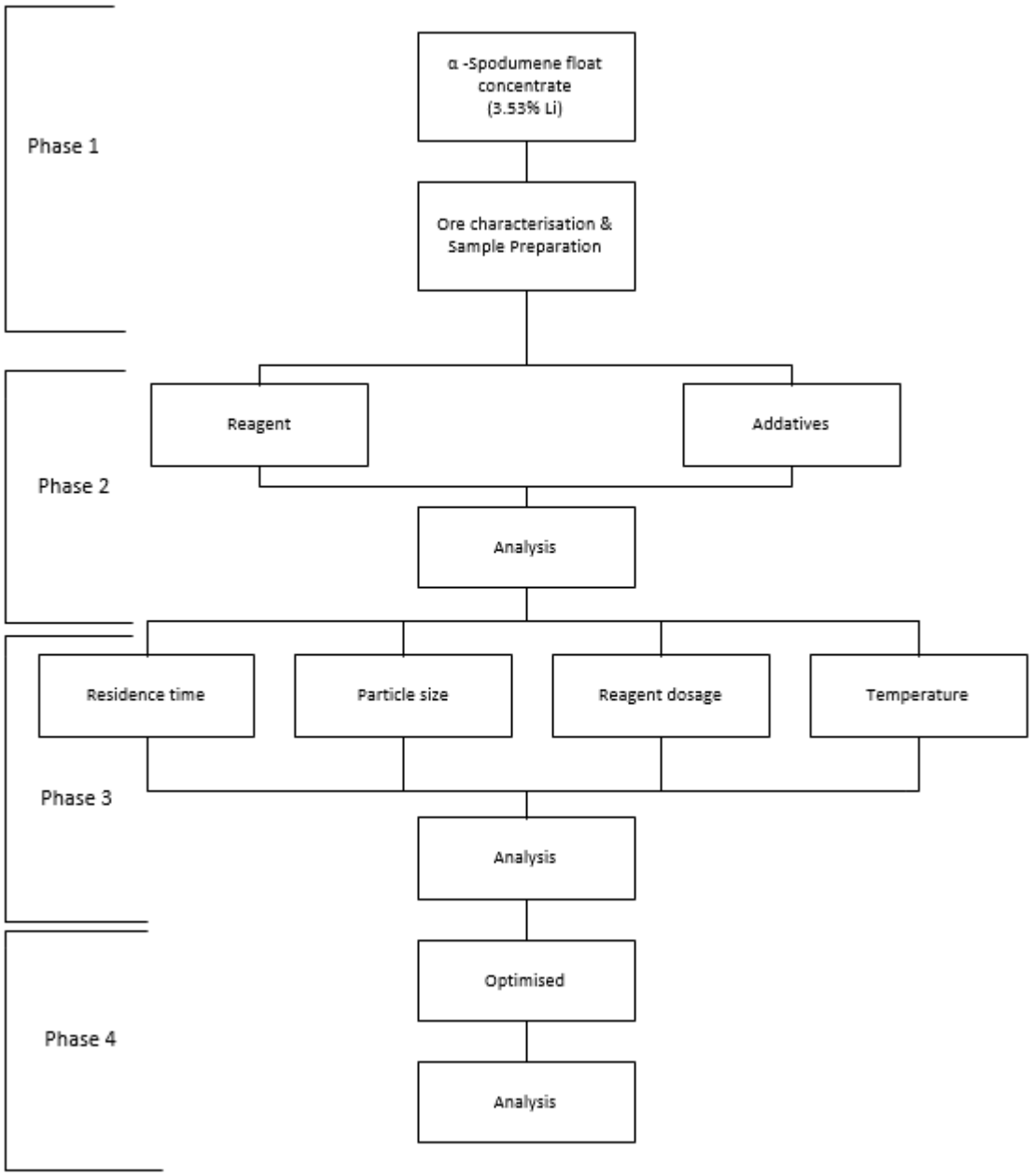

Figure 17: Project's test work flowsheet .

Phase 1 of the test work conducted consisted of ore characterisation and sample preparation, in order to establish a baseline understanding of the spodumene ore utilised throughout the project. Phase 2 was the initial investigative test work conducted around the leaching of the spodumene ore. An investigation into leaching agents and additive additions resulted in a baseline being established for further research. The leaching agent that yielded the highest lithium extraction was then selected to progress to phase 3 of the test work where variations in residence time, particle size, regent dosage and temperature were investigated. From the investigations conducted, optimal leaching conditions are determined and utilised in the final optimised test. Each phase of test work is analysed utilising a variety of analytical quantitative and qualitative techniques such as inductively coupled plasma mass spectrometry (ICP), elemental assay and X-ray diffraction analysis (XRD). The respective results collected at the conclusion of each phase of test work provided the foundations for the next phase of investigations. This resulted in a progressive investigation into the caustic leaching of spodumene, hence displaying the follow on approach implemented throughout this project.

3.1 Experimental material

The desire to investigate the caustic leaching of α-spodumene has resulted in a beneficiated spodumene concentrate being obtained from the Greenbushes Lithium Operation own by Talison Lithium Pty Ltd. Characterisation of the beneficiated spodumene concentrate and investigations into caustic leaching agents are discussed in detail throughout this section. These initial investigations were conducted with the aim of establishing a foundation on the inputs towards the leaching process, so that the leaching investigations conducted were accountable.

3.1.1 Ore characterisation

The characterisation of the spodumene concentrate utilised throughout this project was completed utilising elemental assays, XRD and particle size analysis techniques. The elemental assay results are tabulated in Table 2, below.

Table 2: Elemental assay results for the spodumene flotation concentrate utilised throughout this project

Element	%
Silver (Ag)	<0.001
Aluminium (Al)	14.000
Barium (Ba)	<0.001
Beryllium (Be)	0.001
Bismuth (Bi)	0.001
Calcium (Ca)	0.020
Cadmium (Cd)	<0.001
Cobalt (Co)	<0.001
Chromium (Cr)	0.080
Copper (Cu)	0.004
Iron (Fe)	1.020
Potassium (K)	0.200
Lithium (Li)	3.530
Magnesium (Mg)	<0.040
Manganese (Mn)	0.040
Molybdenum (Mo)	<0.001
Sodium (Na)	0.120
Nickel (Ni)	0.001
Phosphorous (P)	0.020
Lead (Pb)	<0.003
Silicon dioxide (SiO_2)	63.600
Strontium (Sr)	<0.001
Titanium (Ti)	0.020
Vanadium (V)	0.004
Yttrium (Y)	0.010
Zinc (Zn)	<0.010

The assay results indicate that the flotation concentrate is 3.53% lithium or 7.60% lithium oxide (Li_2O). The major constituents of the concentrate are Li, Al (14.00%) and SiO_2 (63.60%) contents that account for 81.13% of the elements analysed. The 7.60% Li_2O found within the concentrate utilised for this project is considered relatively high grade as the Li_2O content in pure spodumene is estimated to be 8.03%. The 1.02% iron (Fe) found within the concentrate accounts for 65.56% of the total impurities present, further suggesting a high grade concentrate was utilised for this project.

Figure 18 displays the XRD analysis conducted on the float concentrate utilised throughout this project. The concentrate displayed similar peaks to those expected from a spodumene concentrate as suggested by The International Centre for Diffraction Data (International Centre for Diffraction Data 2009).

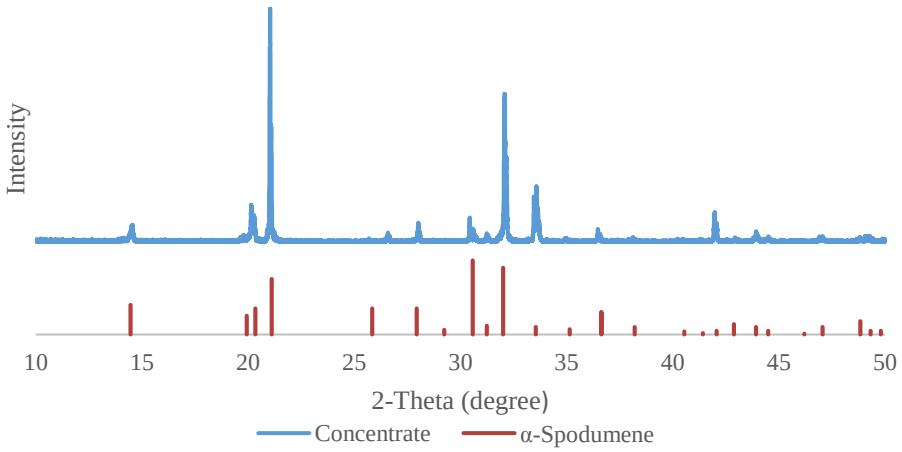

Figure 18: XRD analysis on the spodumene concentrate utilised throughout this project

A particle size analysis on the spodumene concentrate was conducted utilising a Microtrac S3500 laser sizer. Figure 19 displays the results of the laser sizing, of which indicate that the P_{80} of the concentrate is 325µm.

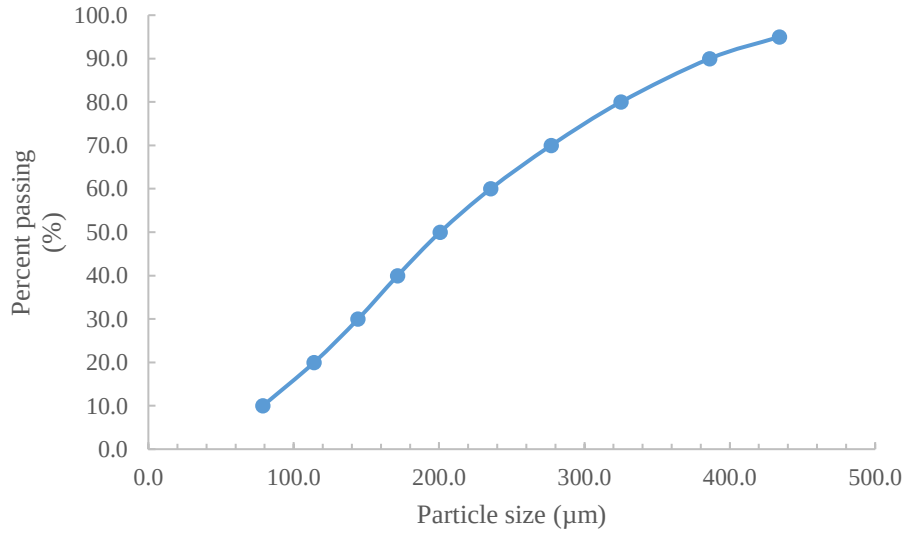

Figure 19: Particle size analysis conducted on the spodumene concentrate with the Microtrac flex S3500 laser sizer

3.1.2 Reagents

The investigation into the caustic leaching of α-spodumene has led to the selection of specified reagents throughout this section. Sodium hydroxide was initially investigated due to its inexpensive nature and regular occurrence throughout relative literature. Through further investigation it was found that quartz (SiO_2) readily dissolves in the presence of H_2O as displayed by Figure 20 below (Queneau and Berthold 1986, Crundwell 2017, Choi et al. 2013). The nucleophilic attack that occurs between the water molecule and the quartz matrix

results in the dissolution of the quartz and gives rise to the production of silicic acid, as displayed in equation (52) (Choi et al. 2013, Crundwell 2017).

$$SiO_{2\,(s)} + 2H_2O_{\,(l)} \rightarrow H_4SiO_4 \qquad (52)$$

Investigations conducted by *Crundwell (2017)* and *Queneau and Berthold (1986)* suggest that the removal rate of the SiO cation from the quartz matrix is enhanced within increasing concentrations of hydroxide ions. This suggest that quartz dissolution is enhanced within alkaline media. Crundwell suggests that this is due to the rapid intermediate reactions that are represented by equations (53) and (54) below.

$$SiO_{\,(s)} + OH^-_{\,(aq)} \rightarrow SiO(OH)^+_{\,(aq)} \qquad (53)$$

$$SiO(OH)^+_{\,(aq)} + OH^-_{\,(aq)} + H_2O_{\,(l)} \rightarrow H_4SiO_{4\,(aq)} \qquad (54)$$

Further research conducted by *Crundwell (2017)* suggested that both lithium and sodium ions behave as catalyst towards promoting the dissolution of quartz. *Crundwell (2017)* proposed that the positive changes in the surface potential difference at the Si-O-Si interface retarded the removal of the hydroxide anions thus accelerating the dissolution of the silicate matrix.

Earlier investigations conducted by *Dove (1999)* drew similar conclusions that were proposed by *Crundwell.* Furthermore, *Dove* suggested that the presence of aluminium and iron cations within the quartz matrix inhibited the dissolution of the quartz. The inhibiting mechanism that these cations introduce towards the dissolution of silica remain undefined and are worthy of greater research, however their retarding influence on the dissolution of quartz is reported across numerous studies (Choi et al. 2013, Lier et al. 1960).

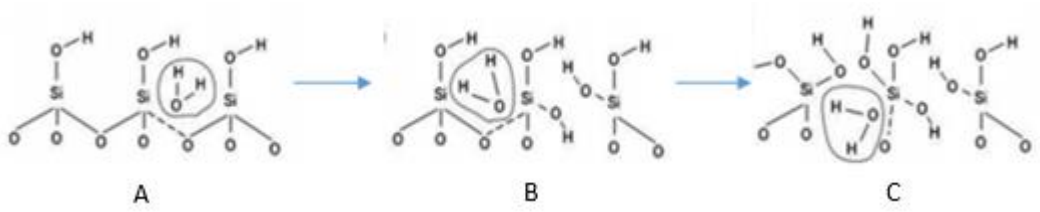

Figure 20: Depiction of the nucleophilic dissolution mechanism for quartz in water, adapted from Choi et al. (2013).

Due to the relative applicability of this phenomenon towards spodumene, an in-depth investigation was deemed appropriate. The results of this investigation are present throughout section 4 and discussed in relative detail throughout section 5.

3.1.2.1 Sodium hydroxide

Sodium hydroxide (NaOH), also known as caustic soda is an inorganic hydroscopic compound that consists of a sodium cation (Na^+) and hydroxide anion (OH^-). Due to the highly soluble nature of the compound, it is often utilised as a strong caustic base within the pharmaceutical, manufacturing and mining industries (Zumdahl 2013). Sodium hydroxide reacts exothermically when it comes into contact with water. The exothermic reaction that occurs is due to the dissociation of the sodium and hydroxide ions, resulting in an alkaline solution.

ThermoFisher Scientific's Ajax Finechem sodium hydroxide mini pearls were utilised as leaching agents throughout this project. Manufactured for analytical purposes the individual assays for each of the 500g containers utilised throughout this project guaranteed a minimum purity of 97% NaOH (ThermoFisher 2015). The significant impurities included sodium carbonate (1.5%), potassium (0.1%) and phosphate (0.05%) species all of which were maintained below their specified maximum quantities.

3.2 Equipment

The leaching component of this project was conducted utilising an autoclave so that pressurised leaching conditions could be investigated. Solid-liquid separation of the leach product is conducted utilising a Buchner funnel that operates under the influence of vacuum. Relevant solid and liquid samples are collected for analysis and storage. Supporting equipment utilised throughout this project including relevant meters, probes and ancillary equipment are discussed in greater detail in Appendix B1-equipment.

3.2.1 Autoclave

A Parr® series 4523 stirred reactor was utilised as the leaching vessel for the entirety of this project. The autoclave setup consisted of two main components that consisted of a one litre autoclave with an Alloy 400 lining and a fixed reactor head that held the cooling coil, magnetic stirrer and sealing gasket. The Alloy 400 clave-lining consists of two-thirds nickel and one-third copper that is high resistant to caustic environments (Parr Instrument Company 2009). The Polytetrafluoroethylene (PTFE) gasket that seals the clave to the fixed reactor head allowed for leaching operations to be conducted at a maximum operating threshold of 623.15 K and 20,000 kPa, hence providing a means to investigate volatile leaching systems.

A Parr® 4848 modular PID controller was utilised to control the operating temperature, pressure and stirring rate of the autoclave. The 4848 controller utilised throughout the project

managed to maintain the operating temperature of the autoclave within ± 5 K of the set point. The magnetic stirrer was maintained at a constant 300 rpm to ensure sufficient mixing conditions and minimise vortexing. The operating pressure of the system was directly proportional to the operating temperature and hence was directly influenced by the temperature controller. Safety equipment such as the burst disk line and the pressure dead head node were isolated and operated as independent systems in order to ensure a relativity safer operating environment for the technicians. A diagram of the 4523 reactor and 4848 controller utilised throughout this project can be seen in Figure 48, found in Appendix B.

3.3 Test work methodology

The project was initially broken down into four phases of test work as illustrated in Figure 17, above. The sample preparation and ore characterisation of the spodumene concentrate utilised as feed material for the leaching operation was initially investigated before any leach tests were conducted. The characterisation of the spodumene concentrate included a 26 element assay suite, an XRD analysis and a particle size analysis of which can be evaluated in section 3.1.

Once characterised the spodumene concentrate was quantitatively riffle split into 13 representative sub samples ready to be utilised as feed material for the leaching investigation. The methodology for the leaching test work conducted is summarised in section 3.3.2. The respective solid residues and leach liquors for each leach conducted were collected and sub sampled for analysis. The analysis of the leach products included: elemental assays, XRD analysis of the solids residues, ICP analysis of the leach solutions and SEM imaging, of which is all discussed in section 4.

Throughout the life of the project the relative success of the investigations conducted were based around the overall accountability of the results collected, with the extraction efficiency of the lithium a targeted objective rather than an indicator for success.

3.3.1 Sample preparation

The concentrate utilised throughout the project was a 1.5-kilogram charge of spodumene concentrate, that consisted of 3.53% lithium. A 1-kilogram charge was initially riffle split into 13 separate 80 gram charges. These 80 gram charges were utilised as the feed material for the leaching process. An initial sizing analysis was conducted utilising a Microtrac flex S3500 laser sizer, recording a P_{80} of 325µm, of which was directly utilised as feed material to the leaching process.

Two of the 80-gram flotation concentrates were milled to a P_{80} of 106µm and 32µm respectively. These chargers were utilised to investigate the influence of particle size on the extraction of lithium under the specified leaching conditions. All charges were then stored in the laboratory at ambient temperature, ready for the leaching operation. A 80-gram sub sample of the remaining concentrate was riffled out from the remaining sample and analysed for its moisture content. The moisture analysis was conducted in duplicate to establish a moisture content of the concentrate ore utilised as feed material for the life of the project. The feed moisture analysis was conducted in a commercial laboratory where a weighed (to four decimal places) quantity of concentrate was placed in a sealed container and left in a 343.15 K oven for 72 hours. The sample was removed after the 72-hour period and a post mass collected, accounting for any excess water that may have existed within silicate lattice the concentrate.

3.3.2 Leaching methodology

A Parr® series 4523 stirred reactor was utilised as the leaching vessel throughout this project. Prior to the leaching operation commencing a pre-check and pressure test were conducted on all the relevant leaching equipment, as to ensure the vessel was safe for operation.

The autoclave was initially charged with NaOH solution and α-spodumene concentrate with the resulting slurry having its mass, pH and Eh recorded. Once charged the autoclave was fixed to the reactor head and pressurised to 1000 kPa with a BOC gas cylinder (Linde Group 2018). The warm up sequence was initiated once the vessel had stabilised at 1000 kPa. The heating sequence occurs at 278.15 K/ min to the specified operating temperature, of which the 4848 PID controller utilised maintains within a ± 5 K operating range. The system was allowed to operate under constant temperature and pressure over the course of a range of specified residence times. At the end of the experiment, the autoclave was cooled to 323.15 K by recirculating cooled water through the cooling coil and the contents of the autoclave is discharged.

The post weight of the clave was recorded prior to the contents of the autoclave being filtered via a Buchner filter. Two Whatman™ grade 1 filter papers are utilised throughout the filtration process. The filtrate collected during the initial filtration process had its density, pH and Eh values recorded and a sub sample was collected for solution assay. The solids are then washed two times with 1 litre of de-ionised water (DI) in order to wash away any excess alkali. A sub sample of the wash solution is collected and the remaining is discarded. After the two DI washes the solids are collected, dried and weighed prior to being blended,

homogenised and split for analysis. A test work flowsheet displaying the steps taken during a leach test is attached in Appendix B1.

3.4 Analysis techniques

Throughout the life of this project, analytical techniques were utilised to qualitatively analyse the spodumene concentrate and leaching products. A combination of a peroxide fusion digest and ICP-MS were utilised for elemental analysis. X-ray powder diffraction (XRD) was deemed appropriate for mineralogical analysis due to the crystalline nature of the leach materials. SEM scanning was conducted in order to characterise the leach feed and residues while forming conclusions on the leaching mechanisms that occurred throughout the process.

3.4.1 Elemental assays

Elemental assays were conducted on all feed material and leach products that were utilised throughout this project. The ICP-MS data was then converted to standardised data and implemented in relevant calculations that assessed the extraction efficiency of the leach process. The resulting data is displayed throughout section 4 with the relevant tabulated data and process methodology found in Appendix B2.

3.4.1.1 Solid residue assays

A peroxide fusion digest was conducted prior to being analysed by inductive coupled plasma mass spectrometry. The peroxide fusion was conducted utilising a sodium peroxide (Na_2O_2) flux and a ventilated furnace. Once the sample underwent heat treatment it was allowed to cool. The product from the fusion process was then dissolved in dilute acidic solution at a 5:100 ratio and applied directly the ICP-MS for elemental analysis. The elements analysed throughout this project include: lithium, potassium, silicon and sodium with two of the optimised tests also incorporating a copper and aluminium analysis.

3.4.1.2 Solution assays

All the leach liquors throughout this project were analysed via direct spray dilution applied directly to an ICP-MS machine. The solution assays were analysed for lithium, silicon, sodium and potassium contents, with the optimised tests also incorporating a copper and aluminium analysis.

3.4.2 X-ray diffraction analysis

X-Ray powder diffraction analysis was utilised to characterise the spodumene concentrate and leach residues. XRD evaluates the electromagnetic backscatter collected off crystalline compounds at specific angles of incidence and various electromagnetic intensities

(International Union of Crystallography 1999). The diffraction pattern generated by the crystalline powders is unique to specific compounds inter atomic molecular arrangements, allowing for identification to occur when compared to certified reference patterns. The ICDD's data base was utilised as the reference material for this project, with the results generated displayed in section 4.2.1 and discussed in detail throughout section 5.

The XRD analysis utilised a 10° to 50° range of analysis as it was evaluated that most of the prominent 'peaks' of spodumene and relevant lithium compounds occurred within this range (Botto 1985, International Centre for Diffraction Data 2009). The operational methodology utilised for this phase of the test work is discussed in further detail in Appendix B1- Supporting equipment section.

3.4.3 Scanning electron microscopy

Scanning electron microscopy (SEM) was utilised to visually analyse the spodumene concentrate and selected leach residues throughout this project. The external morphology, orientation and crystalline structures of the specific samples were analysed and compared against literature sources with the objective of further understanding the physical alterations that have occurred within the leaching process.

A bench top JEOL JCM-6000 SEM was utilised to complete this task, where samples were set in a carbon coated holders prior to SEM analysis. These samples were observed in the secondary electron mode with an acceleration voltage of 5 kV. A comparative analysis on the images collected against various sources of literature is discussed in detail throughout section 4.2 and 5.

4. Results

The investigation into the leaching of α-spodumene has resulted in 10 alkaline leaches being conducted. Table 3 displays the operating parameters that were investigated throughout this project and has the relevant lithium extraction and accountabilities tabulated for each respective test.

Table 3: Summary table of the leaching variables investigated and their respective lithium extraction and accountability

Test Nº #	Atmosphere (Air/CO_2)	NaOH (Moles)	Temperature (Kelvin)	Residence time (Hr's)	Particle size (µm)	Li extraction (%)	Li accountability (%)
1	Air	**8**	573.15	3	325	23.62	82.63
2	Air	**12**	573.15	3	325	32.41	89.78
3	Air	**14**	573.15	3	325	41.48	105.26
4	Air	14	**533.15**	3	325	37.41	104.08
5	Air	14	**553.15**	3	325	40.52	100.80
6	Air	14	573.15	**1**	325	28.93	100.00
7	Air	14	573.15	**6**	325	44.25	96.19
8	Air	14	573.15	3	**32**	31.11	105.7
9	Air	14	573.15	3	**106**	32.41	102.83
10	**CO_2**	14	573.15	3	325	40.76	87.46

From the range of operating conditions investigated it was determined that the optimal leaching parameters for the direct leaching of α-spodumene are as follows: 14 molar NaOH leaching lixiviant, 573.15 K operating temperature, 6 hour residence time and a beneficiated spodumene concentrate consisting of a P_{80} at 325µm. From the tests conducted it can be approximated that the lithium extraction efficiency of this system would be consistently in excess of 40%, with the results collected in this study indicating that 44.25% is achieved.

XRD characterisation displays a significant reduction in the amount of lithium found within all of the leach residues, with sodium-silicate based hydrates forming in its absence. SEM scanning further suggests that leaching has occurred within this system due to the presence of leach pits and corroded particle boundaries. From the results displayed throughout this section a summary on the proposed behaviour of the leaching system investigated can be found in section 5, with recommended future research discussed in section 6.

4.1 Leaching of α-spodumene

The leaching of α-spodumene was evaluated over the course of ten alkaline pressure leaches. From the solution analysis conducted it was found that lithium extraction exhibited a strong linear correlation with increasing NaOH dosages (Figure 21) and operating temperatures (Figure 24). The investigation into the influence of residence time on lithium extraction efficiency resulted in logarithmic trend being established as the leach duration increased linearly at shorter operational times and plateaued as the leach duration increased. The influence of decreasing particle size exhibited an inverse influence on lithium extraction, as decreasing the P_{80} of the feed material from 325µm to 32µm resulted in 10.37% decrease in the amount of lithium extracted (Figure 30).

A sodium substitution and silicon dissolution analysis was to evaluate the influence of each of the operating variables investigated. Table 10 found in Appendix B3 summarises all relevant balances, extractions and accountabilities for each respective element and their response to changes in NaOH dosage, operating temperatures, residence time and particle size.

The dissolution of silicon was found to linearly increase within increasing NaOH dosage, operating temperatures and residence times. The influence of particle size on the dissolution of silicon exhibited linear trends, that suggested that silicon dissolution was minimised (32.14%) at a P_{80} of 106µm and maximised (37.64%) at a P_{80} of 325µm. Sodium was analysed with respect to its change in mass percent in the leach residue compared to the initial amount of sodium found in the feed material. From the ratio calculated the amount of sodium substituted into the leach residue can be readily accessed. From the results collected it became evident that sodium substitution increased linearly with increasing NaOH dosages, operating temperatures and residence times. As established with the silicon analysis, it was found that sodium substitution was minimised (95.78%) at the P_{80} of 106µm and maximised (99.60%) at a P_{80} of 325µm.

4.1.1 Effect of reagent dosage

To investigate the effect of NaOH dosage on the leaching of α-spodumene, three independent experiments were carried out at 8, 12 and 14 molar concentrations. Throughout these experiments other operational variables remained fixed. These variable included: leaching temperature of 573.15 K, 3 hour leach duration and a P_{80} of 325µm for the concentrate utilised as feed material.

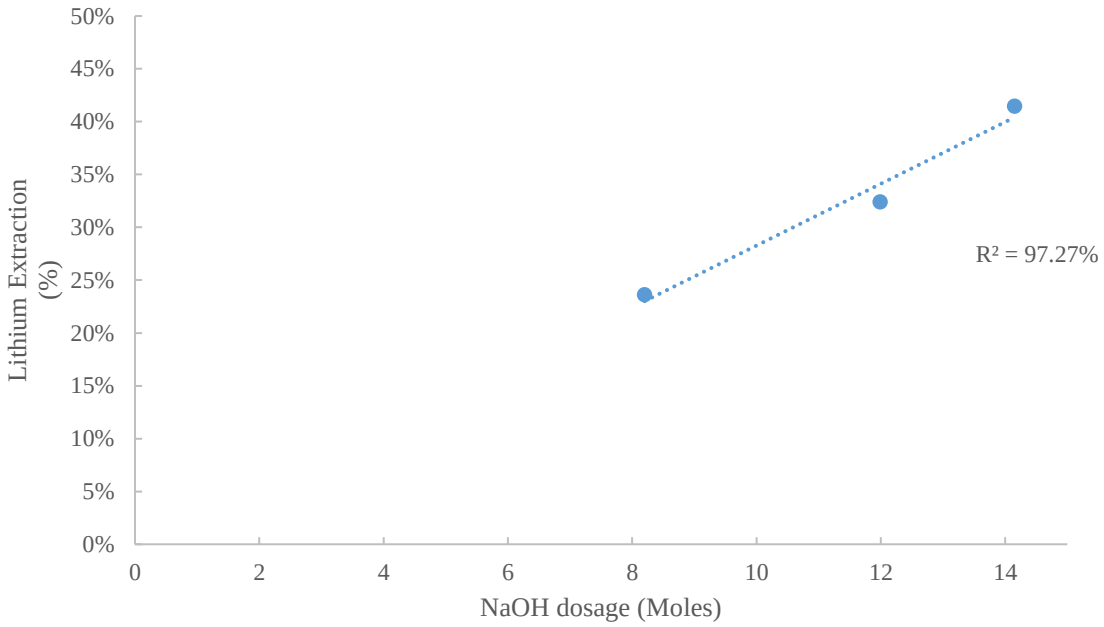

Figure 21: NaOH dosage vs lithium extraction

As displayed in Figure 21 above the dosage of NaOH has a significant influence on the extraction efficiency of lithium. The increased reagent dosage from 8 to 12 molar NaOH resulted in an 8.79% rise in the amount of lithium extracted. A further 9.07% was extracted when the NaOH dosage was raised from 12 to 14 moles. The highest extraction of lithium was 41.48% when leached in a 14 molar NaOH solution, while the 8 molar solution produced the lowest extraction efficiency of 23.62%.

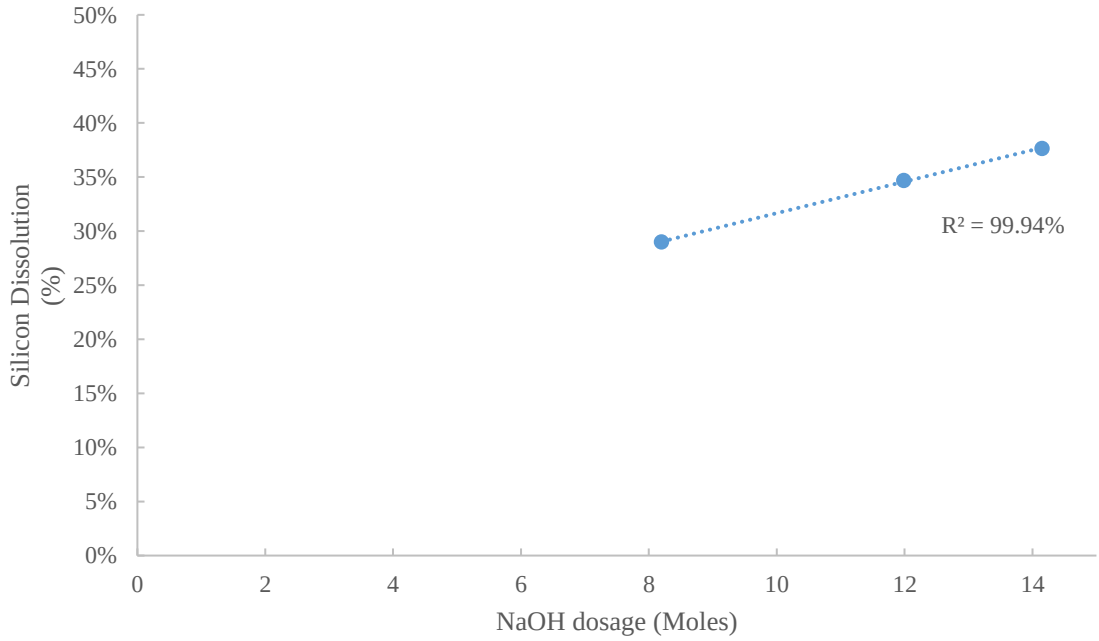

Figure 22: NaOH dosage vs silicon dissolution

Figure 22 displays the linear relationship between NaOH dosage and silicon dissolution. The rise from 8 to 12 molar NaOH dosage sees a rise in silicon dissolution by 5.70%, while 12 to 14 molar NaOH sees a further 2.94% silicon dissolved. The maximum amount of silicon dissolved occurred in the 14 molar solution and was calculated to be 37.64%, while the lowest silicon dissolution (28.99%) occurred in the 8 molar NaOH solution.

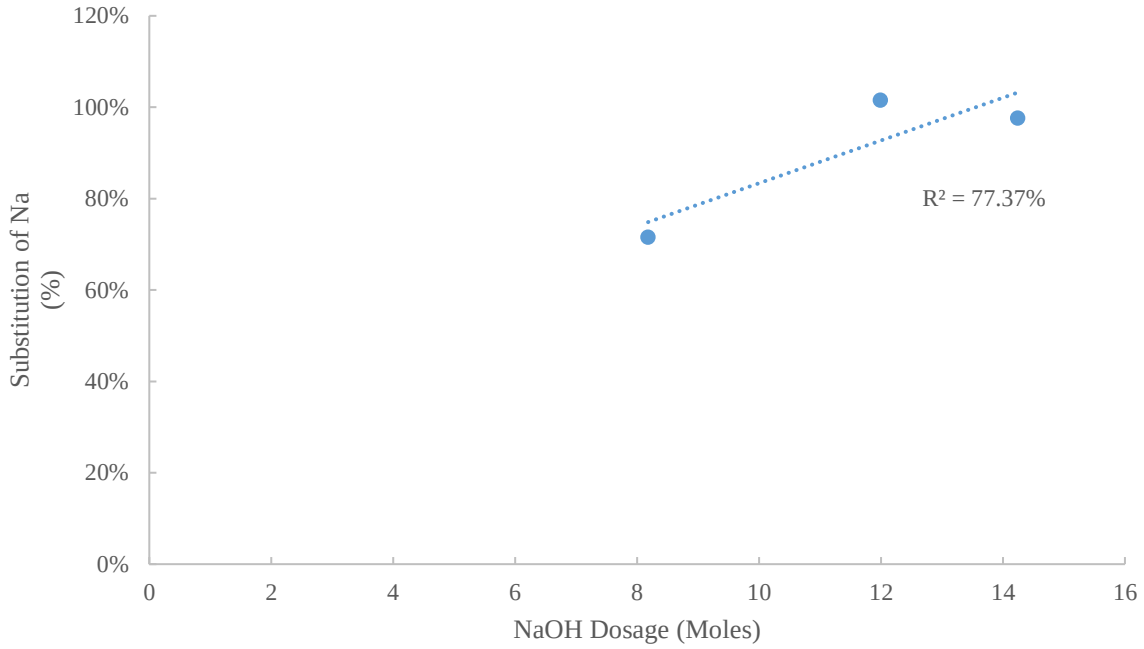

Figure 23: NaOH dosage vs sodium substitution

Figure 23 displays the linearized relationship that exists between increasing NaOH dosage and the amount of sodium substituted into the leach residue. The increase from 8 to 12 molar solution sees a 29.96% rise in the amount of sodium reporting to the leach residue. The adjustment from 12 to 14 molar sees a 3.89% decrease in the amount of sodium reporting to the leach residue. The largest quantity (101.53%) of sodium reporting to the leach residue occurred under the influence of a 12 molar NaOH lixiviant, with the lowest quantity (71.57%) of sodium reported utilising the 8 molar solution.

4.1.2 Effect of temperature

The effect of temperature on the leaching of α-spodumene was investigated from a range of 533.15 K to 573.15 K. Throughout these experiments other operating variables remained fixed. These variable include: NaOH dosage of 14 moles, 3 hour leach duration and a P_{80} of 325µm for the concentrate utilised as feed material.

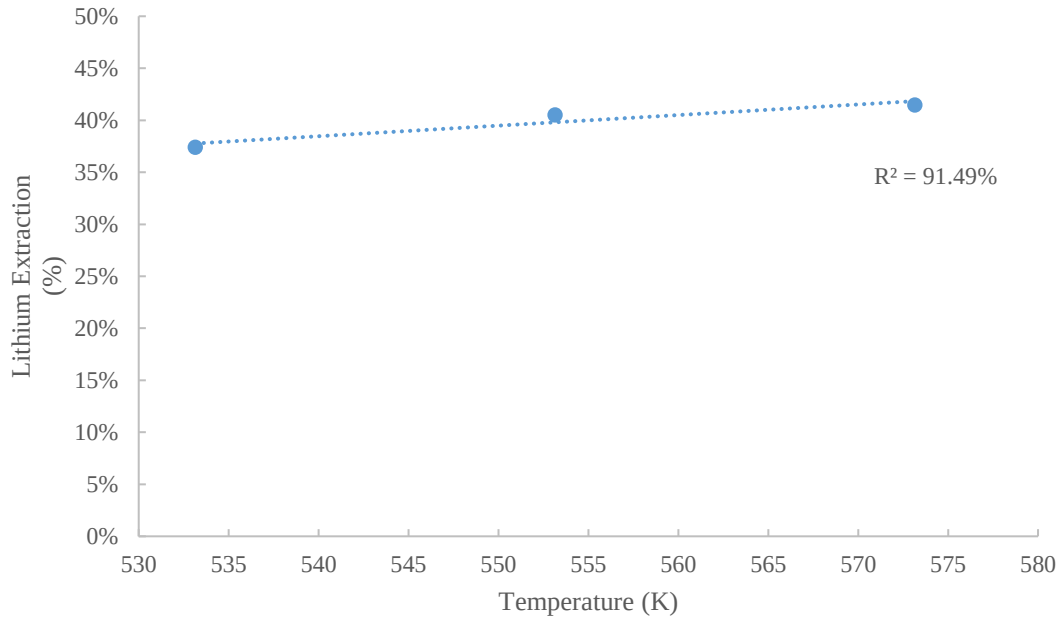

Figure 24: Temperature vs lithium extraction

As displayed in Figure 24 it was concluded that the rise in operating temperatures investigated resulted in a slight increase in the extraction efficiency of lithium. The rise in operational temperatures from 533.15 K to 553.15 K resulted in a 3.11% increase in the amount of lithium extracted, while the rise from 553.15 K to 573.15 K resulted in a further 0.96% extracted. The highest extraction efficiency of 41.48% occurred at 573.15 K.

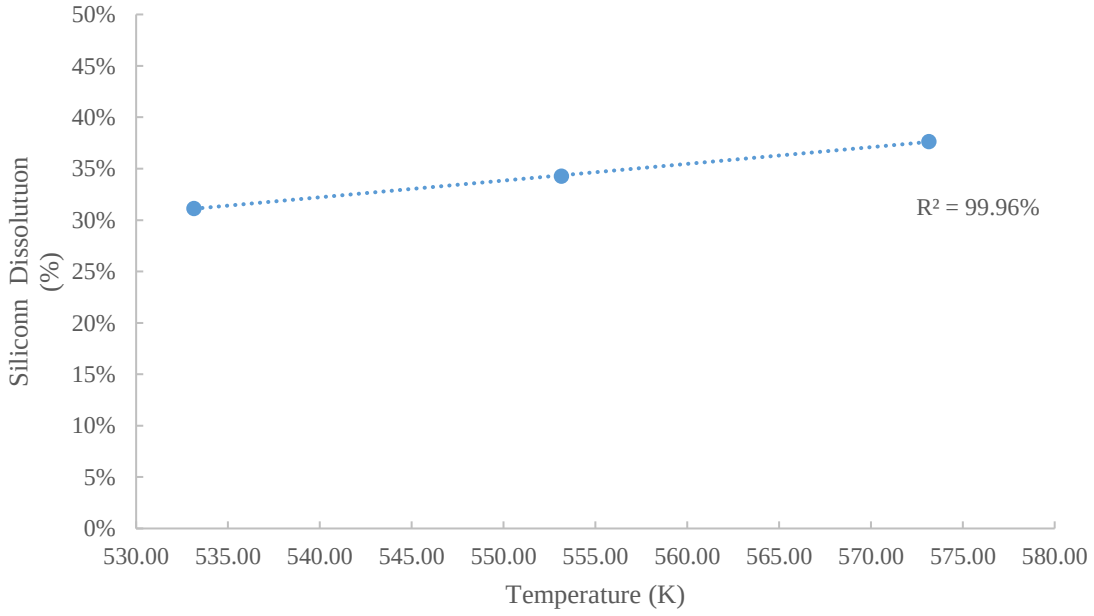

Figure 25: Temperature vs silicon dissolution

Figure 25 displays the positive linear relationship that exists between increasing silicon dissolution and rising operating temperatures. At the operating temperature of 533.15 K, 31.14% silicon dissolution occurs. When the operating temperature is increased to 553.15 K a further 3.14% of the silicon is dissolved until the maximum silicon dissolution is achieved (37.64%) at 573.15 K.

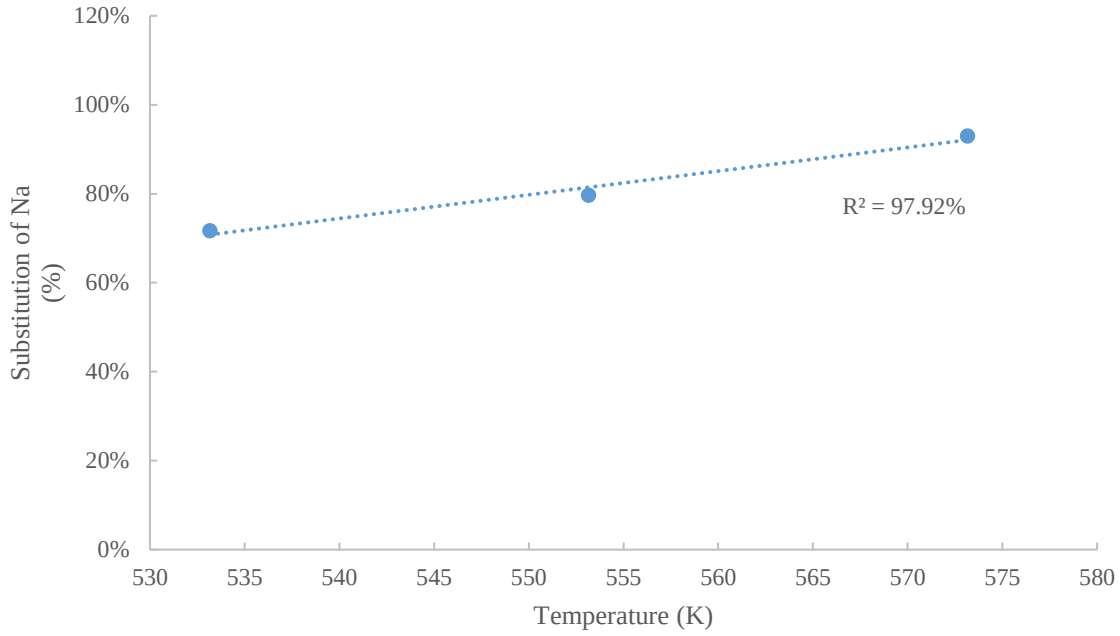

Figure 26: Temperature vs sodium substitution

Figure 26 displays the linear relationship that existing between rising operating temperatures and the increasing amount of sodium reporting to the leach residue. A 7.96% rise in the amount of sodium reported to the leach residue when the operating temperature was raised from 533.15 K to 553.15 K. When the operating temperature was raised to 573.15 K a further 13.34% of sodium reported to the leach residue. The largest quantity of sodium reporting to the leach residue occurred at 573.15 K and was estimated to be a 92.99% increase on the initial quantity of sodium found in the feed material.

4.1.3 Effect of residence time

The influence of residence time on the leaching of α-spodumene was investigated over the course of 1, 3 and 6 hour tests. Throughout these experiments other operating variables remained fixed. These variable include: NaOH dosage of 14 moles, leaching temperature of 573.15 K and a P_{80} of 325µm for the concentrate utilised as feed material.

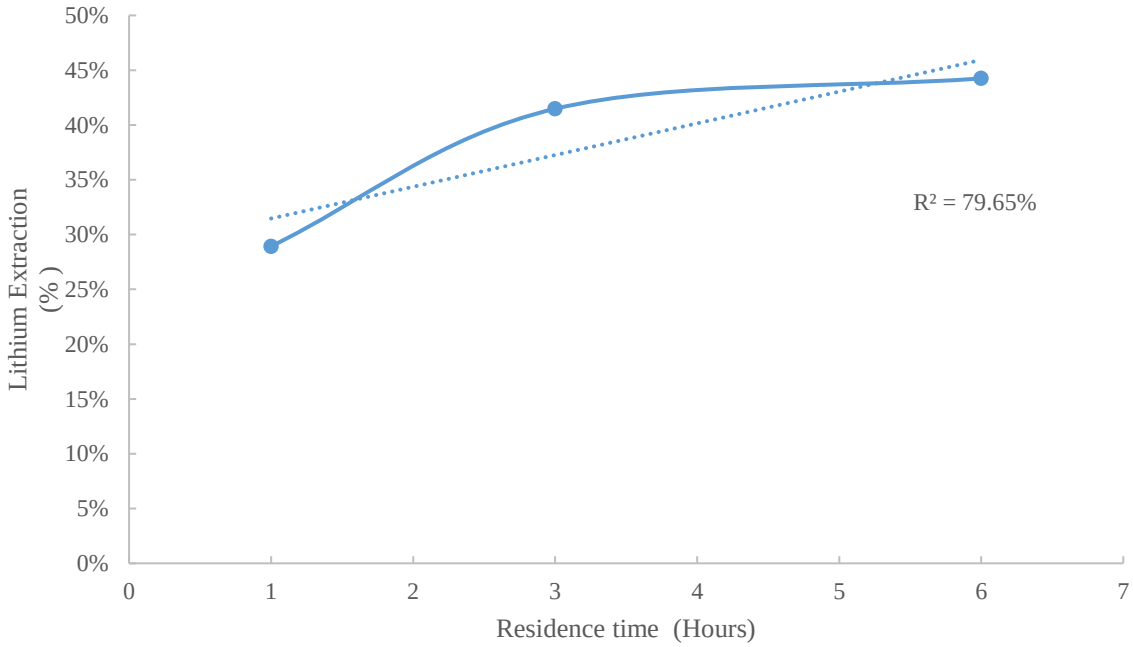

Figure 27: Residence time vs lithium extraction

Figure 27 displays that the residence time of the leaching operation had a significant influence on the extraction efficiency of lithium. Lithium extraction increased proportionally as the leach duration increased, with the 1 to 3 hour interval resulting in a 12.55% increase in the amount of lithium extracted. The 3 to 6-hour leach interval resulted in a further 2.77% lithium being extracted, with a final lithium extraction of 44.25% achieved. The trend of the graph displays a logarithmic relationship between increasing residence time and relative extraction efficiencies of lithium.

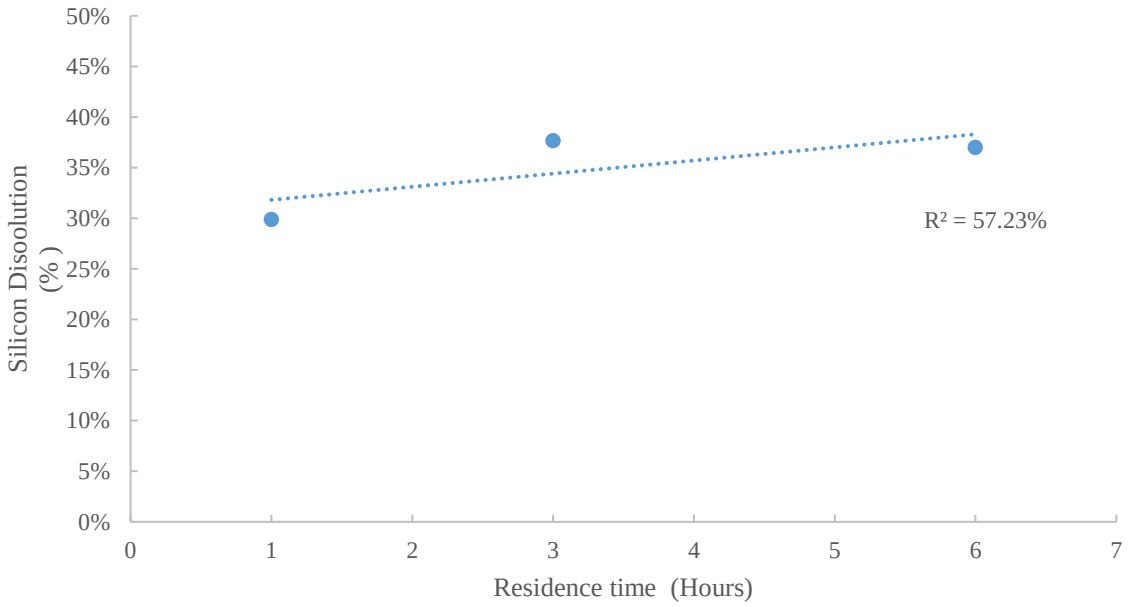

Figure 28: Residence time vs silicon dissolution

Figure 28 displays the linear relationship that exists between longer residence times and higher quantities of silicon dissolution. Similar to the trend exhibited by lithium, the silicon analysis indicates that there was a 7.77% rise in silicon dissolution from the 1 to 3-hour residence times investigated. The 3 to 6-hour interval resulting in a 0.64% reduction of the total amount of silicon dissolved. The highest percentage of silicon dissolution (37.64%) occurred at the 3-hour residence time investigated.

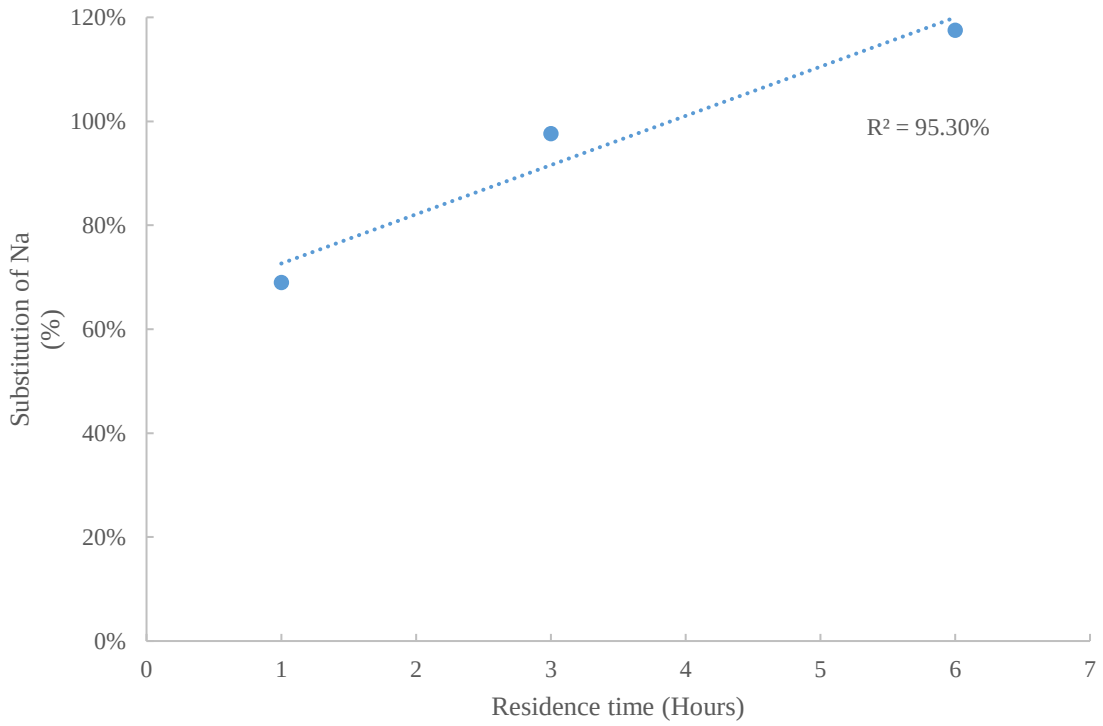

Figure 29: Residence time vs sodium substitution

Figure 29 displays the linear correlation that exists between longer residence times and the rising percentage of sodium substituted into the leach residue. The 1 to 3-hour interval investigated displays a 28.65% rise in sodium substitution while the 3 to 6-hour interval increased sodium substitution by a further 19.91%. The highest substitution of sodium (117.55%) occurred at the 6-hour residence time investigated.

4.1.4 Effect of particle size

Experiments to investigate the effect of particle size on the leaching of α-spodumene were investigated at P_{80}'s of 32, 106 and 325µm. Throughout the tests other operating variables remained constant. These variables include: NaOH dosage of 14 moles, a leaching temperature of 573.15 K and a 3 hour leach duration.

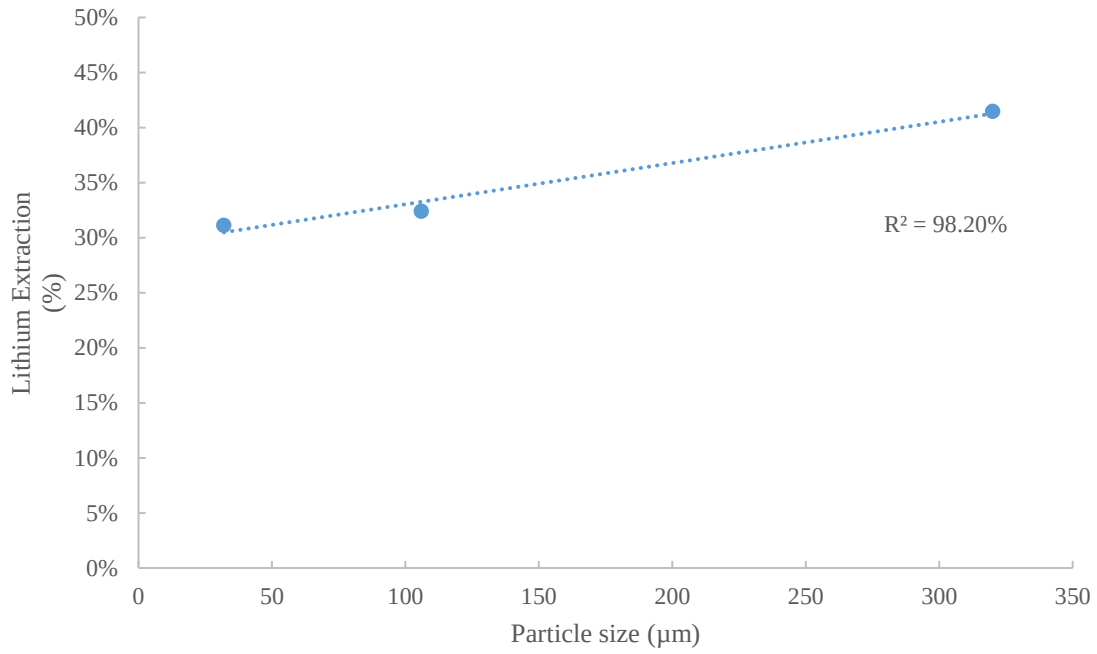

Figure 30: Particle size vs lithium extraction

Figure 30 displays the inverse relationship that was established between particle size and the extraction efficiency of lithium throughout this project. It was evaluated that at a P_{80} of 325µm the corresponding lithium extraction was 41.48 %, while at a P_{80} of 32µm the extraction was reduced to 31.11%. From the results collected it is suggested that the highest extraction efficiency (41.48%) of lithium occurs at a P_{80} of 325µm.

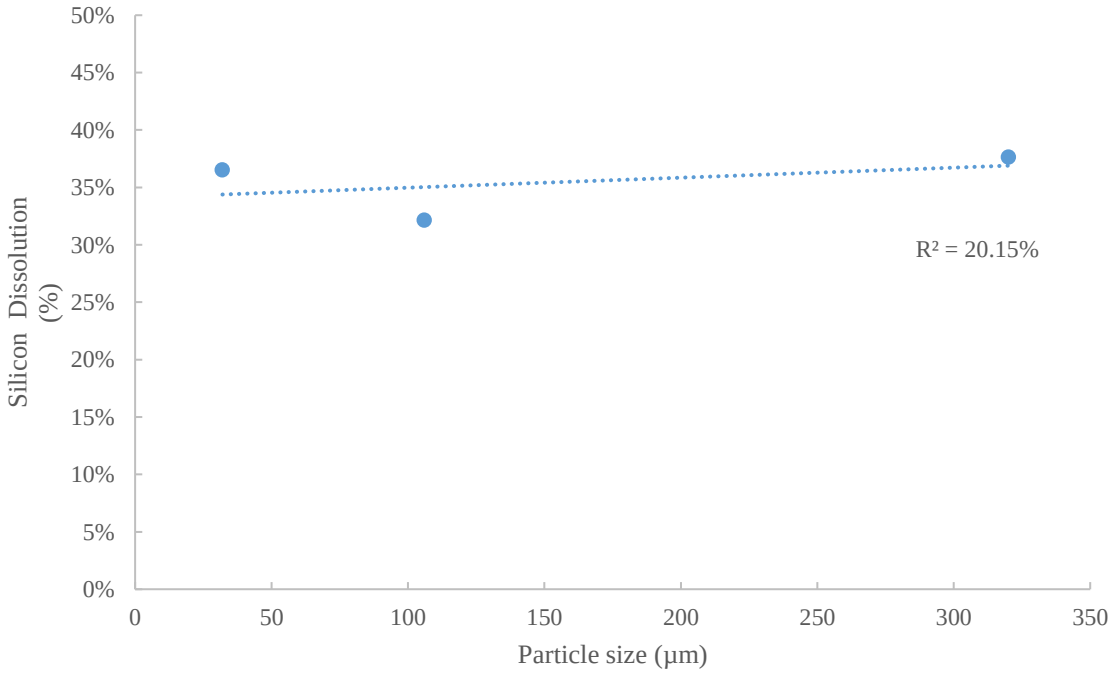

Figure 31: Particle size vs silicon dissolution

The linear relationship that exists between decreasing particle size and increasing silicon dissolution is represented by Figure 31. From the resulted collected it is suggested that maximum silicon dissolution occurs at the 325µm P_{80}, of which is narrowly followed by the 32µm (1.11% lower than that of the 325µm material). Silicon dissolution is at its lowest at the P_{80} of 106 µm material (32.14%).

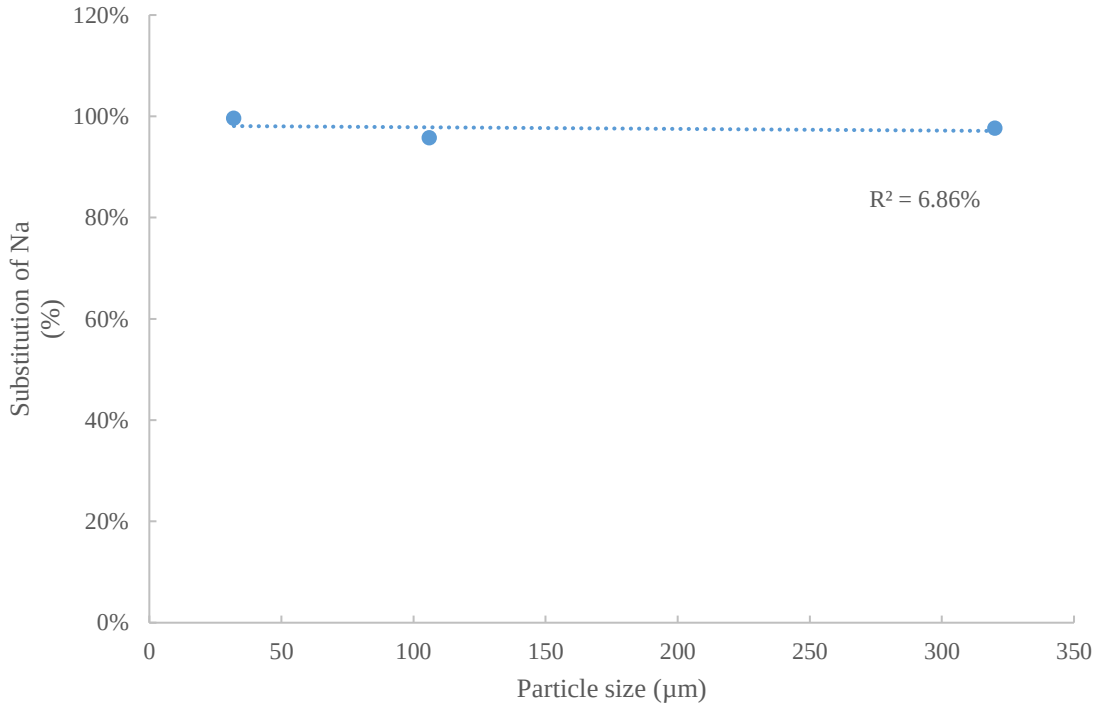

Figure 32: Particle size vs sodium substitution

Figure 32 displays the relationship that exists between particle size and the substitution of sodium. Exhibiting similar trends to those displayed with the silicon analysis the 106µm material has the smallest percentage of sodium substitution occurring (95.78%), while the 325 and 32µm samples have 97.64% and 99.60% respectively.

4.2 Analysis of leach residue

The solids utilised and generated throughout this project were analysed via XRD and SEM analysis. From analysing the physio-chemical alterations of the leach residues and comparing them against the starting feed material, conclusions towards potential leaching mechanisms can be made. The XRD, SEM and assay data are all complied in order to accurately access the leaching system, of which is discussed in detail throughout section 5.

4.2.1 X-ray diffraction analysis

XRD analysis was conducted on all the samples utilised and generated throughout this project. The influence of each leaching variable investigated had its respective residue analysed via XRD in order to access the mineralogical changes that have occurred within the leaching process. The data generated was plotted against literature collected from the ICDD data base in order to characterise each of the residues. Figure 33 to Figure 36 throughout this section display the XRD results, with section 5 discussing the trends in greater detail.

By analysing the XRD results it is evident that there is a significantly reduced amount of lithium associated with the leach residues when compared to the initial spodumene feed. *Kuang et al. (2018)* evaluated a β-spodumene autoclave system where it is suggested that a chemo-selective ion exchange occurs between the lithium ions of the β-spodumene and the sodium ions present in the leach lixiviant. Although physically different β-spodumene consists of the same fundamental constituents to that of α-spodumene, it can be suggested that *Kuang's* proposed ion exchange reaction mechanism is applicable to the α-spodumene system investigated in this study. Although a detailed kinetic study is required to prove this proposed theory, it is evident via the XRD results that lithium only exists in minor quantities within the leach residue and that sodium-silicate based hydrates have reformed in their absence.

The XRD analysis indicates clear morphological alterations to the crystal structure in all of the leach residues, when compared to the initial feed material. These alterations are present in all of the leach residues that were produced throughout this project. The influence of reagent dosage, temperature, particle size and residence time all displayed similar trends, in their XRD results. It was identified that as reagent dosage, temperature, particle size and residence time all increased in their respective orders of magnitude, sodium-silicate based hydrates were also found in greater concentrations within the leach residues.

4.2.1.1 Effect of reagent dosage

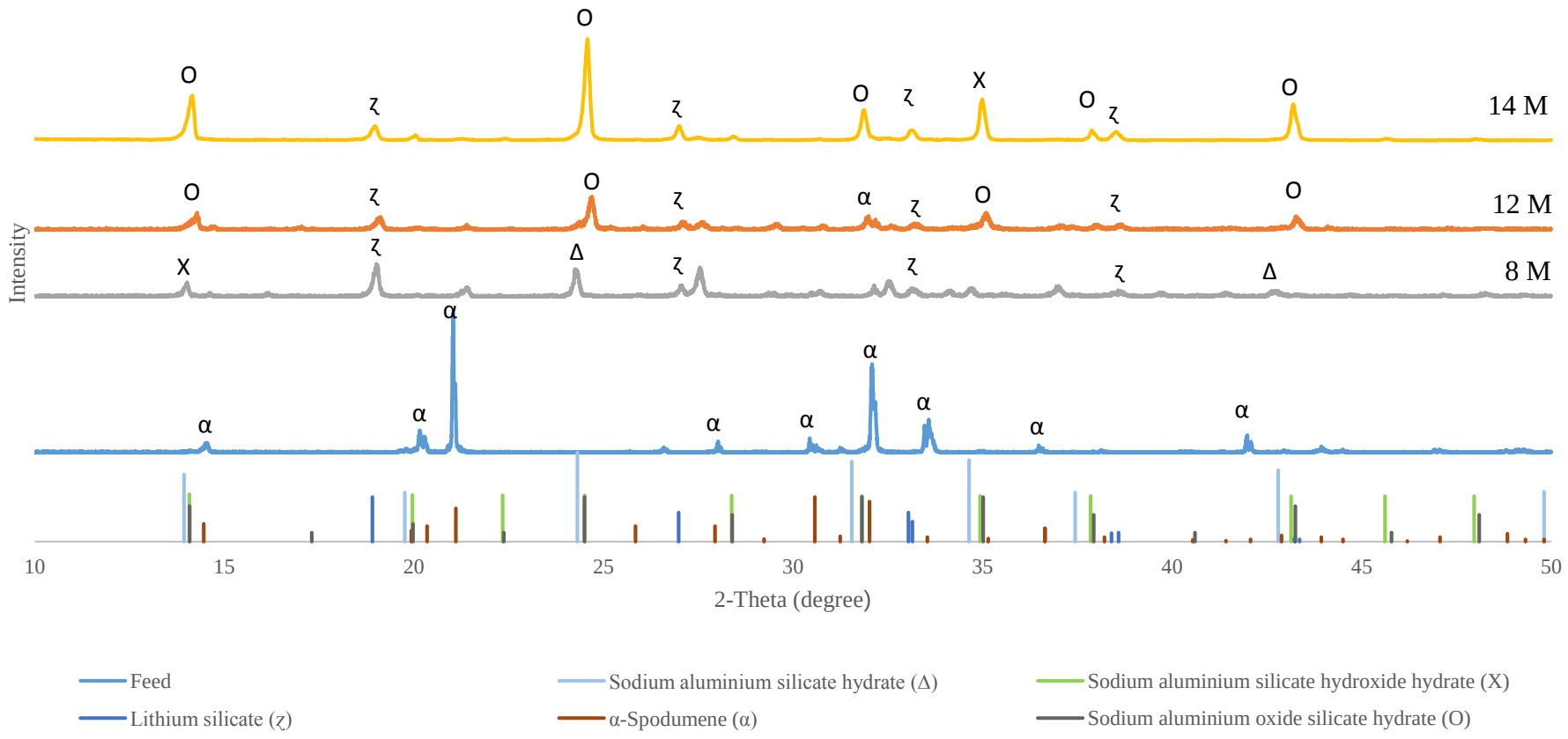

Figure 33: XRD analysis of the leach residues for the 8 molar, 12 molar and 14 molar caustic leaches investigated

4.2.1.2 Effect of temperature

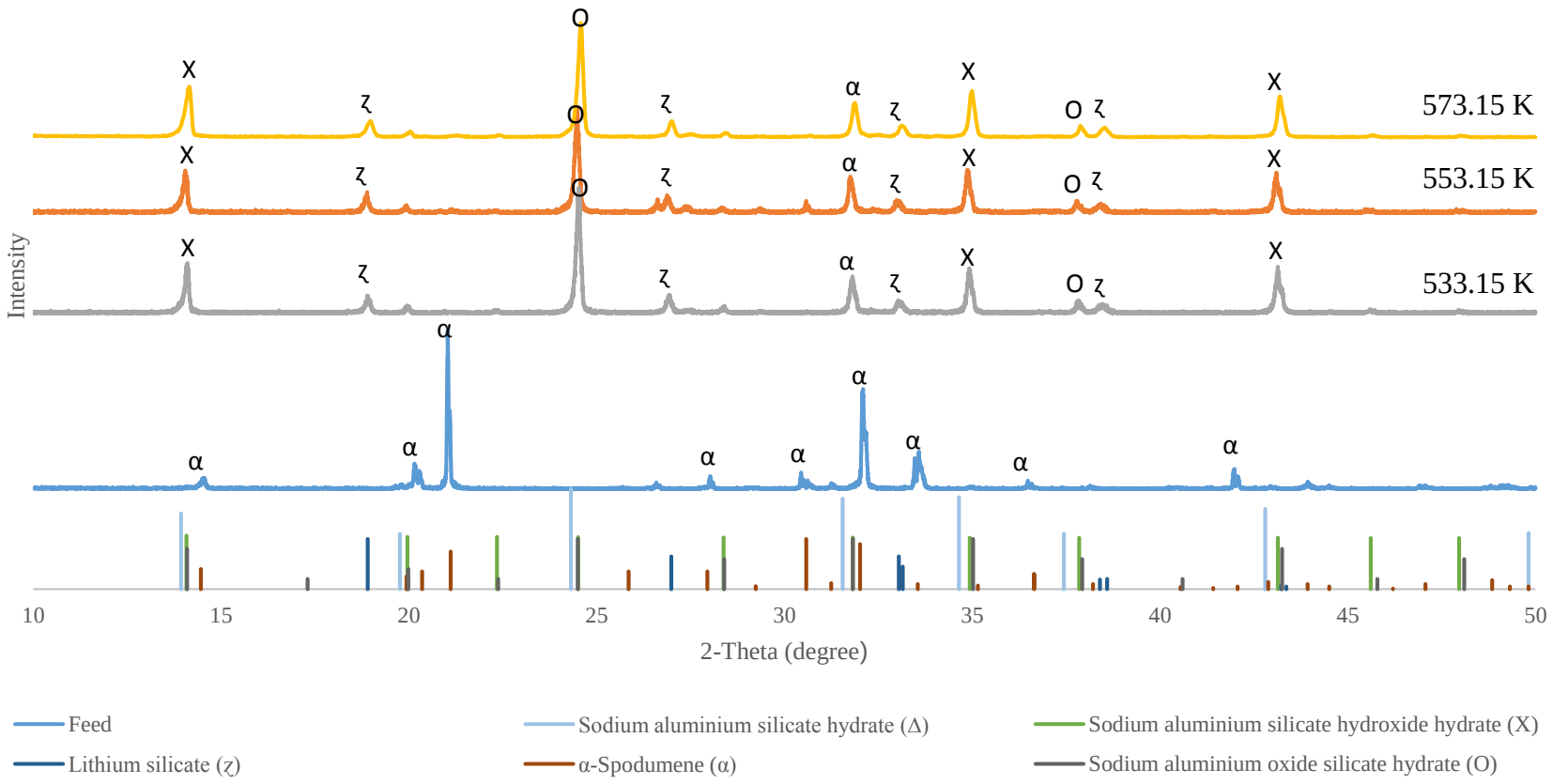

Figure 34: XRD analysis of the leach residues for the 533.15 K, 553.15K and 573.15K leaching temperatures investigated

4.2.1.3 Effect of residence time

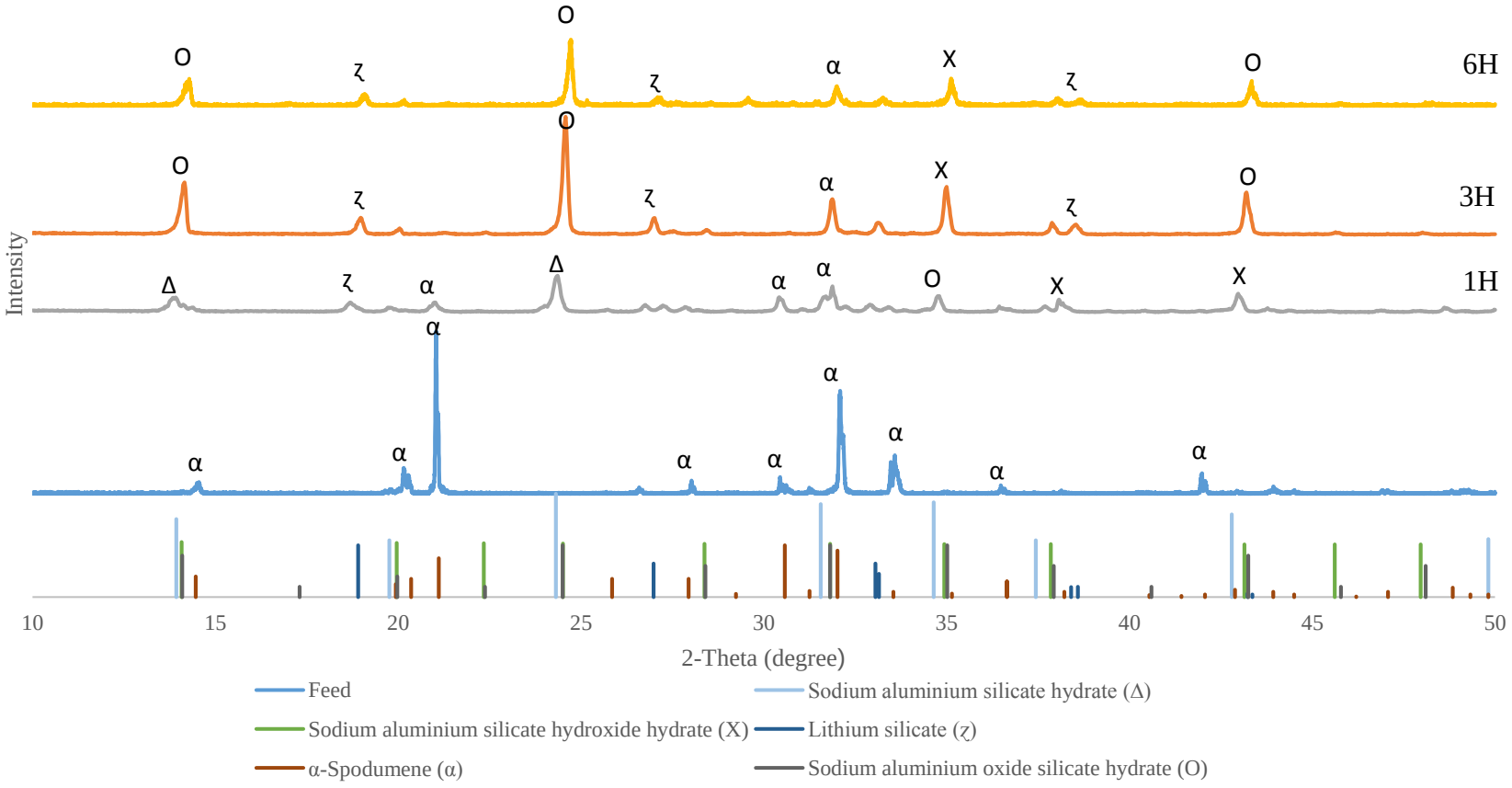

Figure 35: XRD analysis of the leach residues for the 1, 3 and 6 hour residence times investigated

4.2.1.4 Effect of particle size

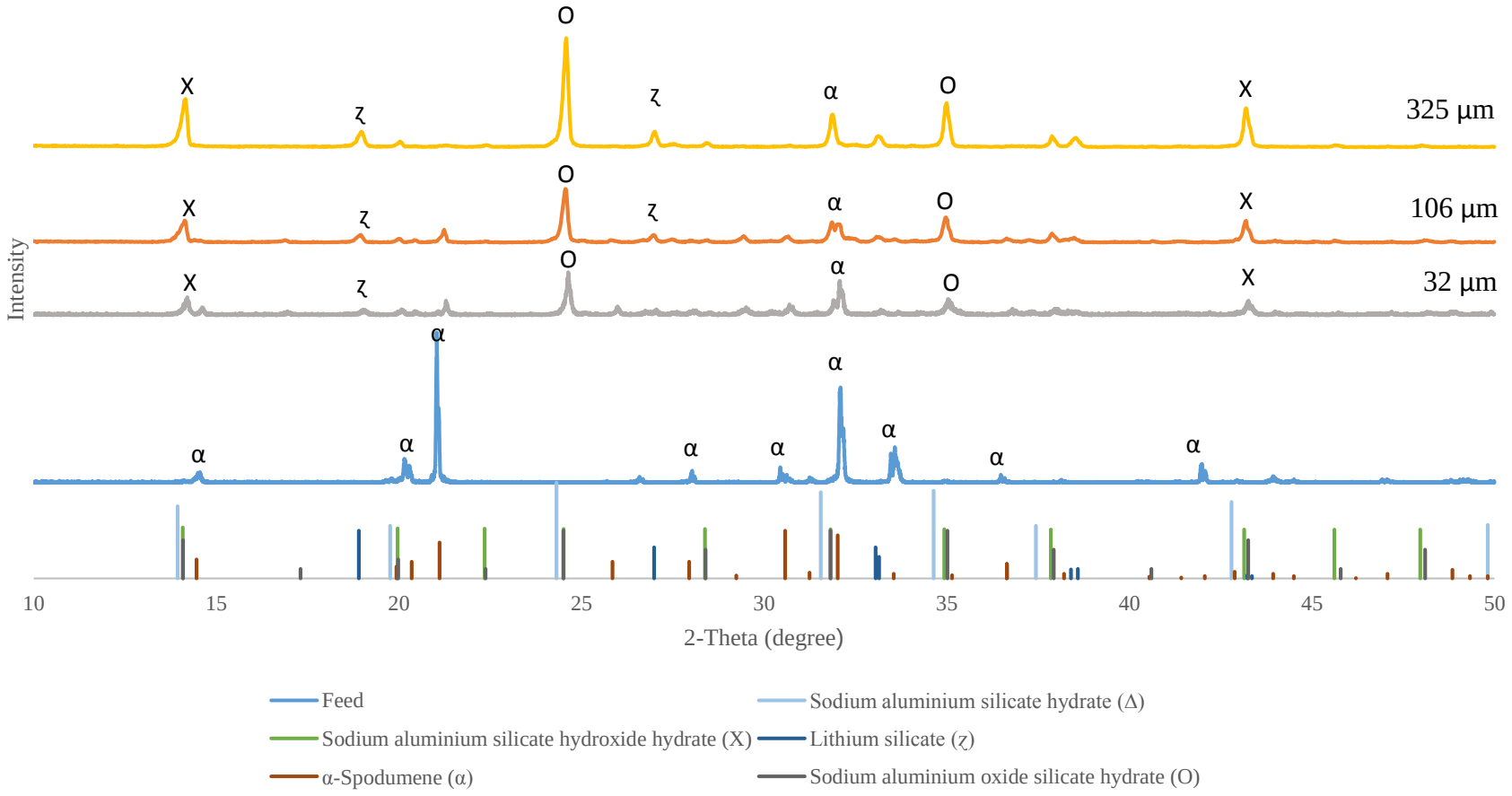

Figure 36: XRD analysis of the leach residues for the 32, 106 and 325µm particle sizes investigated

4.2.2 Scanning electron microscope

SEM imagining was conducted on sub samples of the spodumene concentrate and the Test 3 leach residue. As displayed in Figure 37 below the spodumene concentrate consists of jagged crystalline structures that are relatively uniform. The imaging of the concentrate displays a homogenous composition, with little variation in the intensity of the grey scale imaging collected.

Figure 37: SEM image of the 325µm spodumene concentrate utilised throughout this project

Figure 38 displays the leach residue generated from the following leach conditions: 573.15 K, 4 molar NaOH, 3 hour residence time and an initial P_{80} of 325µm. The initial 200µm imaging that was captured displays a uniform, homogenous sample that clearly displays "pitting" within the embedded residue. Pitting is a physical characteristic of a leached residue (Absolon 2008, Babu et al. 2002). Figure 39 is a close up of the leach "pit" found at point A on Figure 38. The pit generated appears to have been chemically corroded from the boundary of the particle as a result of reactive compounds solubilising within the silicate matrix. The rounded edges of the leach residue displayed in Figure 38 and Figure 39 in comparison to feed material found in Figure 37 suggest that the spodumene concentrate underwent morphological alterations. These alterations are consistent with those expected from dissolution reactions suggesting that a leaching reaction has occurred (Babu et al. 2002).

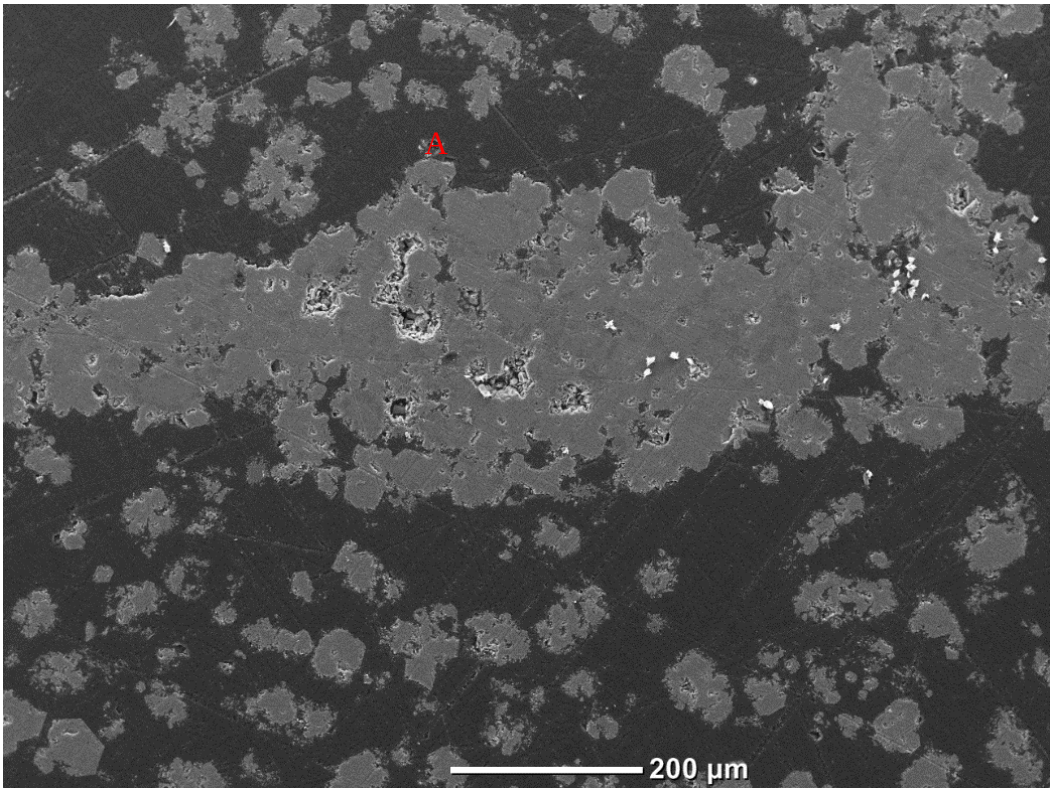

Figure 38: SEM image of the specified leach residue

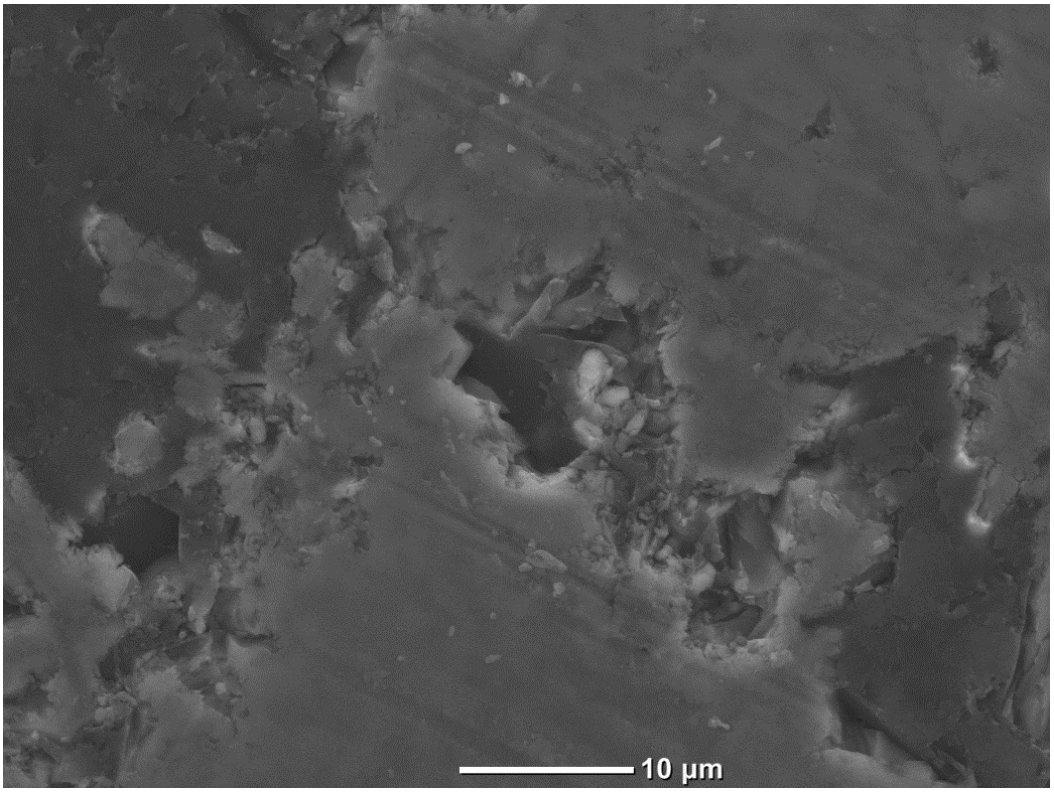

Figure 39: SEM image of the specified leach pit at point A in Figure 29

5. Discussion

5.1 Leaching of α-spodumene

The information from the results displayed throughout section 4 suggest that the leaching of α-spodumene readily occurs when operating under alkaline leaching conditions. Under the operating conditions investigated it was determined that the optimal operating parameters for maximising the extraction efficiency of lithium occurred under the following conditions: a 14 molar NaOH leaching lixiviant, 573.15 K operating temperature, a 6 hour residence time and a P_{80} of 325μm.

From the operating variables investigated it was determined that NaOH dosage had the most significant influence on the extraction efficiency of lithium. This was followed consequentially by the influence of particle size, residence time and operating temperature. From interpreting the elemental assay, XRD and SEM data collected, it is suggested that a chemo-selective ion exchange occurs between the lithium and silicon ions present within α-spodumene and the sodium ion present in the leach lixiviant (Kuang et al. 2018). The XRD analysis conducted indicates that the formation of anhydrous sodium silicate based hydrates has occurred in significant quantities within the leach residue, while the lithium silicate feed material almost completely reacted. Elemental assay results supported the XRD analysis by indicating that an average of 91.02% sodium had being substituted into the leach residue, when compared against its initial feed material. To investigate the proposed chemo-selective ion exchange mechanism further an SEM analysis was conducted on a leach residue (Test 3) that had been previously assayed. The assays conducted on the leach residue indicated that: 41.48% of the lithium had been extracted, 37.63% silica and 1.1% aluminium dissolution had occurred. It was also noted that a 154.00% rise in the sodium contents of the leach residue occurred, when compared to the initial feed material. The results from the elemental assay analysis on the spodumene feed material and respective leach residue are depicted in Figure 40, below.

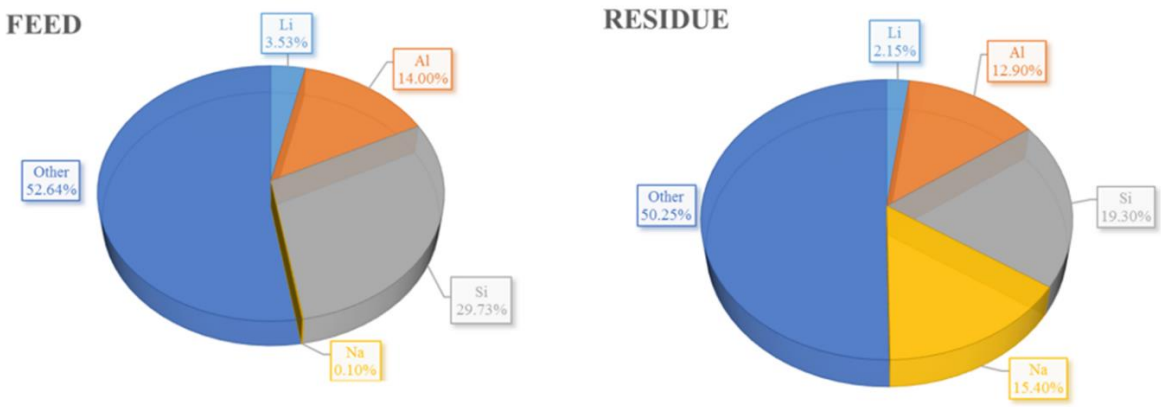

Figure 40: Feed vs residue comparison from the elemental assay data collected for Test 3

The SEM imaging that was conducted on the samples depicted in Figure 40 are found in section 4.2.2. As often associated with leaching reactions the presence of "pits" and corroded particle boundaries indicate that dissolution of the feed material had occurred. Electron Dispersive X-ray (EDX) analysis is a recommended future study as a means to further characterise the surface mineralogy of the leach residues and establish a greater understanding towards the leaching mechanisms of the system.

From the investigations conducted the following reactions are proposed for the direct leaching of α-spodumene utilising a NaOH lixiviant:

1) $NaOH_{(aq)} + LiAlSi_2O_{6\ (s)} \rightarrow LiOH_{(aq)} + NaAlSi_2O_{6\ (s)}$

5.2 Geo-polymorphs of silica

Throughout the leaching test work conducted it was observed that amorphous silica gels were present within the leach filtrates and wash solutions. The viscous nature of these gels inhibited the filterability of the autoclave product. Due to the dissolution of silicon in alkaline media, the formation of siliceous gels was expected within the leach products (Crundwell 2017). An attempt to characterise the siliceous products was conducted with the resulting data and literature studies suggesting that the most probable gel formed is sodium silicate ($(Na_2O)_x . SiO_2$) (Crundwell 2017, Queneau and Berthold 1986).

During the filtration of the autoclave products it was observed that density separation had occurred within the leach filtrate and wash solutions, as displayed in Figure 41 below.

Figure 41: Washate from test 3, displaying a clear separation occurring within the flask

An ICP-MS analysis was conducted on the two different layers that formed in the wash solution during Test 3. The summary of the resulting analysis is tabulated in Table 4 below.

Table 4: ICP-MS results on the grab samples conducted on the two different 'layer' formed in the wash solution for test 3

Element	Top washate (g/L)	Bottom washate (g/L)	Filtrate (g/L)
Li	0.04	2.02	2.91
Si	1.80	10.10	8.89
Na	3.86	175.80	246.70

From the assays conducted it is suggested that the separation of the wash solution had occurred due to differences in density. The concentration of lithium, silicon and sodium found within the 'bottom' wash solution further indicate that a siliceous gel had formed and that it separates rapidly within an aqueous water media, due to its increased density.

6. Conclusion and recommendations

This study aimed to investigate the direct leaching of α-spodumene in alkaline media by addressing the influence of reagent dosage, operating temperature, residence time and particle size. From the study conducted the research concluded that:

- α-spodumene can be leached directly in caustic solutions
- The extraction efficiency of lithium under optimised conditions was limited to approximately 46%
- Diffraction patterns generated by SEM and XRD analysis on the leach residues shows that the crystalline spodumene is almost fully converted to an amorphous-hydrated material

Recommendations for further investigations include:

- Further test work be conducted to evaluate the recovery efficiency at higher NaOH concentrations
- Test work to assess the formation of potential by-product siliceous materials
- A kinetics study on the leaching system be conducted in order to identify the leaching mechanisms and inhibiting factors
- EDX analysis be conducted on the leach residues to further characterise the surface mineralogy of the leach products

References

Absolon, V.J. 2008. A comparasion of biological and chemically induced leaching mechanisms of chalcopyrite Adelaide: University of South Australia.

Alexander, P.P. 1947. Method of Producing Lithium Hydride and Hydrides Of Other Alkali Metals Massachusetts, Unisted States of America.

AMEC. 2018. Grasping the Lithium opportunity Association of Mining and Exploration Companies.

Archambault, M, and C Olivier. 1968. Carbonising roast of lithium bearing ores. Quebec, Canada.

Averill, W.A, and D.L. Olson. 1978. "A review of extractive processes for lithium from ores and brines " *Energy* no. 3:305-313.

Babu, M.N, K.K Sahu, and B.D. Pandey. 2002. "Zinc recovery from sphaleraite concentrate by direct oxidative leaching with ammonium, sodium and potassium persulphates." *Hydrometallurgy* no. 64 (2):119-129.

Barbosa, L.I, N.G Valente, and J.A Gonzalez. 2013. "Kinetic study on the chlorination of B-spodumene for lithium extraction with Cl2 gas." *Thermochimica Acta* (557):61-67.

Barbosa, L.I., G. Valente, R.P. Orosco, and J.A. Gonzalez. 2014. "Lithium extraction from b-spodumene through chlorination with chlorine gas." *Minerals Engineering* no. 56:29-34.

Birney, M. 2017. Lithium Australia in funding and off-take for SiLeach tech. *Buisness News Western Australia*, October 31.

Botto, I.L. 1985. "Structural and spectroscopic properties of leached spodumene in the acid roast processing." *Materials Chemistry and Physics* no. 13 (5):423-436.

Bridgetown, Shire of. 2016. Discover Greenbushes. Paper Napkin Creative.

Brown, T. 2016. Lithium. Nottingham: Minerals UK.

Chen, Y., Q. Tian, B. Chen, X. Shi, and T. Liao. 2011. "Preparation of lithium carbonate from spodumene by a sodium carbonate autoclave process." *Hydrometallurgy* no. 109:43-46.

Cho, J., Y.J. Kim, and B. Park. 2000. "Novel LiCoO2 Cathode Material with Al2O3 Coasting for a Li Ion Cell." *American Chemical Society* no. 12 (12):3788-3791.

Choi, Jung-Hae, Yong-Seok Seo, and Byung-Gon Chae. 2013. "A study of the pressure solution and deformation of quartz crystal at high pH and under high stress." *Nuclear Engineering and Technology* no. 45 (1):53-60. doi: https://doi.org/10.5516/NET.06.2012.024.

Choubey, P.K, M Kim, R.R Srivastava, J Lee, and J Lee. 2016. "Advance review on the exploitation of the prominent energy-storage element: Lithium. Part I: From mineral and brine resources." *Minerals Engineering* (89):119-137.

Crundwell, Frank K. 2017. "On the Mechanism of the Dissolution of Quartz and Silica in Aqueous Solutions." *ACS Omega* no. 2 (3):1116-1127. doi: 10.1021/acsomega.7b00019.

Dean, J.A. 1999. *Lange Handbook of Chemistry*. New York: McGRAW-HILL, INC.

DeYoung, D.H. 1991. Production of Lithium by Direct Electrolysis of Lithium Carbonate United States of America

Di, Y., Z. Wang, S. Tao, and N. Feng. 2013. "A novel vacuum aluminothermic reduction lithium process." *John Wiley & Sons: 4th international symposium on high temperature metallurgical processing*:11-17.

Dove, Patricia M. 1999. "The dissolution kinetics of quartz in aqueous mixed cation solutions." *Geochimica et Cosmochimica Acta* no. 63 (22):3715-3727. doi: https://doi.org/10.1016/S0016-7037(99)00218-5.

Ellestad, R.B, and K.M Leute. 1950. Method of extracting lithium valuables from spodumene ores. Minneapolis,Minnesota, United States of America.
Free, M.L. 2013. *Hydrometallurgy fundamentals and Applications*. New Jersey: John Wiley & Sons Inc.
Fuerstenau, M.C., and K.N. Han. 2003. *Principals of Mineral Processing*. Colorado: Society for Mining, Metallurgy and Exploration Inc.
Gains, L., J. Sullivan, A. Burnham, and I. Belharouak. 2011. Life-Cycle Analysis for Lithium-Ion Battery Production and Recycling. Paper read at Transportation Research Board 90th Annual Meeting, at Washington, DC.
Galaxy Resources Limited. 2011. Galaxy Resources Ltd.
Griffin, A. 2017. Corporate Position Statement, August 2017. Perth, Western Australia: Lithium Australia.
Grosjean, C., P.H. Miranda, M. Perrin, and P. Pogg. 2012. "Assessment of world lithium resources and consequences of their geographic distribution on the expected development of the electric vehicle industry." *Renewable and Sustainable Energy Reviews* no. 16:1735-1744.
Gummow, R.J., M.W. Thackeray, W.I.F. David, and S. Hull. 1992. "Structure and electrochemistry of lithium cobalt oxide synthesised at 400°C." *Materials Research Bulletin* no. 27 (3):327-337.
Guo, H., G. Kuang, H. Wang, H. Yu, and X. Zhao. 2017. "Investigation of Enhanced Leaching of Lithium from α-Spodumene Using Hydrofluoric and Sulfuric Acid." *Minerals* no. 205 (7):1-16.
Habashi, F. 1986. "Pyrometallurgy." In *Principals of Extractive Metallurgy.* New York: Gordon and Breach Science Publishers.
Halmann, M., M. Epstien, and A. Steinfeld. 2012. "Carbothermic reduction of aluminia by natural gas to aluminium and syngas: A thermodynamic study." *Mineral Processing and Extractive Metallurgy Review* no. 5 (33):352-361.
Hampel, C.A. 1972. "Lithium Electrowinning " In *Encyclopedia of Electrochemistry* 778-779. Huntington, New York: Krieger.
Hazen, R.M, and L.W Finger. 1984. "Comparative Crystal Chemistry: In this young and developing discipline, the variations in crystal structure with temperature, pressure, and composition are used to investigate interatomic forces." *American Scientist* no. 72 (2):143-150.
Hocking, M., J. Kan, P. Young, C. Terry, and D. Begleiter. 2016. Lithium 101. Sydney, Australia: The Deutsche Bank, Markets Research
Hurlbut, C.S. 1971. *Dana's Manual of Mineralogy*. New York: Wiley.
Ingham, P.D., I.R. White, and S. Jackson. 2011. Greenbushes Lithium Operations. NI 43-101 Technical Report prepared for Talison Lithium Ltd. . Perth, Western Australia: Talison Lithium Ltd.
International Centre for Diffraction Data. 2009. ICDD. JCPDS.
International Union of Crystallography. 1999. The Prinicpals of X-ray Diffraction.
Ionode Pty Ltd. 2015. Ionode Sealed Gel Electrodes.
Jaskula, B.W. 2017. Lithium. Reston, Virginia, United States: United States Geological Survey
Julien, C., G.A. Nazri, and A. Rougier. 2000. "Electrochemical performances of layered LiM1-Y M'y O2 (M= Ni, Co; M'= Mg, Al, B) oxides in lithium batteries " *Solid State Ionics* (135):121-130.
Kipouros, G.J., and D.R. Sadoway. 1998. Toward New Technologies for the Production of Lithium. Toronto: Journal Of Minerals

Konar, B, D.G Kim, and I Jung. 2018. "Critical thermodynamic optimization of the Li2O-Al2O3-SiO2 system and its application for the thermodynamic analysis of the glass-ceramics." *Journal of the European Ceramic Society*.
Kuang, G., Y. Liu, H. Li, S. Xing, F. Li, and H. Guo. 2018. "Extraction of lithium from β-spodumene using sodium sulfate." *Hydrometallurgy*.
Kulifeev, V.K., V.P. Tarasov, O.N. Krivolapova, and V.V. Miklushevskiy. 2007. New trends in the development of the lithium metallurgy. Paper read at Names 2007, 3rd France-Russia Seminar, at Metz, France
Lier, J. A. Van, P. L. De Bruyn, and J. Th G. Overbeek. 1960. "The soluability of quartz." *The Journal of Physical Chemistry* no. 64 (11):1675-1682. doi: 10.1021/j100840a017.
Linde Group. 2018. Air. Linde Group
Lithium Australia. 2016. About SiLeach.
London, D. 2014. "A petrologic assessment of internal zonation in granitic pegmatites." *Lithos* no. 184-187:74-104.
Mao, H. 1996. Simplified preparation of LIPF6 based electrolyte for non-aqueous batteries. Burnaby, Canada.
Mayer, S.T. 1999. Mixed Lithium Maganese Oxide and Lithium Nickel Cobalt Oxide Positive Electrodes California, United States of America.
Meshram, P., B.D. Pandey, and T.R Mankhand. 2014. "Extraction of lithium from primary and secondary sources by pre-treatment, leaching and separation: A comprehensive review." *Hydrometallurgy* no. 150:192-208.
Mindat. *Spodumene* 1993-2018. Available from https://www.mindat.org/min-3733.html.
Moon, K.S., and F.W. Douglas. 2003. "Surface crystal chemistry in selective flotation of spodumene (LiAl[SiO3]2) from other aluminosilicates." *International journal of mineral processing* no. 72:11-24.
Munoz, J.L. 1969. "Stability relations of LiAISi206 at high pressures." *Minerological Society of America* (2):203-209.
Nicholson, C.I. 1946. Production of lithium compounds. Ottawa, Ontario, Canada.
OutoTec. *HSC Chemictry (7.0), Chemical Reactions and Equalibrum Calculations*. Outotec Pty Ltd 2017. Available from http://www.outotec.com/products/digital-solutions/hsc-chemistry/.
Parr Instrument Company. 2009. Stirred Reactors and Pressure Vessels. Moline, Illinois: Parr Instrument Company.
Partington, G.A., and N.J. McNaughton. 1995. "A Review of the Geology, Mineralization, and Geochronology of the Greenbushes Pegmatite, Western Australia." *Economic Geology* no. 90:616-635.
Pauling's, L. 1932. "The nature of the chemical bond. IV. The energy of single bonds and the relative electronegativity of atoms." *Journal of the American Chemical Society* no. 9 (54):3570-3582.
Phillips, S.L, and D.L Perry. 1995. *Handbook of inorganic compounds*. New York: CRC Press.
Pidgeon, L.M., and J.M. Touguri. 1962. "High-temperature studies of metallurgical process part 11. The thermal reduction of calcined dolomite with silicon." *CanadIan Journal of Chemistry* no. 40:1769-1776.
Queneau, Paul B., and Cornelius E. Berthold. 1986. "Silica in Hydrometallurgy: An Overview." *Canadian Metallurgical Quarterly* no. 25 (3):201-209. doi: 10.1179/cmq.1986.25.3.201.
Rio Tinto. 2014. Rio Tinto Serbia Highlights Innovating to Develop New Resources. Rio Tinto, Serbia.

Rosales, G.D., M.C. Ruiz, and M.H. Rodriguez. 2014. "Novel process for the extraction of lithium from β-spodumene by leaching with HF." *Hydrometallurgy* no. 147:1-6.
ROWE Scientific Pty Ltd. 2018. Products-pH buffers. edited by ROWE Scientific Pty Ltd.
Salakjani, N. Kh., P. Singh, and A.N. Nikoloski. 2016. "Mineralogical transformations of spodumene concentrate from Greenbushes, Western Australia. Part 1: Conventional heating." *Minerals Engineering* no. 98:71-79.
Souza, S.O., G.M. Ferraz, and S. Watanabe. 2004. "Effects of Mn and Fe impurities on the TL and EPR properties of artificial spodumene polycrystals under irradiation." *Nuclear Instruments and Methods in Physics Research* no. 218 B:259-263.
Takeda, O., M. Li, T. Toma, K. Sugiyama, M. Hoshi, and Y. Sato. 2014. "Electrowinning of Lithium from LiOH in Molten Chloride." *Journal of The Electrochemical Society* no. 161 (14).
Talison Pty Ltd, Lithium. 2018. Talison Lithium Vividgroup.
ThermoFisher. 2015. ThermoFisher Catalouge. ThermoFisher Scientific Inc.
Thomas, R, and P Davidson. 2016. "Revisiting complete miscibility between silicate melts and hydrous fluids, and the extreme enrichment of some elements in the supercritical state — Consequences for the formation of pegmatites and ore deposits." *Ore Geology Reviews* (72):1088-1101.
Tianqi Lithium. 2018. Tianqi Lithium Australia. Tianqi Lithium Corporation
TPS Australia. 2018. TPS WP-80. TPS.
Tran, T., and V.T. Luong. 2015. "Lithium Production Processes." In *Lithium Process Chemistry*, 81-124. Gwangju, Korea: Elsevier Inc.
U.S. Department of Health and Human Services. 2004. The Facts About Chlorine New York, United States if America: State Goverment of New York
University of Minnesota. 2010. Pyroxene.
Vikström, H., S. Davidson, and M. Höök. 2013. "Lithium availability and future production outlooks." *Applied Energy* no. 110:252-266.
Walker, W.Q. 2015. Short course on lithium ion batteries: Fundamentals, Thermal preformance and Understanding Paper read at TFAWS 2015 Short Course on Lithium-ion Batteries, at Houston, United States of America.
Wang, T, Y Tong, B Jahn, T Zou, Y Wang, D Hong, and B Han. 2007. "SHRIMP U–Pb Zircon geochronology of the Altai No. 3 Pegmatite, NW China, and its implications for the origin and tectonic setting of the pegmatite." *Ore Geology Reviews* no. 32 (1-2):325-336.
Wanhill, R.J.H. 2014. "Chapter 15 – Aerospace Applications of Aluminum–Lithium Alloys." In *Aluminum-lithium Alloys* 503-535. Butterworth & Heinemann.
Williams, P. 2017. Biggest lithium mine doubles with Greenbushes expansion. March 17.
Yaksic, A., and J.E. Tilton. 2009. "Using the cumulative availability curve to assess the threat of mineral depletion: The case of lithium." *Resources Policy* no. 34:185-194.
Yan, X.Y., and D.J. Fray. 2010. "Molten salt electrolysis for sustainable metals extraction and materials processing – A review." In *Electrolysis: Theory, Types and Applications* 1-48. Cambridge, United Kingdom: Nova Science Publishers, Inc. .
Zelikman, A.N., O.E. Krein, and G.V. Samsonov. 1996. "Lithium." In *Metallurgy of Rare Metals*, 458. Washington D.C.: National Science Foundation.
Zumdahl, S.S. 2013. *Chemical Principles* Illinois, United States of Amercia Brooks/ Cole, Cengage Learning

Appendices

Appendix A - Literature review

This section is incorporated as supporting data for the literature review section of this thesis found in section 2.

Appendix A1 - Relevant tables

Table 5: Lithium based minerals structural formulae and theoretical lithium contents, adopted from Meshram et al. (2014).

Mineral	*Formula*	*Lithium Content (%)*
Spodumene	$LiAlSi_2O_6$	3.73
Lepidolite	$LiKAl_2F_2Si_3O_9$	3.56
Amblygonite	$LiAlFPO_4$	4.74
Triphylite	$LiFePO_4$	4.40
Petalite	$LiAlSi_4O_{10}$	2.27
Bikiaite	$LiAlSi_2O_6.H_2O$	3.28
Eucryptite	$LiAlSiO_4$	5.53
Montebrasite	$Li_2O.Al_2O_3.2SiO_2$	3.93
Jadarite	$LiNaSiB_3O_7(OH)$	3.39
Zinnwaldite	$LiKFeAl_2F_2Si_3O_{10}$	1.7
Hectorite	$Na_{0.3}(Mg, Li)_3Si_4O_{10}(F, OH)_2$	0.56
Zabuyelite	Li_2CO_3	18.75

Table 6: Reported methods and their experimental profiles for the extraction of lithium from β-spodumene, adopted from Kuang et al. (2018).

Methods	*Reagents/Process*	*Direct Product*	*Drawbacks*	*% Li extracted*	*Reference*
Sulfuric acid method	Roasting with 93 % H_2SO_4 (1.4 times higher than theoretical usage) at 523 K for 30 min. Consequential water leach. Roasting with $CaCl_2$ at ore/$CaCl_2$ molar ratio 1:2 and 900 °C for 120 min.	Li_2SO_4	Acid gas emission, high concentration reagents.	92%	(Meshram et al. 2014)
Alkaline processing	Sintering of α-spodumene in the presence of CaO for one hour, followed by a 4-hour water leach at 95ºC. 10:1 L/S ratio at	LiOH	Significant quantities of impurities in the product, massive reagent consumption, CO_2 emissions, complex processing	84%	(Meshram et al. 2014)
Chlorination roasting method	Roasting with pure Cl_2 at 1100 °C for 150 min.	LiCl	High leaching temperature, corrosion resistant equipment required.	90.2	(Barbosa et al. 2014)
Hydrofluoric acid method	Leaching with 7 % HF (S/L ratio 1.82 %, w/v) at 75 °C for 20 min.	LiF	Highly toxic reagent.	90	(Guo et al. 2017)
Sodium carbonate method	Autoclaving with Na_2CO_3 at L/S ratio 4 mL/g, Na/Li ratio 1.25 and 225 °C for 60 min.	Li_2CO_3	Complex steps and high reagent cots.	First step: 94 Second step: 91	(Kuang et al. 2018)

Table 7: Thermodynamic data of spodumene, and lithium products at standard conditions.

Name and Formula	*Molecular weight*	*Molar Volume*	$\Delta H°_{298.15}$	$\Delta G°_{298.15}$	$\Delta S°_{298.15}$	*Cp*	*Ref*
	g/mol	*cm^3*	*kcal /mol*	*kcal/mol*	*kcal/mol.K*	*cal/mol.K*	
Water aqueous (H_2O)	18.02	18.069	-68.315	-56.678	16.718	17.98	(Dean 1999, OutoTec 2017)
Lithium (Li)	6.94	13.017	-	-	-	5.925	(Dean 1999, OutoTec 2017)
Lithium aqueous ion (Li^+)	6.94	-	-66.552	-70.005	11.582	14.259	(Dean 1999, OutoTec 2017)
Lithium Oxide (Li_2O)	29.88	14.76	-142.897	-134.117	-29.447	12.998	(Dean 1999, OutoTec 2017)
Lithium Carbonate (Li_2CO_3)	73.89	-	-290.640	-270.578	-67.288	23.008	(Dean 1999, OutoTec 2017)
Lithium Hydroxide (LiOH)	23.95	-	-115.894	-104.904	-36.860	11.654	(Dean 1999, OutoTec 2017)
Lithium Chloride (LiCl)	42.39	-	-97.578	-91.780	-19.445	11.398	(Dean 1999, OutoTec 2017)
α-Spodumene ($LiAlSi_2O_6$)	186.09	58.37	-730.091	-688.676	-138.908	38.002	(Dean 1999, OutoTec 2017)
β-Spodumene ($LiAlSi_2O_6$)	186.09	78.22	-723.399	-683.772	-132.909	38.911	(Dean 1999, OutoTec 2017)
Analcime ($NaAlSi_2O_6$)	220.16	97.49	-939.680	-886.272	-179.130	48.959	(Dean 1999, OutoTec 2017)

Table 8: Solubility of lithium products at variating temperatures (g/100g H_2O) (Dean (1999), Phillips and Perry 1995) .

Li-Salts	*273.15*	*293.15*	*313.15*	*333.15*	*353.15*	*373.15*
Li_2CO_3	1.54	1.33	1.17	1.01	0.85	0.72
LiCl	69.20	83.50	89.20	98.40	112	128
Li_2SO_4	36.10	34.80	33.70	32.60	31.40	-
$LiHCO_3$	5.80	5.74	-	-	-	-

Appendix A2 - Relevent figures

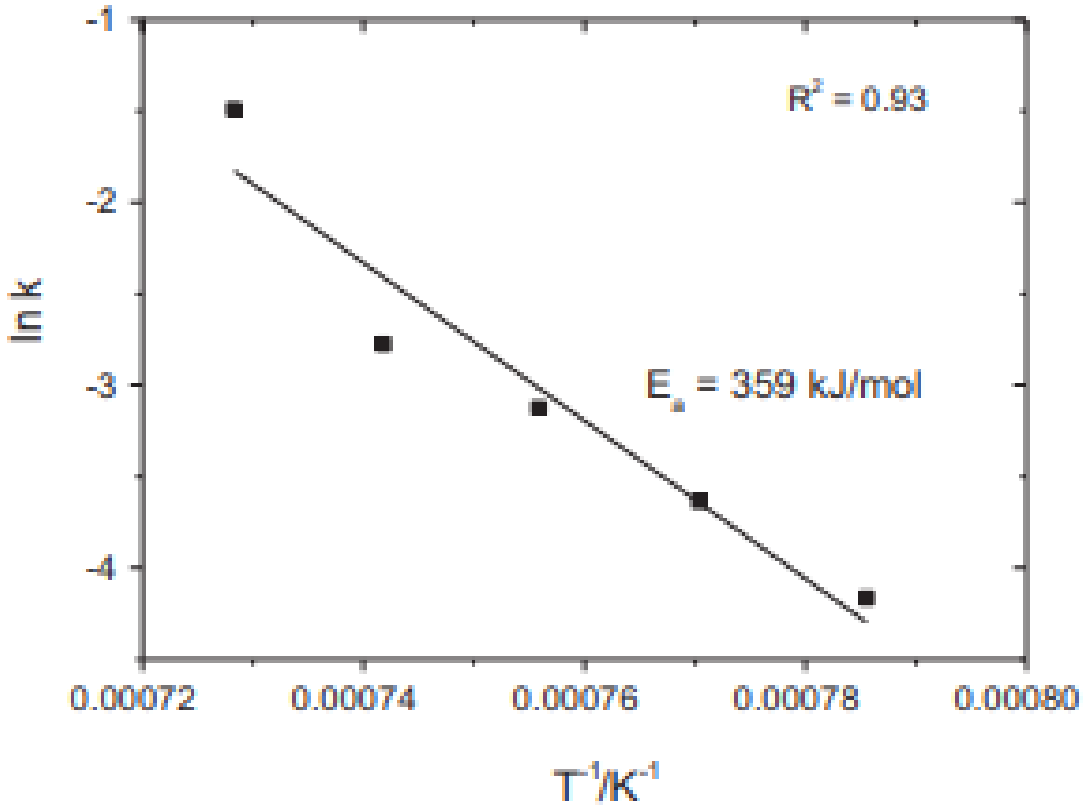

Figure 42: Arrhenius plot for the chlorination of β-spodumene, adopted from Barbosa et al. (2013)

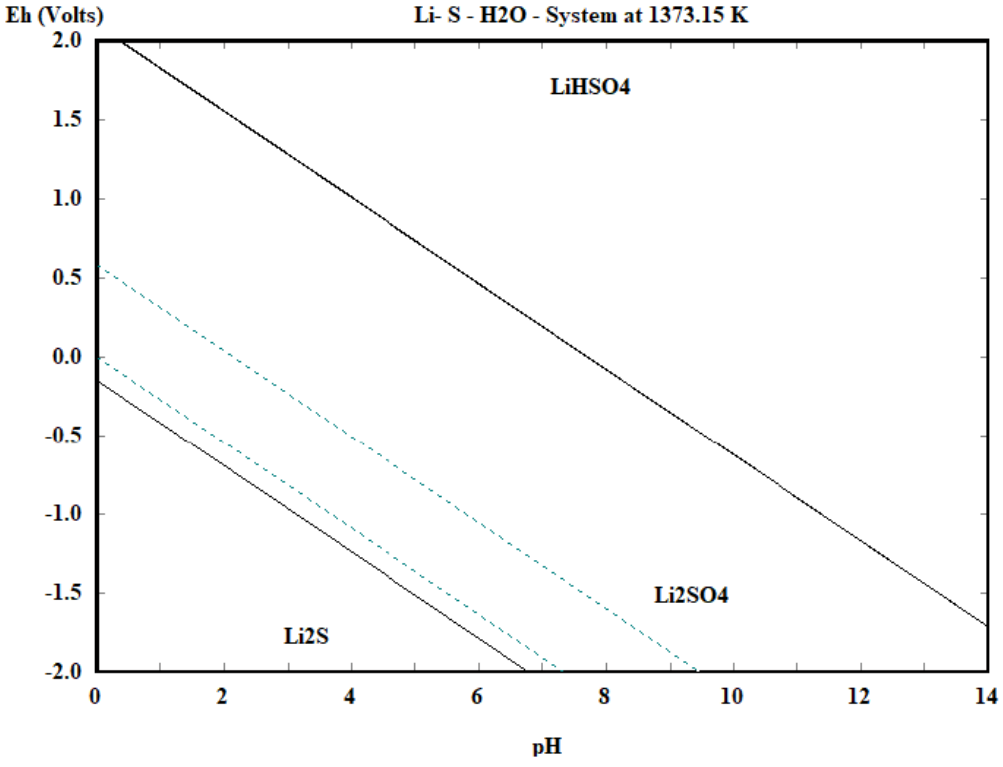

Figure 43: Eh-pH diagram of Li-S-H_2O system at 1373.15 K, adopted from OutoTec (2017)

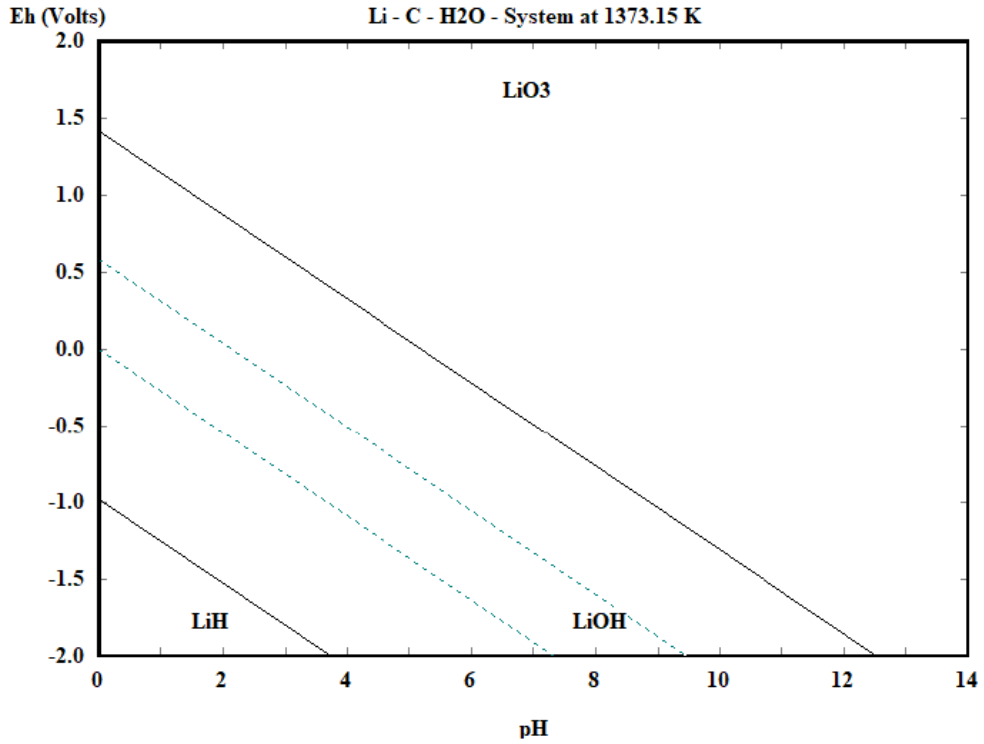

Figure 44: Eh-pH diagram of Li-C-H_2O system at 1373.15 K, adopted from OutoTec (2017)

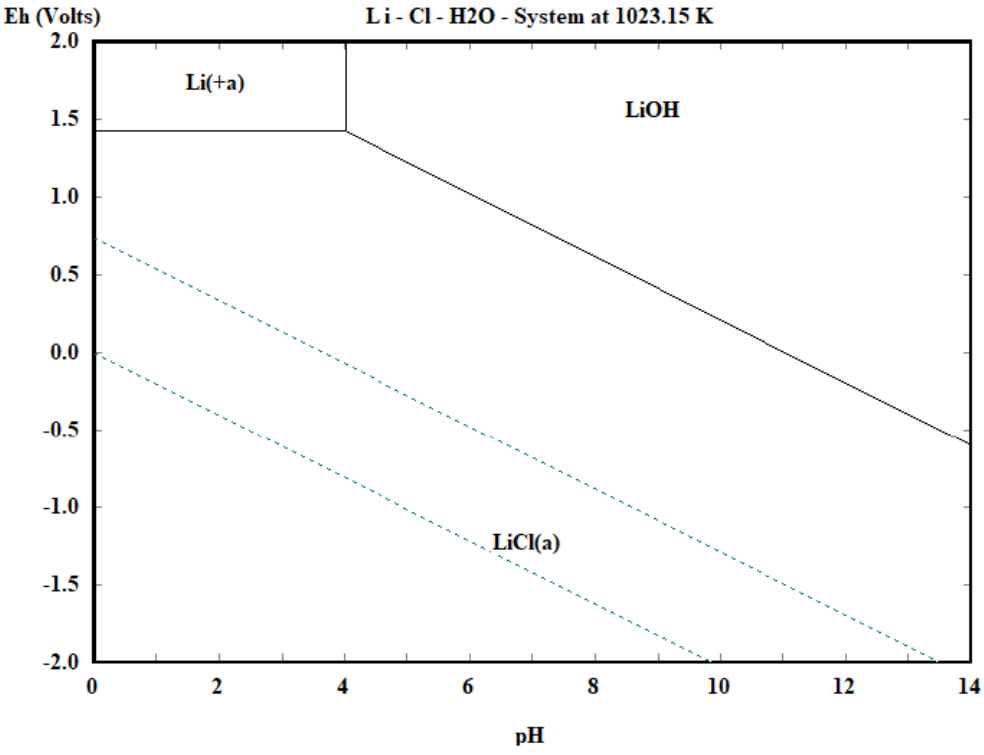

Figure 45: Eh-pH diagram for a Li-Cl-H_2O system at 1023.15 K, adopted from OutoTec (2017)

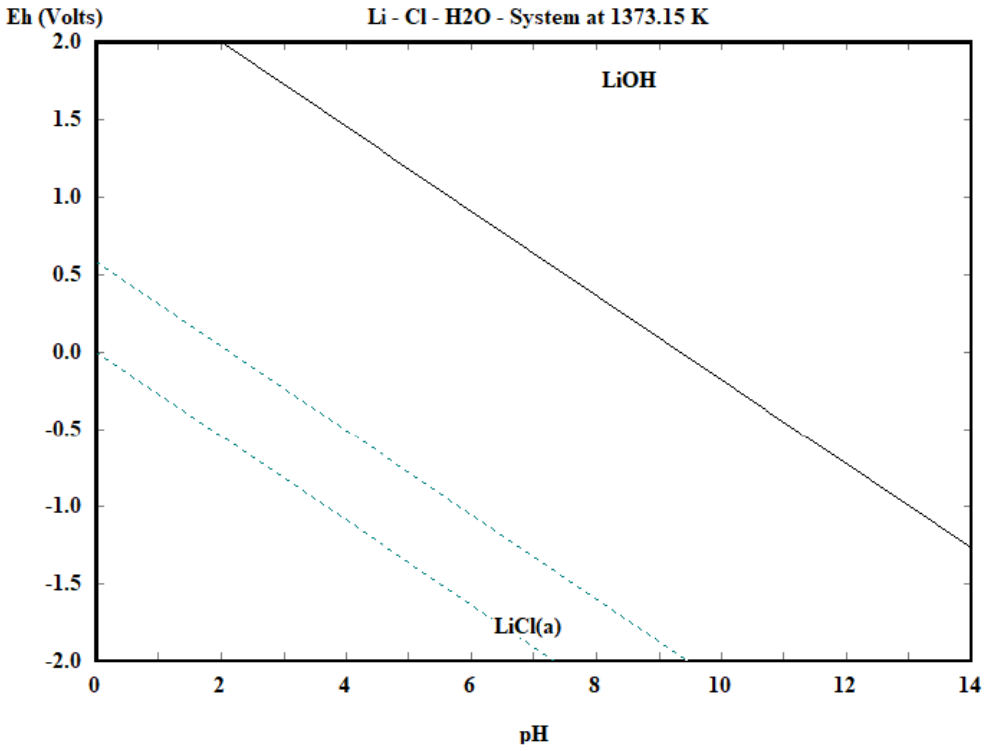

Figure 46: eH-pH diagram for a Li-Cl-H_2O system at 1373.15 K, adopted from OutoTec (2017)

Appendix A3 - Lithium ion batteries

The primary components of lithium ion batteries are the anode, cathode, electrolyte and separator (Figure 20) (Mao 1996). The cathode consists of an aluminium foil that is coated in lithium cobalt oxide ($LiCoO_2$) or lithium nickel dioxide ($LiNiO_2$). The anode consists of copper foil that is coated in graphene. The electrolyte consists of a super saturated solution of lithium hexafluorophosphate ($LiPF_6$). The lithium ions present in the electrolyte intercalate/de-intercalate between the anode and cathode, stimulating an exchange on electrons within the cell. This process is stimulated from the redox reaction occurring at the anode and cathodes, represented by equations 55 and 54 below.

Overall Cell Reaction

$$CoO_2 + LiC_2 \rightarrow LiCoO_2 + C_6 \text{ of which } E^0_{298\ K} = 4V \quad (55)$$

Cathodic Reaction

$$CoO_2 + Li^+ + e^- \rightarrow LiCoO_2 \quad (56)$$

Anodic Reaction

$$LiC_6 \rightarrow Li^+ + C_6 + e^- \quad (57)$$

The redox flow throughout the battery sees the discharge point occurring at the cathode, and charging point occurring at the anode (Figure 20). The cycling of charges between the two electrodes stimulates a flow of electrons in an external circuit, which provides the battery with a point connection to an external circuit.

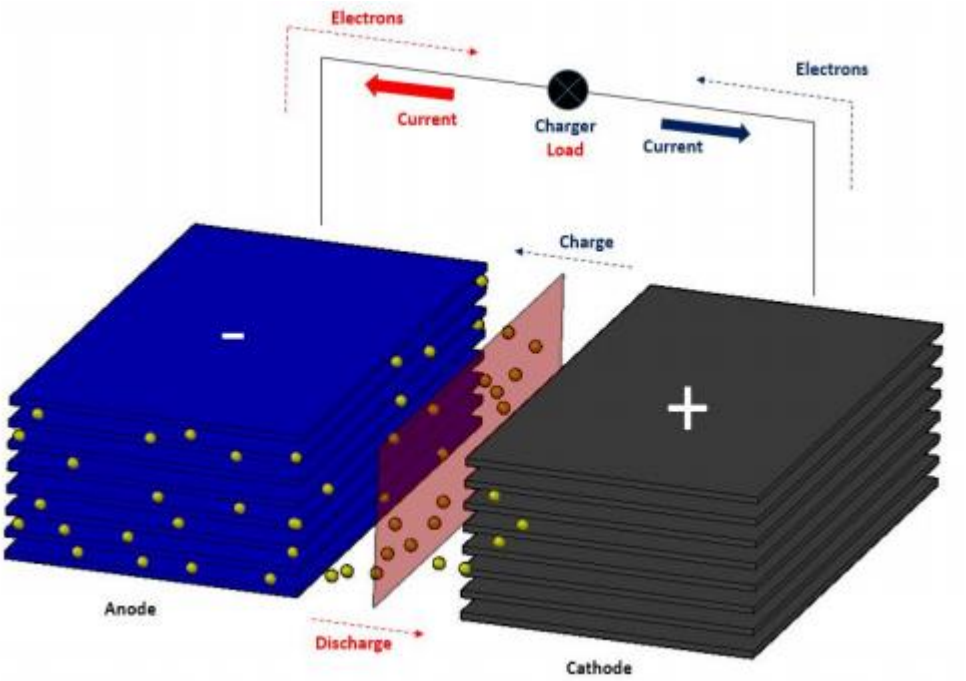

Figure 47: Schematic of a battery displaying the flow of ions, adopted from Walker (2015)

The Binding agents

The binding agents utilised by $LiCoO_2$ contains 10 g of polyvinlidene fluoride (PVDF) powder and 100 mL of dimethylformamide (DMF) of which are combined together and mixed at 323.15 K for 1 hour. 50g of cathode oxide is combined with 5.40 g of SFG-15 graphite adhesive and 2.10 g of carbon. Finally, approximately 16.55 g of additional DMF was added to the mixture as a smoothing agent.

The final cathode is meant to consist of 90 weight % of cathodic material, 5 weight % carbon and 5% binding agent.

Appendix B - Supporting experimental material

Appendix B1 - Supporting equipment

Equipment

Parr instruments Autoclave reactor system

Parr instruments 4523 general purpose reactor system in conjunction with a 4848 PID controller and Alloy 400 autoclave lining were utilised as the leaching system throughout this project (Parr Instrument Company 2009).

Figure 48: Parr instruments 4523 general purpose reactor system utilised throughout this project, adopted from Parr Instrument Company (2009)

TPS WP-80 pH-MV-Temperature meter (TPS Australia 2018)

A pH-MV-Temperature probe purchased from TPS Australia was utilised as the meter throughout the experiments conducted. This meter utilised standard rechargeable A2 batteries and was calibrated prior to each test being conducted.

*Figure 49: TPS's WP-80 pH- MV- Temperature meter*_ENREF_75*TPS Australia (2018).*

Ionode Pty Ltd.'s IH- 40C pH probe (Ionode Pty Ltd 2015).

Ionode's IH-40C pH probe was utilised throughout the tests conducted. The product specifications of the probe are attached in Table 9, below.

Figure 50: Ionode's IH-40C pH probe (Ionode Pty Ltd 2015)

Table 9: Product specifications of TPS's IH-40C probe (Ionode Pty Ltd 2015).

Body:	Polypropylene
Temp Range:	0 - 60°C
pH Range:	0 - 14 pH
pH Sensor:	C Glass Bullet
Reference:	Double Junction Ag/AgCl Gel
Slope:	>97%
Zero pH:	7.0 ± 0.5
Cable Length:	1m. Standard (Max. 20m)

The probe was stored in 3 molar KCl solution when not in use and was washed with de-ionised water prior and post use. The probe was also calibrated prior to each test utilising standard pH buffer solutions at pH of 4,7 and 10. The buffer utilised throughout this project was ROWE Scientific's standardised buffer solutions (ROWE Scientific Pty Ltd 2018).

Supporting operational material

The attached material is supporting operation procedures for the XRD and SEM. A flowsheet for a standard leach utilising the autoclave is also attached for greater understanding.

Leaching flowsheet

Below is a simplified test work flowsheet conducted on all leaches, it is assumed that all prestart checks and safety procedures have been addressed prior to this point:

1. Tare a 500 mL plastic beaker on a scale and place 240.00 g of DI water into the tared beaker
2. Weigh out *x* g of NaOH utilising 4 decimal point scale
3. Pour all NaOH into 500 mL beaker holding the 240g of DI water (MAKE SURE TO HAVE A WATCH GLASS OVER THE TOP OF BEAKER, to reduce evaporation losses due to exothermic nature of reaction taking place) Caution HOT.
4. Wait for caustic solution to reach ambient temperature and weigh solution mass before heading to autoclave room
5. Place spodumene sample into pre weighed empty autoclave
6. Pour entire contents of caustic solution into clave and record the pH and initial mass. Weigh the 500 mL beaker after this to account for losses.
7. Begin autoclave assembling procedure by mounting the autoclave into the fixed reactor head. Make sure to evenly secure the clamps and tighten the bolts appropriately. Refer to specialised assistance is required.

8. Pre load the autoclave with 200 kPa worth of pressure to ensure assemblage has occurred correctly. Check for leaks with soapy water. If no leaks, then pressurisation can occur.
9. Pressurise to 1000 kPa.
10. Remove gas loading assembly by closing off the gas bottles isolation valve followed by the attached regulators valve. Once closed the two isolation valves on the autoclave head can be closed. The two safety valves that operate in series across the gas link connecting the gas bottle to the clave can then be closed.
11. Once all gas valves are isolated, the pressure line connecting the autoclave to the gas bottle can be disconnected. (BE WARY OF ANY RESIDUAL PRESSURE TRAPPED IN THE LINE)
12. Once disconnected and the autoclave is sealed and pressurised the heating sequence can begin. The impellor can also be set to the standardised 300 rpm to begin agitating the contents of the autoclave.
13. Wait within a safe but accessible vicinity to the autoclave to evaluate its heating sequence to ensure a stable operation. Turn on the ventilation system to the room.
14. Record time, temperature and pressure once the autoclave has reached operating temperature. Repeat this process every 15 minutes to account for a safe and stable operation.

END LEACH (ENSURE ALL CORRECT PPE IS WORN)

15. Once predetermined residence time has been achieved the cooling sequence can be initiated. Set operating temperature to ambient temperature of the room and step away.
16. Wait outside of the autoclave operational area for it to cool via its internal cooling system
17. Once cooled to ambient temperature commence de-pressurisation by slowing venting the autoclave through one of its marked gas vent valves.
18. Begin the de-assembling sequence.
19. Weigh the contents of the autoclave and record its pH. Take photos and record any necessary observations.
20. Assemble a Buchner filter under the influence of a vacuum. Line the filter with two Whatman^{TM} grade 1 filter papers.

21. Mix and pour the entire contents of the autoclave into the filter and allow separation to occur.
22. Collect a 20 mL sample of the filtrate for solution analysis. Dilute the 20 mL sample in 100 mL of DI utilising a volumetric flask. Shake flask and pour 30 ml from the contents of the volumetric flask into a sterile vial, for assay.
23. Collect all the contents of the volumetric flak by placing the residual solution into new sterile 100 mL sample container.
24. Tare a 10ml volumetric flask on a 4 decimal point scale. Place 10 ml of the leach filtrate into the 10 ml volumetric flask and recorded the mass. From the mass of the solution the specific gravity of the solution is determined (refer to B3 for calculations).
25. Once the mass of the 10 ml volumetric flask is collected, the contents can be emptied back into the bulk filtrate in the Buchner filter. Take and record a pH reading of the filtrate to ensure solution is stable. Pour entire contents of filtrate into a 500 mL plastic container for storage.
26. Begin washing cycle of the residue by utilising DI water as a wash solution. Make sure the entire contents of the autoclave is emptied into the Buchner filter. Once the entire contents of the autoclave is cleared leave it aside to dry.
27. Fill the contents of Buchner funnel to the 1000 ml mark on the vacuumed flask utilising the DI water. Make sure to pour the DI water into bed level volumes, ensuring the solid residues are being "washed'.
28. Collect a sample of the wash solution for assay (20 mL is sufficient). Dispose of the remainder.
29. Repeat the wash steps another two times with DI water to ensure the solid residues are washed. Collect 20 mL subsample of the wash for assay.
30. Collect the washed solids from the Buchner filter and place them in the 60-degree oven for drying (leave for 2 days to dry sufficiently).
31. Weigh the dried post mass of the clave to account for samples sticking to the clave
32. Weigh the solid samples after two days' worth of drying and split into two even portions by mass.
33. Ring pulverise one half of the residue sample for XRD and peroxide fusion digestion and ICP-MS analysis. The remaining half is riffle split out into a 5 g representative sample for SEM analysis. All residues are then bagged and stored in a secured, cool dry pace.

XRD

Starting the machine:

1. Confirm power connection to water cooler and the XRD has been switched on.
2. Turn rotary switch on.
3. Select the ‘Control power on’ button located on the spellman DF3 panel.
4. Ensure correct slits have been inserted into XRD.
5. Select the ‘X Ray On’ button located on the generator control panel
6. Ensure start up voltage is set to 20 kV and current at 10 mA.
7. After 10 minutes, slowly raise the voltage to 35 kV and the current to 28 mA.
8. Place prepared samples into their respective holders.
9. Start up the visX112E operating software and set up the data collection
10. Start the Auto Loader Batch to allowing sample analysis.

Turning off Instrument:

1. Turn kV and mA down to start values of 20 kV and 10 mA.
2. Select the ‘X-Ray off’ button to turn off generator.
3. Turn off the water cooler.
4. Turn off rotary switch to shut down power to XRD.

SEM

Sample Preparation:

Resin

1. Prepare the resin mixture by adding Epohy Resin and EpoFix Hardener at a ratio of 5 to 1 to a large weigh boat. Mix consistently for 2 minutes to ensure resin is homogenous.
2. Add solid sample to the base of a 25 mm SEM sample mould.
3. Top up mould with resin mixture and leave to set overnight.
4. Remove set resin sample from mould, polish and place in a vacuum desiccator overnight.
5. Undertake sample carbon coating process.

Tabs

1. Place 20 g worth of sample into weigh boat and spread until uniform layer covers the face of the boat.
2. Remove SEM tab from the package and remove protect sheath from the sticky face of the tab.
3. Place sticky face of the tab into the sample, allowing for sample to attach to the face
4. Attach the correct SEM plate for loose particle analysis and conduct SEM operation

SEM/EDX Operation:

1. Turn on computer, select JCM-6000 login and wait for software to load. Ensure aperture is in correct position.
2. Select the ON/OFF button to turn on SEM and select the 'Vent' button on the computer screen.
3. Slowly open the SEM door once the chamber has released.
4. Carefully place the sample into holder and place into the SEM sample stage, securing the latches.
5. Slowly close and secure SEM door, holding for 2 seconds.
6. Once the SEM chamber evacuation has been complete and the software has run a full auto adjustment, SEM images can be taken.

SEM/EDX Sample Removal and Shutdown:

1. Select 'filament' in the software interface and allow to cool for 2 minutes.
2. Select the 'Vent' button, allow chamber to vent and the door to release.
3. Slowly pull out door, loosen latches and remove sample holder from SEM.
4. Close the chamber door, hold for 2 seconds and wait for chamber to evacuate.
5. Select the 'Power Off' button in the software interface, select 'yes' to the alert message and 'ok' to the following message.
6. Exit the SEM computer software

Appendix B2 - Supporting results section

Supporting experimental data and analysis is found throughout this section. This includes all supporting assay data, calculated balances and operational variables.

Relevant tables

Table 10: Summary table of the leaching variables investigated and their respective lithium extraction, silicon dissolution and sodium reformation with corresponding accountabilities

Test Nº # 	Atmosphere (Air/CO_2) 	NaOH (Moles) 	Temperature (Kelvin) 	Residence time (Hr's) 	Particle size (μm) 	Li extraction (%) 	Li accountability (%) 	Si dissolution (%) 	Si accountability (%) 	Na reformation in leach residue (+ %) 	Na accountability (%)
1	Air	**8**	573.15	3	325	23.62	82.63	28.98	100.99	71.57	146.80
2	Air	**12**	573.15	3	325	32.41	89.78	34.69	96.60	101.53	106.41
3	Air	**14**	573.15	3	325	41.48	105.26	37.63	85.67	97.64	130.28
4	Air	14	**533.15**	3	325	37.41	104.08	31.14	97.81	79.65	122.07
5	Air	14	**553.15**	3	325	40.52	100.80	34.28	86.27	92.99	109.11
6	Air	14	573.15	**1**	325	28.93	100.00	29.00	100.00	68.99	120.61
7	Air	14	573.15	**6**	325	44.25	96.19	37.17	86.49	117.55	134.87
8	Air	14	573.15	3	**32**	31.11	105.7	36.52	90.41	99.60	128.79
9	Air	14	573.15	3	**106**	32.41	102.83	34.64	106.66	95.78	135.23
10	**CO_2**	14	573.15	3	325	40.76	87.46	44.77	82.12	81.68	141.42

Table 11: Summary table of relevant operating variables and measured pH, specific gravity and feed moisture of each test.

Test Nº # 	Feed (g) 	Residue (g) 	Pre leach pH (0-14) 	Post leach pH (0-14) 	Loading pressure (kPa) 	Average operational pressure at temp (kPa) 	Pressure flux upper and lower bounds (max/min, %) 		Specific gravity of filtrate (g/mL) 	Feed moisture (%)
1	80.0022	79.8900	10.76	12.03	1000	7950	3.02	4.40	1.27	0.0083
2	80.0270	79.8901	10.00	11.28	1000	7360	1.63	4.48	1.34	0.0083
3	80.0019	76.8610	10.92	12.03	1000	5720	4.90	7.34	1.39	0.0083
4	80.0022	79.9800	10.37	11.38	1000	4100	5.37	9.76	1.43	0.0083
5	80.0000	79.9902	10.37	12.07	1000	5260	6.08	3.42	1.41	0.0083
6	80.0000	74.3301	10.94	11.43	1000	6660	1.05	2.55	1.40	0.0083
7	80.0110	79.9203	10.92	11.18	1000	6600	3.49	5.00	1.39	0.0083
8	80.0014	78.9000	10.37	11.94	1000	6790	2.36	6.63	1.39	0.0083
9	80.0001	79.5480	10.93	11.33	1000	6990	1.29	5.01	1.40	0.0083
10	80.0017	69.8720	10.89	11.76	1000	4900	6.12	12.25	1.39	0.0083

Table 12: Raw ICP-MS results conducted on the spodumene concentrate utilised as feed material throughout this project.

Element	Ag (ppm)	Al (%)	Ba (ppm)	Be (ppm)	Bi (ppm)	Ca (ppm)	Cd (ppm)	Co (ppm)	Cr (ppm)	Cu (ppm)	Fe (%)	K (ppm)
	<2	14.0	<5	10	<10	200	<5	<5	800	44	1.02	2000

Element	Li (%)	Mg (ppm)	Mn (ppm)	Mo (ppm)	Na (ppm)	Ni (ppm)	P (ppm)	Pb (ppm)	SiO2 (%)	Sr (ppm)	Ti (ppm)	V (ppm)	Y (ppm)	Zn (ppm)
	3.53	<400	400	<5	1200	10	200	25	63.6	2	<200	<40	<100	14

Table 13: Analysis and balance on test 1- 8M NaOH leach conducted

	Ore (g)	NaOH (g)	DI (g)	Solution (g)		Total out (g)	Residue (g)	Soln out (mL)	SG filtrate (g/mL)		
	80.0022	83.34	240.00	242.61		388.00	79.89	242.61	1.270		
Element	Feed (%)	Feed (g)				Residue (%)	Residue (g)	Aq (g/L)	Wash (g/L)	Extraction (%)	Accountability (%)
Li	3.53	2.82				2.70	2.16	0.43	0.29	23.62	82.63
Si	29.79	23.79				21.10	16.89	17.48	11.91	28.98	100.99
Na	-	0.12				10.90	8.71	156.95	97.95	+ 71.51	146.80

Table 14: Analysis and balance on test 2- 12M NaOH leach conducted

	Ore (g)	NaOH (g)	DI (g)	Solution (g)		Total out (g)	Residue (g)	Soln out (mL)	SG filtrate (g/mL)		
	80.03	133.44	240.00	371.17		435.00	79.89	264.60	1.342		
Element	Feed (%)	Feed (g)				Residue (%)	Residue (g)	Aq (g/L)	Wash (g/L)	Extraction (%)	Accountability (%)
Li	3.53	2.82				2.40	1.91	1.95	0.42	32.41	89.78
Si	29.79	23.79				19.50	15.54	24.02	4.12	34.69	96.60
Na	-	0.12				15.40	12.30	214.55	47.78	+ 101.53	106.41

Table 15:Analysis and balance on test 3- 14M NaOH leach conducted this is also the baseline test

	Ore (g)	NaOH (g)	DI (g)	Solution (g)		Total out (g)	Residue (g)	Soln out (mL)	SG filtrate (g/mL)		
	80.0019	166.68	240.00	404.88		446.00	76.86	265.57	1.390		
Element	Feed (%)	Feed (g)				Residue (%)	Residue (g)	Aq (g/L)	Wash (g/L)	Extraction (%)	Accountability (%)
Li	3.53	2.82				2.15	1.65	2.91	2.06	41.48	105.26
Si	29.79	23.79				19.30	14.83	8.98	11.90	37.63	85.67
Na	-	0.12				15.40	11.84	246.70	179.66	+ 97.64	130.28

Table 16: Analysis and balance on test 4- 533.15 K leach conducted

	Ore (g)	NaOH (g)	DI (g)	Solution (g)		Total out (g)	Residue (g)	Soln out (mL)	SG filtrate (g/mL)		
	80.0022	166.68	240.00	404.06		465.00	79.98	268.86	1.432		
Element	Feed (%)	Feed (g)				Residue (%)	Residue (g)	Aq (g/L)	Wash (g/L)	Extraction (%)	Accountability (%)
Li	3.53	2.82				2.20	1.77	3.05	1.31	37.41	104.08
Si	29.79	23.79				20.48	16.38	19.22	6.39	31.14	97.81
Na	-	0.12				12.1	9.68	285.25	114.60	+ 79.65	122.07

Table 17: Analysis and balance on test 5- 553.15 K leach conducted

	Ore (g)	NaOH (g)	DI (g)	Solution (g)		Total out (g)	Residue (g)	Soln out (mL)	SG filtrate (g/mL)		
	80.0000	166.68	240.00	404.06		460.00	79.99	269.06	1.412		
Element	Feed (%)	Feed (g)				Residue (%)	Residue (g)	Aq (g/L)	Wash (g/L)	Extraction (%)	Accountability (%)
Li	3.53	2.82				2.10	1.68	3.35	0.99	40.52	100.80
Si	29.79	23.79				19.50	15.63	13.37	4.80	34.28	86.27
Na	-	0.12				14.10	11.28	270.95	76.42	+ 92.99	109.11

Table 18: Analysis and balance on test 6- 1hour residence time leach conducted

	Ore (g)	NaOH (g)	DI (g)	Solution (g)		Total out (g)	Residue (g)	Soln out (mL)	SG filtrate (g/mL)		
	80.0000	166.68	240.00	404.85		469.00	74.33	285.24	1.398		
Element	Feed (%)	Feed (g)				Residue (%)	Residue (g)	Aq (g/L)	Wash (g/L)	Extraction (%)	Accountability (%)
Li	3.53	2.82				2.70	2.01	2.87	0.89	28.93	100.00
Si	29.79	23.79				22.44	16.68	15.71	9.59	29.90	100.40
Na	-	0.12				11.30	8.40	283.25	93.20	+ 68.94	120.61

Table 19: Analysis and balance on test 7- 6 hour residence time leach conducted

	Ore (g)	NaOH (g)	DI (g)	Solution (g)		Total out (g)	Residue (g)	Soln out (mL)	SG filtrate (g/mL)		
	80.0110	166.68	240.00	404.90		455.00	79.92	269.84	1.390		
Element	Feed (%)	Feed (g)				Residue (%)	Residue (g)	Aq (g/L)	Wash (g/L)	Extraction (%)	Accountability (%)
Li	3.53	2.82				1.97	1.57	2.65	1.58	44.25	96.19
Si	29.79	23.79				18.70	14.95	10.80	10.06	37.17	86.49
Na	-	0.12				17.80	14.23	265.35	161.73	+ 117.55	134.87

Table 20: Analysis and balance on test 8- 32 µm P_{80} leach conducted

	Ore (g)	NaOH (g)	DI (g)	Solution (g)		Total out (g)	Residue (g)	Soln out (mL)	SG filtrate (g/mL)		
	80.0014	166.68	240.00	404.89		460.00	78.90	273.60	1.393		
Element	Feed (%)	Feed (g)				Residue (%)	Residue (g)	Aq (g/L)	Wash (g/L)	Extraction (%)	Accountability (%)
Li	3.53	2.82				2.47	1.95	2.45	1.36	30.99	105.9
Si	29.79	23.79				19.20	15.12	9.71	13.74	36.41	90.56
Na	-	0.12				15.30	12.07	260.05	147.69	+ 99.60	128.79

Table 21: Analysis and balance on test 9- 106 µm P_{80} leach conducted

	Ore (g)	NaOH (g)	DI (g)	Solution (g)		Total out (g)	Residue (g)	Soln out (mL)	SG filtrate (g/mL)		
	80.0001	166.68	240.00	404.10		468.00	79.89	278.03	1.397		
Element	Feed (%)	Feed (g)				Residue (%)	Residue (g)	Aq (g/L)	Wash (g/L)	Extraction (%)	Accountability (%)
Li	3.53	2.82				2.40	1.92	3.55	0.92	32.14	111.95
Si	29.79	23.79				19.50	15.55	25.39	9.94	34.63	106.67
Na	-	0.12				14.60	11.61	334.65	90.94	+ 95.78	135.23

Table 22: Analysis and balance on test 10- CO_2 leach conducted

	Ore (g)	NaOH (g)	DI (g)	Solution (g)		Total out (g)	Residue (g)	Soln out (mL)	SG filtrate (g/mL)		
	80.0017	166.68	240.00	404.90		453.00	69.87	275.63	1.390		
Element	Feed (%)	Feed (g)				Residue (%)	Residue (g)	Aq (g/L)	Wash (g/L)	Extraction (%)	Accountability (%)
Li	3.53	2.82				2.46	1.72	2.65	2.09	39.14	87.46
Si	29.79	23.79				8.61	13.14	8.61	14.59	44.77	82.14
Na	-	0.12				14.20	9.92	260.30	196.22	+ 81.68	141.42

Relevant figures

A comparative pie graph (Figure 51) was constructed around Test 3, displaying the elemental composition of the feed and residue materials. Figure 51 displays the 41.48% lithium extraction, 37.63% silica and 1.1% aluminium dissolution, with a 154.00% rise of the sodium present in the leach residue against the initial sodium concentration in the feed material. A detailed discussion on the potential reaction mechanisms of this leaching system can be found throughout section 5, with future studies recommended in section 6.

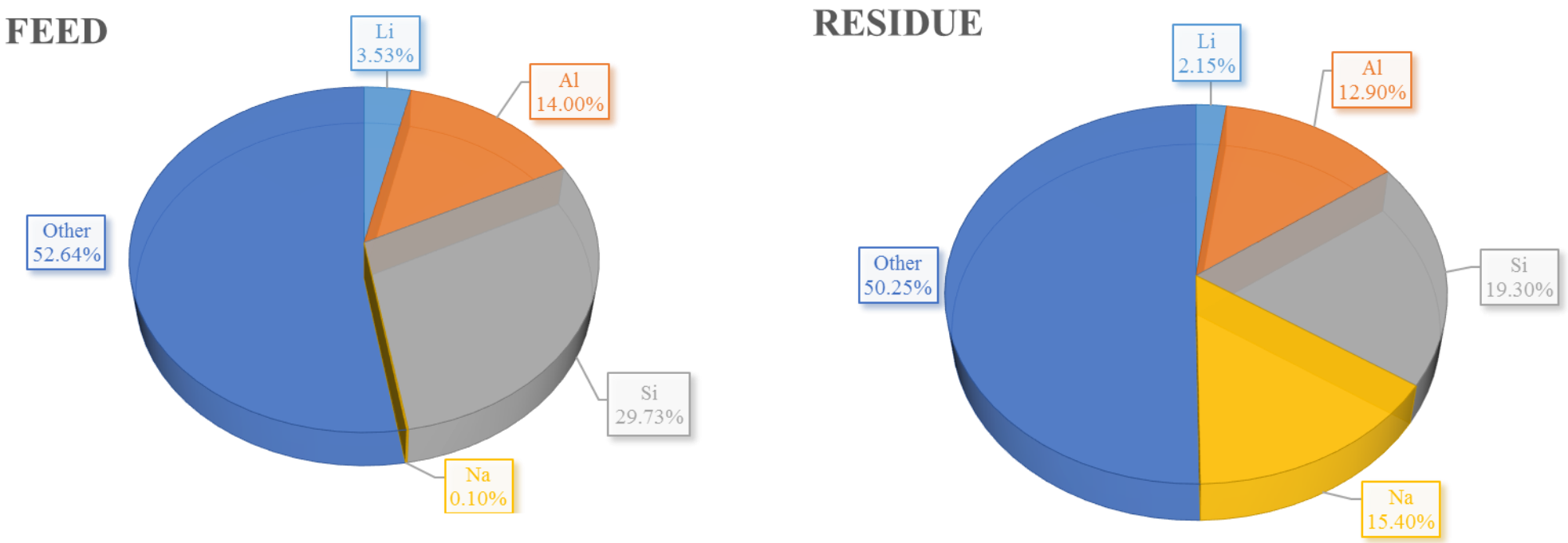

Figure 51: Feed vs residue comparison from the ICP-MS data collected for test 3

Table 23: ICP MS results for test 3's grab sample on the separated layers of the filtrate and wash solution

	Ore (g)	NaOH (g)	DI (g)	Solution (g)		Total out (g)	Residue (g)	Soln out (mL)	SG filtrate (g/mL)			
	80.0019	166.68	240.00	404.88		446.00	76.86	265.57	1.390			
Element	Feed (%)	Feed (g)				Residue (%)	Residue (g)	Aq (g/L)	Wash (top) (g/L)	Wash (bottom) (g/L)	Extraction (%)	Accountability (%)
Li	3.53	2.82				2.15	1.65	2.91	0.04	2.02	41.48	105.26
Si	29.79	23.79				19.30	14.83	8.98	1.80	10.10	37.63	85.67
Na	-	0.12				15.40	11.84	246.70	3.86	175.80	+ 97.64	130.28

Appendix B3 - Supporting calculations

Na: Li molar equivalence calculations, ensuring that Na isn't the limiting reagent

Solving for Li contents in spodumene sample utilised in this project

$= 80\ g\ (ore) \times 3.53\ \%\ (feed\ assay) = 2.824\ g$ of Li in spodumene concentrate

Therefore, there is:

$$\frac{6.941\frac{g}{mol}\ (Li)}{186.09\frac{g}{mol}of\ (spodumene)}$$

$$= 3.72992\ \%\ Li\ in\ spodumene\ (Theoretical)$$

So calculating for Na in NaOH

$$\frac{22.9898\frac{g}{mol}\ (Na)}{39.997\frac{g}{mol}of\ (NaOH)}$$

$$= 57.478811\ \%\ Na\ in\ NaOH\ (Theoretical)$$

Therefore, to find the 1:1 ratio for Li: Na

$$\frac{80.00g\ (ore)}{186.0899\frac{g}{mol}of\ (spodumene)}$$

$$= 0.429899742\ mol$$

Of which

$$\frac{3.53\ \%\ (Li\ actual)}{3.72992\ \%\ (Li\ in\ spodumene, theoretical)}$$

$$= 94.64009452\ \%\ compared\ to\ theoretical$$

Therefore

$$= 0.429899742\ mol\ \times\ 94.64009452\ \%$$

So the moles of Li in concentrate is:

$$= 0.4068575437\ moles\ of\ Li\ in\ the\ ore$$

Accounting for the OH in NaOH

$$n = \frac{m}{M}$$

$$0.4068575437\ moles = \frac{x}{39.997\ \frac{g}{mol}}$$

$$x = \ 16.27308118\ g\ @\ 100\%\ NaOH$$

Therefore, accounting for the impurities present (97.5 % is the purity of NaOH utilised throughout this project.

$$x = \frac{16.27308118}{100} \times 0.975$$

$$15.86625415\ g\ @\ 97.5\%\ NaOH$$

Therefore, dosage required is:

$$= 16.27308118\ g + \ 0.4068270295\ g$$

$$= 16.68\ g$$

Therefore, for 80 g of spodumene ore 16.68 g of NaOH is required for a 1:1, Li: Na ratio.

NaOH molar calculations

Mass of NaOH (g)	Mass of DI (g)	Total Mass (g)	Specific gravity (g/mL)	Volume of solution (L)	NaOH (g/L)	Moles of NaOH (actual moles)
83.34	240.00	323.34	1.270	0.25	327.34	8.18
133.44	240.00	373.44	1.342	0.28	479.53	11.99
166.68	240.00	406.68	1.390	0.29	569.70	14.24

Specific gravity calculations

Once the flask is tared

$$Specific\ gravity = \frac{x\ (mass)}{10\ mL}$$

$$x\frac{g}{L} = \frac{x\frac{g}{mL}}{1000}$$

Accountability calculations

$$\sum \frac{in}{out}\ per\ element\ or\ compound$$

Na substitution calculations

$$Na\ substitution\ (\%) = \frac{Na\ in\ residue - Na\ in\ feed}{Na\ in\ feed}$$

This is interpreted as an addition in % terms from the initial mass of Na in the feed material.

Appendix B4 - Supporting grind establishment data

106µm

Table 24: Grind establishment conducted on spodumene concentrate to achieve P_{80} of 106µm

Size fraction (µm)	Weight (g)	Weight (%)	Cumulative passing (%)
(+) 320	0.9	1	99
320-200	4.8	6	93
200-150	5.2	6	86
150-100	10.1	13	74
100-50	38.7	48	20
(-) 50	21.3	27	5
Total	80.0	100	-

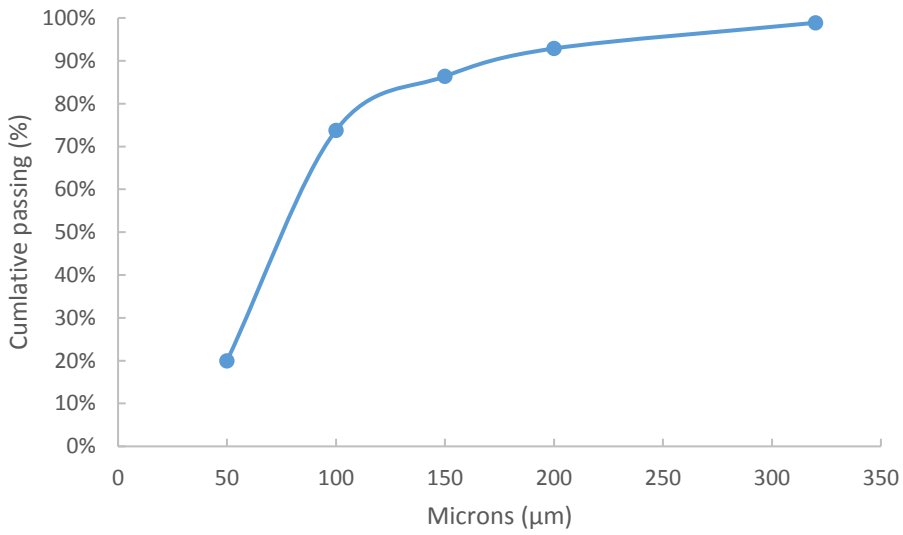

Figure 52: Laser sizing curve displaying the P_{80} is 106µm

32µm

Table 25: Grind establishment conducted on spodumene concentrate to achieve P_{80} of 32 µm

Size fraction (µm)	Weight (g)	Weight (%)	Cumulative passing (%)
(+) 100	3.9	5	95
100-75	2.1	3	93
75-50	3.8	5	88
50-32	10.0	13	75
(-) 32	60.2	75	0
Total	80.01	100	100

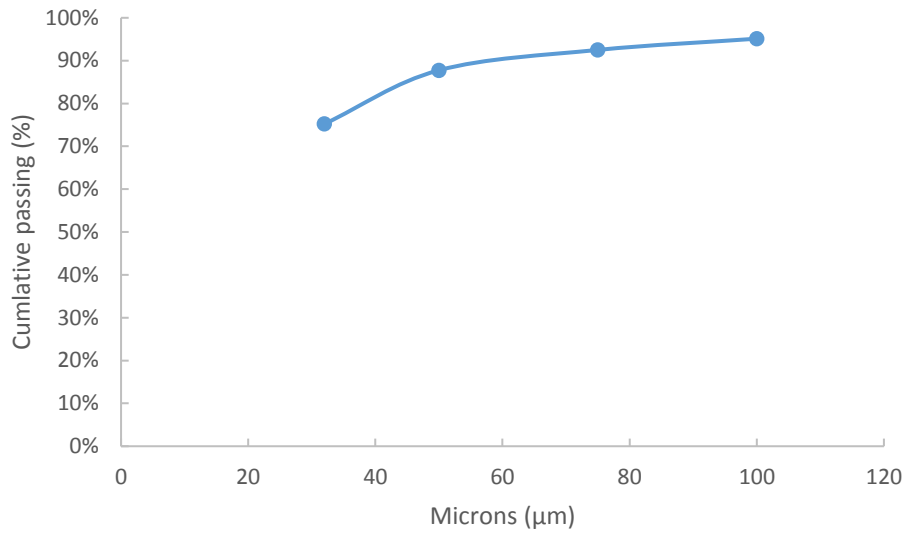

Figure 53: Laser sizing curve displaying the P_{80} is 32µm

Appendix B5 - Pictures

Figure 54: Picture captured of test 3's wash solution

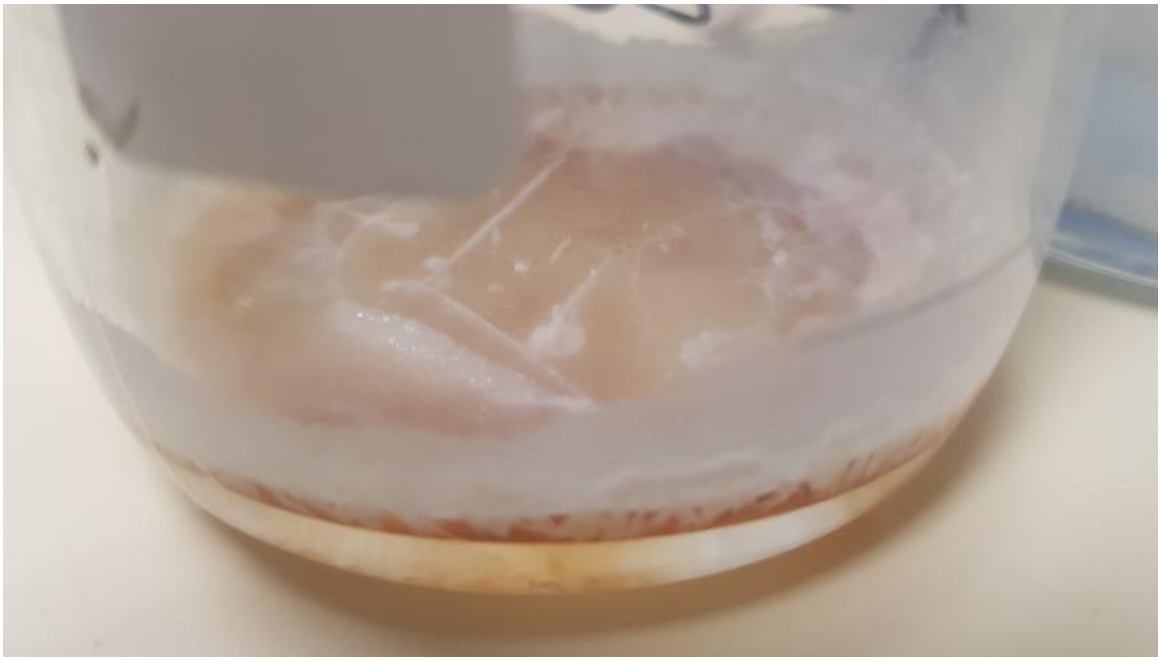

Figure 55: Picture of test 3's filtrate once it was evaporated off after 3 days of drying in a 333.15 K oven.

Figure 56: Leach residue for test 3